Version of Record: https://www.sciencedirect.com/science/article/pii/S0924424721001825
Manuscript_2be962e830d6330ac7015dc3934bc731

Acoustics at the nanoscale (nanoacoustics): A comprehensive literature review.

Part I: Materials, devices and selected applications

Chang Peng[a], Mengyue Chen[a], James B. Spicer[b], and Xiaoning Jiang[a,*]

[a] *Department of Mechanical and Aerospace Engineering, North Carolina State University, Raleigh, NC 27695, USA*

[b] *Department of Materials Science and Engineering, The Johns Hopkins University, 3400 North Charles Street, Baltimore, MD 21218, USA*

** Corresponding author: xjiang5@ncsu.edu (Xiaoning Jiang).*

Abstract

In the past decade, acoustics at the nanoscale (i.e., nanoacoustics) has evolved rapidly with continuous and substantial expansion of capabilities and refinement of techniques. Motivated by research innovations in the last decade, for the first time, recent advancements of acoustics-associated nanomaterials/nanostructures and nanodevices for different applications are outlined in this comprehensive review, which is written in two parts. As part I of this two-part review, firstly, active and passive nanomaterials and nanostructures for acoustics are presented. Following that, representative applications of nanoacoustics including material property characterization, nanomaterial/nanostructure manipulation, and sensing, are discussed in detail. Finally, a summary is presented with point of views on the current challenges and potential solutions in this burgeoning field.

Keywords: acoustics, nanotechnology, nanoacoustics, nanomaterials, nanostructures, acoustic microscopy, manipulation, sensing

© 2021 published by Elsevier. This manuscript is made available under the Elsevier user license
https://www.elsevier.com/open-access/userlicense/1.0/

Contents

1. Introduction 2
2. Nanomaterials and nanostructures for nanoacoustics 6
2.1. Active nanomaterials for acoustics 6
2.2. Passive nanomaterials for acoustics 7
2.2.1. Nanoelectrode for acoustics 7
2.2.2. Nanomaterials for laser-generated ultrasound 10
3. Applications of nanoacoustics 15
3.1. Nanoacoustic characterization 15
3.1.1. Scanning acoustic microscopy (SAM) 15
3.1.2. Atomic force acoustic microscopy 17
3.1.3. Laser-based acoustic microscopy 18
3.1.4. Other acoustic microscopies 19
3.2. Nanoacoustic manipulation 20
3.2.1. Generation of SAWs 21
3.2.2. Principle of operation 23
3.2.3. Travelling surface acoustic wave (TSAW) acoustofluidics 23
3.2.4. Standing surface acoustic wave (SSAW) acoustofluidics 26
3.3. Nanoacoustic sensing 27
3.3.1. Sensing principle 28
3.3.2. Chemical sensing 28
3.3.3. Biosensing 29
3.3.4. Other nanoacoustic sensing 31
4. Conclusions and outlook 33
Declaration of competing interest 34
Acknowledgments 34
References 34

1. Introduction

Sound is a mechanical vibration that propagates as acoustic waves in an elastic medium including air, liquid or solid structures. Acoustics is an interdisciplinary science that studies sound, particularly its production, transmission, and effects. Sounds with frequencies above the upper limit of human hearing range (typically 20 kHz) are termed as ultrasound [1].

Ultrasound is usually generated using a suitable transducer which converts electrical energy or other form of energy to acoustic energy [2]. Most of ultrasonic transducers use piezoelectric materials to generate acoustic waves from an alternating electric field using the converse piezoelectric effect. The same transducer can also be used to receive ultrasonic waves using the direct piezoelectric effect.

The first large scale implementation of ultrasound was in the military field near the beginning of World War I (1914) with the introduction of the first underwater sound navigation and ranging system (known as SONAR) [3], which was based on a pulse-echo operation. In the years that followed, many new applications for ultrasound were developed, inspiring the development of new technological advances. In the 1930s, ultrasound was introduced to generate heat to warm the deep tissue in the body, as a means of physical therapy [1]. In the late 1940s, in order to reduce the dependence of radiative medical X-ray imaging, ultrasonic pulse-echo imaging method was developed and applied to diagnostic medicine [3]. In the 1950s, Fellinger and Schmid successfully utilized ultrasound irradiation to promote hydrocortisone ointment delivery into the inflamed tissues for polyarthritis treatment [4]. Since then, the field of diagnostic and therapeutic ultrasound, i.e., medical ultrasound, has become one of the most active research fields and numerous outstanding breakthroughs have been reported. Due to its merits including easy-to-use, low cost, noninvasive assessment as well as no ionizing radiation, ultrasound imaging has been widely and actively used in the areas of gynecology, gastroenterology, angiology, and cardiology [5–9]. Moreover, ultrasound has been applied to promote drug or gene delivery into targeted tissues, including, but not limited to, skin, endothelium, and brain [10]. It has also been applied in treatment of various types of diseases, such as cancer, thromboembolism, and arteriosclerosis [11–14]. Beyond medical applications, ultrasound has also been used for many industrial applications,

including ultrasonic cleaning, welding and processing, as well as non-destructive testing [15–22].

In the early 1980s, nanotechnology and nanoscience started to receive great attention from broad segments of the research community [23]. Nanotechnology is by its nature a highly multidisciplinary collection of fields, which involves chemistry, biology, materials, physics, and medicine. The breakthroughs and advances in nanotechnology have provided various nanoscaled materials and devices with extraordinary characteristics for ultrasound investigations [24–28]. In many ways, the combination of nanotechnology with ultrasonics has revolutionized conventional approaches to use ultrasound. The emergence of different nanomaterials for the support of diagnosis and treatment of numerous kinds of diseases has attracted increasingly more attention over the past few years and has now become an important field of medical ultrasound. Indeed, nanotechnology offers numerous emerging ultrasonic instruments, from lab-on-a-chip devices capable of monitoring and controlling nanoparticles, molecules, and individual cells, to nanoscaled probes for materials properties characterization.

Motivated by the research innovations over the last decade, this review, written in two parts, comprehensively examines, for the first time, recent advancements in the study of acoustics-associated nanomaterials/nanostructures and nanodevices for various applications, as summarized in **Figure 1**. Time and space do not permit us to review all the nanotechnology innovations that have been introduced into ultrasound during the past decade. Instead, the focus will be on the nanomaterials and nanostructures for acoustics, acoustic devices including acoustic sensors, actuators, and transducers involving nanomaterials and nanostructures, as well as nanoacoustic applications including characterization of materials and structures, nanomaterials/structures manipulation, sensing, biomedical imaging, and therapy.

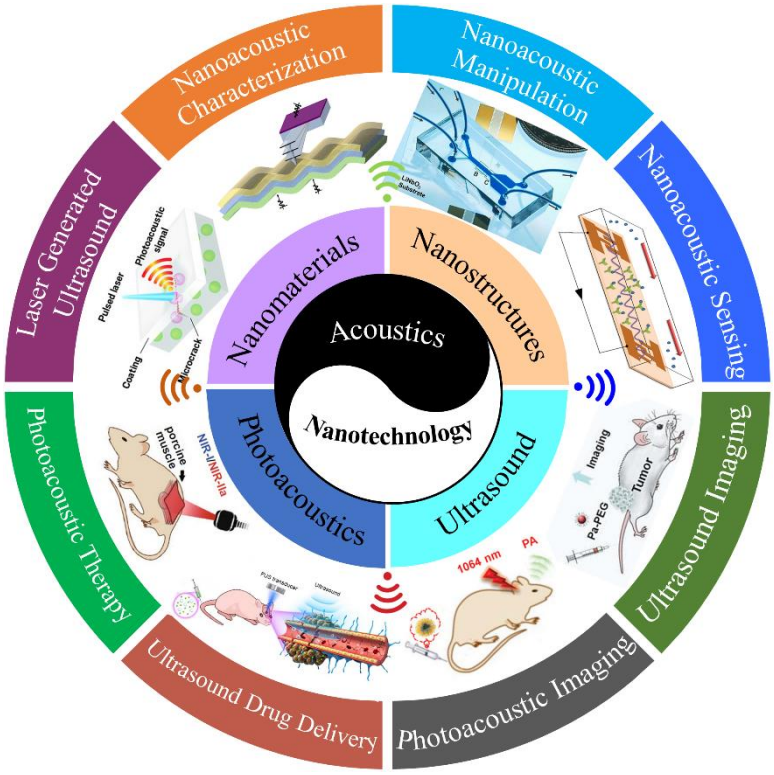

Figure 1. Schematic illustration of integration of acoustics-associated nanomaterials/nanostructures and nanodevices for applications in this review. "Laser generated ultrasound", Reproduced with permission [29]. Copyright 2018, American Chemical Society. "Nanoacoustic characterization", Reproduced with permission [30]. Copyright 2017, American Chemical Society. "Nanoacoustic manipulation", Reproduced with permission [31]. Copyright 2014, National Academy of Sciences. "Nanoacoustic sensing", Reproduced with permission [32]. Copyright 2019, Elsevier. "Ultrasound imaging", Reproduced with permission [33]. Copyright 2020, Ivyspring International Publisher. "Photoacoustic imaging", Reproduced with permission [34]. Copyright 2019, Wiley-VCH. "Ultrasound drug delivery", Reproduced with permission [35]. Copyright 2017, Dove Press Ltd. "Photoacoustic therapy", Reproduced with permission [36]. Copyright 2020, Springer Nature.

As part I of this two-part review, this paper proceeds as follows: in Section 2, active and passive nanomaterials for acoustics will be reviewed in terms of their nanostructures and performances. In Section 3, nanoacoustics for characterization of materials and structures, nanomaterials/structures manipulation, and sensing, will be reviewed focusing on materials, devices, and applications. The last section (Section 4) provides a summary and outlook for research on nanoacoustics.

2. Nanomaterials and nanostructures for nanoacoustics

2.1. Active nanomaterials for acoustics

Due to their superior piezoelectric properties and excellent mechanical properties, one dimensional piezoelectric nanomaterials (e.g. one physical dimension out of nanoscale and the other two dimensions in the nanoscale) have been reported by researchers for acoustics, as summarized in **Table 1**. They consist of lead zirconate titanate (PZT) and polyvinylidene difluoride (PVDF) nanofibers that are applied for acoustic to electric energy conversion. For example, Chen et al. [37] developed PZT nanofiber composites with Au/Cr interdigitated electrodes for acoustic emission detection. The nanofibers were fabricated by employing the electrospinning method, illustrating high piezoelectric constant and mechanical strength. Compared with bulk PZT (0.025 Vm/N) and PZT microfiber (0.059 Vm/N), the g_{33} value of PZT nanofiber (0.079 Vm/N) was much larger, resulting in a higher sensitivity for acoustic sensing. PVDF-based nanostructures have also been widely used as piezoelectric active materials due to their high piezoelectric coefficient and high energy conversion efficiency. Sun et al. [38] fabricated composite PVDF nanofibers with zinc oxide (ZnO) nanorods to enhance the performance of PVDF-based nanofibers for acoustic vibration detection. The PVDF-ZnO composite nanofiber membranes were synthesized by electrospinning combined with hydrothermal method. The nanofiber membranes showed good acoustic-electric conversion properties under low frequency (< 1000 Hz) sound conditions. Compared with PVDF nanofibers at the same sound condition (140 Hz, 116 dB), the composite nanofibers demonstrated three times higher voltage output, which was mainly attributed to the enhanced piezoelectric coefficient of the hybrid nanostructures with ZnO nanorods.

Table 1. The recently reported active nanomaterials for acoustics.

Material	Fabrication method	Diameter	Application
PZT nanofiber [37]	Electrospinning	~ 80 nm	Acoustic emission detection

PZT nanofiber [39]	Electrospinning	50-120 nm	Acoustic emission detection and structural health monitoring
PVDF nanofiber [40]	Electrospinning	310 nm	Noise detection
PVDF-ZnO nanofiber [38]	Electrospinning and hydrothermal	90-140 nm	Acoustic vibration detection
PZT nanofiber [41]	Electrospinning	200 nm	Acoustic vibration detection

2.2. Passive nanomaterials for acoustics

Contrary to active nanomaterials for acoustics that can produce an electrical field when acoustic waves hit them, or can generate acoustic waves under an electrical or magnetic field, passive nanomaterials for acoustics mainly consist of nanoscaled materials assisting acoustic generation/detection as well as interacting with acoustic waves for various applications. They can be categorized into two types: organic nanomaterials (such as organic molecules and semiconducting nanomaterials) and inorganic nanomaterials (such as metallic nanoparticles, metallic nano-patterns, and carbon-based nanomaterials). The thorough review of those types of passive nanomaterials is presented in the following sections corresponding to the different applications. In this section, only the passive nanomaterials for electrode and laser-generated ultrasound are examined.

2.2.1. Nanoelectrode for acoustics

2.2.1.1. Nano-patterned electrode for piezoelectric materials. Relaxor ferroelectric single crystals, particularly the lead magnesium niobate–lead titanate (PMN-PT), have been exploited for a great variety of applications including sensors, ultrasound transducers, and actuators due to their outstanding piezoelectric and dielectric properties [42,43]. The researches related to the properties of relaxor ferroelectric materials have been carried out for about two decades, and now it is widely recognized that the piezoelectric and dielectric properties of a ferroelectric single crystal are closely associated with its domain structures [44]. In order to further improve the properties of ferroelectric single crystals, domain

engineering techniques have been employed by researcher. Patterning nanocomposite electrode, a kind of domain engineering techniques, has been effectively utilized for tailoring the piezoelectric and dielectric properties of ferroelectric materials over the past few years. Chang et al. [45] fabricated manganese (Mn)/gold (Au) composite nanopattern as nanoelectrode on a PMN-PT single crystal surface by using interference lithography method. Combined the Mn/Au nanoelectrode with back switching poling method, the [001] poled PMN-PT single crystal achieved the increase of piezoelectric coefficient d_{33} and dielectric constant by 27% and 25%, respectively. Following that work, in order to explore the relationship between the domain structures and the properties of the PMN-PT with nanoelectrode, the authors employed piezoresponse force microscopy and time-of-flight secondary ion mass spectrometry to study a PMN-PT sample with MnO_x/Au nanocomposite electrode [46] (**Figure 2a**). Their results showed that the single crystal with the patterned nanoelectrode had a d_{33} 36.7% higher and dielectric constant 38.3% higher than the crystal with conventional planar Au electrode. The increased piezoelectric and dielectric properties were attributed to Mn diffusion and doping as well as the fringe effect underneath the edge of the patterned nanoelectrode. Furthermore, Gao et al. [47] employed X-ray diffraction reciprocal space mapping technique to investigate how the patterned nanoelectrode affected domain distribution near the surface region under electric field. It was found that the enhanced properties were mainly attributed to the excess elastic energy stored in the nano domain distribution. Recently, Luo et al. [48] further advanced the study of domain morphology of PMT-PT with patterned nanoelectrode. They found that the domain morphologies varied from the nanoelectrode surface to the crystal interior. Compared with the crystal with planar electrode, the domain wall density of the crystal with nanoelectrode was higher. Moreover, the M phase of the nanoelectrode patterned crystal had higher randomness than that of the planar electrode deposited crystal.

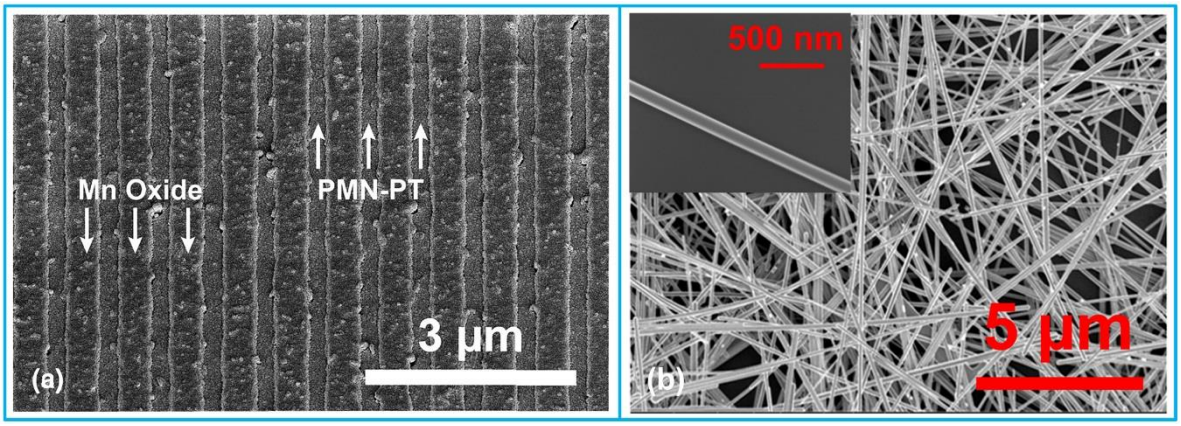

Figure 2. Nanoelectrodes for acoustics. (a) MnO_x nanoelectrode patterned on a PMN-PT single crystal surface. Reproduced with permission [46]. Copyright 2018, Elsevier. (b) SEM images of the silver nanowires. Reproduced with permission [49]. Copyright 2021, IEEE.

2.2.1.2. Silver nanowire electrode for ultrasound transducers. Conventionally, ultrasound transducers are always fabricated with a rigid structure, which cannot maintain a good coupling with the non-planar surfaces, such as human body or human skull, during different applications. The air gaps between the transducer and non-planar surface interface resulting from the poor coupling will lead to ~100% acoustic wave reflection and distortion, thus bringing about unreliable results. Recently, a flexible piezoelectric 1-3 composite structure was developed by Jiang et al. [50,51], which was composed of piezoelectric ceramic and soft elastomer polydimethylsiloxane (PDMS). Because traditional metal-based electrode could not be utilized for continuous bending, a highly stretchable and conductive silver nanowire-based electrode was fabricated for the flexible transducer (**Figure 2b**). The silver nanowires were synthesized by a modified polyol reduction technique [51]. They were randomly oriented to form a dense network on the transducer surface, having an average diameter of ~ 90 nm. Recently, the flexible piezo-composite ultrasound transducer deposited with the silver nanowire-based electrodes has been successfully applied for noninvasive blood pressure sensing applications [8,49].

2.2.2. Nanomaterials for laser-generated ultrasound

2.2.2.1. Photoacoustic effect. The photoacoustic effect, discovered by Alexander Graham Bell in 1880, refers to the generation of acoustic waves from an object being irradiated by pulsed or intensity-modulated light [52]. While there are five main mechanisms responsible for the generation of photoacoustic signal, including dielectric breakdown [53], vaporization or material ablation [54], thermoelastic process [55,56], electrostriction [57], and the radiation pressure [58], for the majority of applications, thermoelastic expansion is the most commonly recognized mechanism for photoacoustic generation and is used widely for biomedical therapy, biomedical imaging, nondestructive inspection, and material characterization.

The fundamental principle of thermoelastic generation of acoustic waves can be simply described as illustrated in **Figure 3a** [52]. When an optical illumination encounters a certain substance, part of the optical energy is absorbed by the substance and converted to heat energy. Therefore, the temperature of the object rises, and thermal expansion takes place at the same time, which generates acoustic waves in the medium. It should be noted that in order to generate acoustic waves in the medium, the heating source must vary with time to produce corresponding temporal variations in pressure.

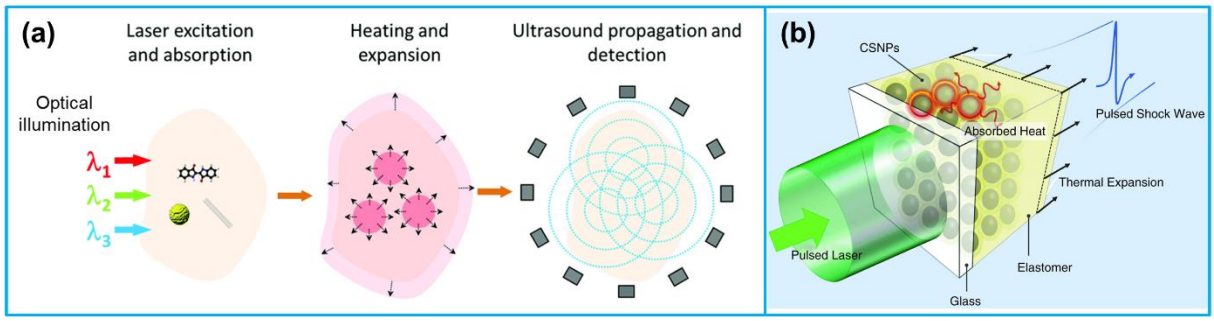

Figure 3. (a) A schematic illustration of the mechanism of photoacoustic signal generation. Reproduced with permission [59]. Copyright 2017, The Royal Society of Chemistry. (b) A schematic representation of laser-generated ultrasound configuration. Reproduced with permission [60]. Copyright 2019, IEEE.

Theoretically, in its simplest formulation, the generation of acoustic waves via the thermoelastic effect is governed by both the heat equation (**Equation 1**) and the acoustic

wave equation (**Equation 2**). For simplicity, only isotropic media will be considered. The temperature distribution which is determined by the heat conduction equation can be expressed as follows [61]:

$$\frac{\partial T}{\partial t} = k\nabla^2 T + \frac{1}{\rho C_p} h(r,t) \quad (1)$$

where T refers to the temperature, k refers to the thermal diffusivity, ρ is the density of the material, C_p is the specific heat capacity, and h is the heating power per unit volume, which relies on both time, t, and position, r.

The inhomogeneous wave equation for the scalar potential ϕ in time domain is shown in the following equation [62]:

$$\nabla^2 \emptyset - \frac{1}{c^2}\frac{\partial^2 \emptyset}{\partial t^2} = \frac{3B}{\rho c^2}\alpha_L T \quad (2)$$

where B is the bulk modulus, c is the speed of longitudinal wave, and α_L is the linear coefficient of thermal expansion. The temperature distribution T which has been determined by **Equation 1** acts as a source term in this equation. Therefore, the pressure field in a medium can be calculated as $p = -B\nabla^2 \emptyset$.

2.2.2.2. Nanomaterials for laser-generated ultrasound. Laser-generated ultrasound has been under investigation and development for several decades and has provided several advantages over conventional piezoelectric transduction techniques such as the ability to perform ultrasonic measurements in a noncontact and remote fashion. Other attractive features of laser-generated ultrasound are its high frequency (MHz), wide bandwidth, as well as high power density [63]. Different from the conventional photoacoustic applications that the laser beam and target medium are directly interacted, laser-generated ultrasound configuration are now commonly composed of an optical absorption layer and a thermal expanding layer, which is much easier and more efficient to convert optical energy into acoustic waves [64]. A typical configuration is shown in **Figure 3b**.

The poor optical-to-acoustical conversion efficiency is considered to be one major drawback that the laser-generated ultrasound based on thermoelastic effect currently has [65]. In order to improve the conversion efficiency, researches have focused predominantly on absorption material which is the most critical component in laser ultrasound transducer. It is highly desirable that the optical absorbing material possesses the properties of large thermal expansion coefficient, low heat capacity and high optical absorption coefficient [66].

In 1963, White [55] proposed that high frequency ultrasound can be generated by laser irradiation of metals, and thin metal films such as Mo [67], Al [67] and Cr [68], However, owing to their small thermal expansion coefficient, the optical-to-acoustical conversion efficiency of metallic films is relatively low [69]. While other material systems might yield higher conversion efficiencies and have been considered previously, the focus of this section is on nanoscaled systems that are engineered specifically to produce enhanced efficiency. For example, Hou et al. [70] developed a 2D gold nanostructure to generate 100 MHz ultrasound, which was composed of gold nanoparticles (AuNPs) sandwiched between a 4.5 μm-thick PDMS layer and a glass substrate. The 2D nanostructure facilitated the creation of laser-generated ultrasonic transducer arrays for high frequency ultrasonic imaging. In another study, Wu et al. [71] reported a AuNPs-PDMS nanocomposite prepared by one-pot synthesis for high efficiency ultrasound generation. Their results demonstrated that the nanocomposite showed a conversion efficiency much higher than that of an Al thin film. Besides AuNPs, Lee et al. [72] demonstrated that an optoacoustic transmitter fabricated by reduced graphene oxide (rGO)-coated thin Al film was able to generate an acoustic pressures 64 times higher than those produced by the Al-alone transmitter. Karabutov et al. [73] studied the use of a 300 nm Al thin film as a transmitter within a temperature range of 3-14 kK and a pressure range of 0.1-4 kbar. The dynamics of the pressure, temperature, and reflectivity of aluminum under these conditions were measured at a nanosecond time resolution. Yoo et al. [74] reported a

high-frequency optoacoustic transmitter which was made by nanostructured germanium (Ge) and PDMS spin coated on top of it. Under pulsed laser excitation, the transmitter generated an acoustic pressure 7.5 times higher than that of a Cr transmitter.

Beyond thin metal films, carbon-based nanomaterials have also been widely used for optoacoustic transmitters to generate broadband and efficient ultrasound transmission (**Table 2**). Compared with metallic thin films, they usually (but not always) illustrate higher ultrasound transmission efficiency. Inspired by the fact that carbon black (CB) is composed of carbon nanoparticles, Hou et al. [75] fabricated an optical absorbing film comprising of a mixture of CB and PDMS spin coated onto a glass substrate (**Figure 4a**). The thin film with a thickness of 11 μm could improve the transduction efficiency by 30 dB. The acoustic power generated by a transmitter made by the film was comparable to a piezoelectric transducer (100 MHz center frequency). In another study, Hou et al. [70] showed that the carbon nanotube (CNT) nanocomposite demonstrated five times enhancement compared to 2D AuNPs nanocomposites (**Figure 4b**). Due to the nanoscale dimension of CNT, the device based on CNT nanocomposite had fast thermalization rate, which could generate high frequency ultrasound efficiently. While AuNPs nanocomposites also possessed this advantage, the outstanding thermal conductivity of the CNTs made the nanocomposite to have better thermal conduction and improved efficiency compared with AuNPs. Carbon nanofibers-PDMS (CNFs-PDMS) thin films have also been reported by Hsieh et al. [69] for high intensity acoustic wave generation (**Figure 4c**), which demonstrated a maximum acoustic pressure 7.6-fold higher than that of using CB-PDMS thin films. Moreover, the optoacoustic conversion efficiency of the CNFs-PDMS composite was much higher than CB-PDMS and metallic thin films. Chang et al. [63] developed a candle soot nanoparticles-PDMS (CSNPs-PDMS) nanocomposite (**Figure 4d**) and the photoacoustic conversion efficiency was compared with CNFs-PDMS, CNTs-PDMS, and CB-PDMS nanocomposites. The ratio of conversion

efficiency for CSNPs-PDMS and other three kinds of nanocomposites was 13:4.9:4.1:1. Following that, Huang et al. [76] fabricated an optoacoustic transmitter using the CSNPs-PDMS nanocomposite, exhibiting superior performance. Using a laser excitation with low fluence (3.57 mJ/cm^2), the energy conversion coefficient and acoustic pressure of the transmitter were measured to be 4.41×10^{-3} and 4.8 MPa, respectively. In another study, Chang et al. [77] concluded that both the thickness of CS/PDMS composite and the carbon volume fraction were important for light absorption. Under a low laser energy input (<1 mJ/pulse), the 2.15 μm-thick CS/PDMS composite could generate a conversion efficiency of 9.69×10^{-3} and an acoustic pressure of 3.78 MPa. Recently, Kim et al. [78] reported a narrowband, ultrasound nondestructive testing method based on a patterned array of CSNPs-PDMS lines as the acoustic signal amplifier. The CSNPs-PDMS array design generated narrowband photoacoustic waves that could filter the undesired wave modes and enhance the subsequent Lamb wave analysis.

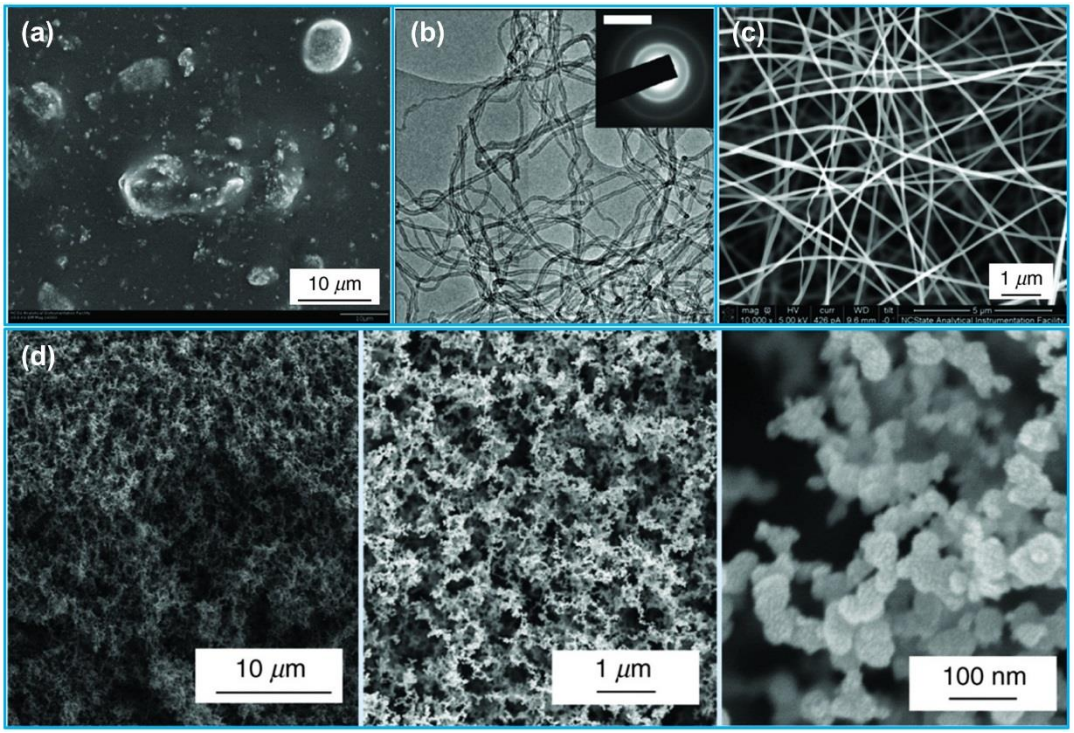

Figure 4. Scanning electron microscopy (SEM) photographs of carbon-based nanomaterials for laser ultrasound nanocomposite transmitters. (a) Carbon black powder-PDMS thin film. Reproduced with permission [69]. Copyright 2015, AIP Publishing. (b) Carbon nanotubes.

Reproduced with permission [79]. Copyright 2014, AIP Publishing. (c) Carbon nanofibers-PDMS thin film. Reproduced with permission [69]. Copyright 2015, AIP Publishing. (d) Coated candle soot nanoparticles on the glass in various resolutions. Reproduced with permission [60]. Copyright 2019, IEEE.

Table 2. The reported nanomaterials for laser ultrasound nanocomposite transmitters.

Nanomaterial	Thickness (μm)	Aperture diameter (mm)	Len material	Focal length (mm)	Transmitting sensitivity at center frequency (MPa/mJ)
CB-PDMS [80]	30	12	Glass	N/A	0.22-0.57 @ 3 MHz
CB-PDMS (concave) [81]	25	12-12.5	Glass	12.4	1.5 @ 14 MHz
CB paint (concave) [82]	20	2	Glass	3.4	0.65 @ 20 MHz
CNT-Au-PDMS (concave) [83]	16	6	Fused silica	5.5	2.67 @ 15 MHz
CNT-Au-PDMS (concave) [84,85]	16	12	Fused silica	11.46	>1.4 @ 15 MHz
CNT-PDMS [79]	20	0.2	Optical fiber	N/A	0.025 @ 18 MHz
CNT-Au-PDMS (concave) [86,87]	16	15	Fused silica	9.2	30 @ 15 MHz
CNT-PDMS [88]	20	0.2	Optical fiber	N/A	> 0.04 @ 19.4 MHz
CNT-PDMS [89]	13.7	0.2	Optical fiber	N/A	0.05 @ 31 MHz
CNF-PDMS [69]	24	12	Glass	N/A	0.7-3.27 @ 3.5 MHz
CSNP-PDMS [63]	25	12	Glass	N/A	28 @ 10 MHz
CSNP-PDMS [90]	18	12	Glass	N/A	2.5 @ 10 MHz
CSNP-PDMS (concave) [91]	24.5	6	Glass	4.71	1.11 @ 14 MHz

3. Applications of nanoacoustics

3.1. Nanoacoustic characterization

3.1.1. Scanning acoustic microscopy (SAM)

The concept of acoustic microscopy was first proposed by Sokolov in 1949 [92]. Since the wavelength of sound at high frequencies can be very short, it is possible to develop an acoustic microscope which has a resolution similar to that of an optical microscope. In 1974 Lemons and Quate demonstrated the first scanning acoustic microscope operating at 150 MHz frequency and providing a 10 μm resolution [92]. In 1985, this group successfully developed a SAM capable of operating in liquid helium at 840 MHz with a wavelength of 260 nm [93].

The technique of SAM has been in use for nearly four decades, and it has been successfully used for imaging interior structures in materials as well as for biology [93].

The principle of the SAM is illustrated in **Figure 5a**. In this technique, an ultrasound transducer generates high-frequency acoustic waves which propagate through a coupling medium and focus on a specimen. The resulting reflected acoustic waves resulting from the acoustic impedance difference at the material interfaces are then acquired and analyzed to generate images, revealing the microscopic features or defects in the specimen. Since the ultrasound imaging resolution increases with the frequency, nanometer-scale resolution of SAM can generally be achieved at frequencies of several hundred gigahertz. However, strong acoustic attenuation in the gigahertz range can occur in the coupling medium. Typically, the frequency of the ultrasonic signal used in SAM is in the range 15–300 MHz, but can be in the GHz for applications that require high resolution with limited penetration depth, i.e., near field ultrasound microscopy [94,95].

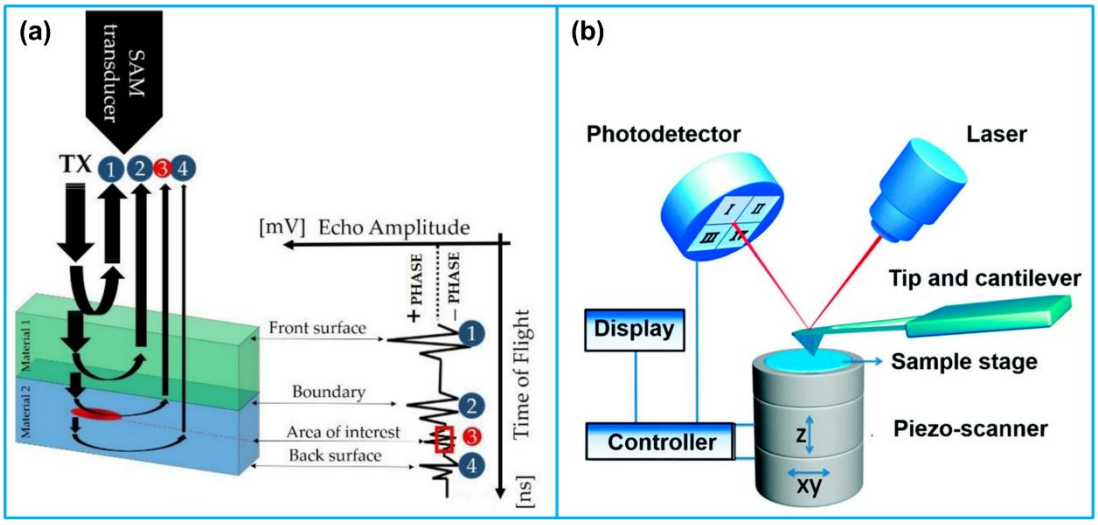

Figure 5. (a) Principles of scanning acoustic microscopy (SAM). Reproduced with permission [96]. Copyright 2019, MDPI. (b) Schematic diagram of atomic force microscopy. Reproduced with permission [97]. Copyright 2015, The Royal Society of Chemistry.

The most important component of a scanning acoustic microscope is the ultrasonic transducer which is usually made of piezoelectric thin film, such as ZnO and $LiNbO_3$ [98]. The transducer is integrated into a rod type of acoustic delay line that's made of quartz or

sapphire, which converts the high frequency electrical signal into acoustic waves. During the application, the exit aperture of the rod is often fabricated into a spherical or conical shape to focus the acoustic beam. There are two modes of operation in a scanning acoustic microscope [98]: reflection mode and transmission mode. In the reflection mode, a single ultrasonic transducer is utilized for transmitting and receiving acoustic signals, which is similar to an ultrasound pulse-echo mode operation. In the transmission mode, two different transducers are applied, and one is used as a transmitter and the other is used as a receiver. The comparison between the reflection mode and transmission mode for applications is described in the literature [93]. The SAM technique is particularly applicable to characterize optically opaque samples that optical characterization methods cannot be effectively utilized.

3.1.2. Atomic force acoustic microscopy

Although SAM can be applied for characterizing spatial variations in the materials and determining interfacial and elastic properties, the spatial resolution of SAM is limited to micrometer and thus hardly to characterize material properties which requires sub-micrometer resolution [99]. In order to improve the resolution for characterization, a scanning probe microscopy (SPM)-based acoustic method has been developed, which utilizes the scanning probe as a local ultrasonic transducer and measures the steady-state elastic force between the probe tip and sample surface (**Figure 5b**) [100,101]. Nowadays, the most commonly used SPM-based characterization techniques which combine of acoustics and atomic force microscopy include atomic force acoustic microscopy (AFAM) and ultrasonic force microscopy (UFM). They can characterize and map of mechanical properties of samples, including metals, semiconductors, and ceramics with nanoscale resolution. For example, AFAM has been reported by many recent studies to successfully measure dynamic Young's modulus of different materials with nanometer resolution, such as nanocrystalline ferrites [102], silicon single crystals [103], PZT ceramics, diamond-like carbon coatings [104], and

clay minerals [105]. During the AFAM measurement, the contact zone between the cantilever tip and sample surface is sonicated by an ultrasonic transducer (**Figure 5b**). The measuring of dynamic Young's modulus is derived from the difference of the cantilever contact resonant frequency relative to its free resonance. The spatial resolution of the AFAM technique is approximately 10 nm [105].

The UFM, adopting a much softer cantilever than the tip-sample contact zone, is a modification of the original AFM setup [106]. While a sample is driven to vibrate at frequency higher than the cantilever resonance by a transducer thereunder, the tip is cyclically contact the sample [100]. The subsurface features of the sample can be mapped by the modulated cantilever vibration. The subsurface features with different elastic properties can also be imaged by controlling the direction of vibration forces [106]. The spatial resolution of the UFM technique is approximately 5 nm.

3.1.3. Laser-based acoustic microscopy

Laser-based ultrasonic (LBU) techniques have also been used for nondestructive material characterization. Compared with ultrasonic technique based on the piezoelectric effect, LBU techniques generate and detect ultrasonic waves without need of an acoustic coupling medium, which can potentially improve the penetration depth of ultrasonic waves during characterization [94]. Moreover, getting rid of the coupling medium is also favorable for the samples which are easily contaminated by the coupling material. For the characterization of nanoscaled features in samples, broadband ultrasonic waves with frequencies up to 1000 GHz are generated by ultrafast laser sources, which show ultrasonic wavelengths up to several hundred nanometers [107–110]. However, in this frequency regime, strong acoustic attenuation will be generated, which limits the sample penetration depth to just the nanoscale [109,110]. Inspired by this, Balogum et al. [94] developed a microscopy technique which can extend the penetration depth to several hundred micrometers. A pulsed laser source was used

to generate broadband acoustic waves and an optical interferometer was applied to detect acoustic waves. In addition, Ahn and Balogun [111] employed a laser-based ultrasonic technique for measuring the bulk elastic properties of nanoporous gold membranes. The technique was non-contact and nondestructive, and the existence of sample inhomogeneity could be revealed based on the dispersion of bulk waves. The reported technique could potentially be utilized for process control during nanoporous structure fabrication.

3.1.4. Other acoustic microscopies

Alternatives to force-based scanning probe microscopy techniques have been investigated that use near-field optical microscopy techniques to locally map ultrasound arrivals with sub-optical wavelength spatial resolution (**Figure 6a**) [99]. These techniques typically use a pulsed laser to produce a broadband ultrasonic source and a scanning near-field optical probe to detect the ultrasonic arrivals. Shekhawat et al. [30] developed a near-field thickness resonance acoustic microscopy technique which can image the subsurface features with large sensitivity and high resolution (**Figure 6b**). Zeng et al. [112] created nanoacoustic resonators by exciting acoustic resonances in the embedded nanoparticles for characterizing the physical properties of surrounding matrix materials. Femtosecond pulsed laser light was employed to excite the nanoparticle acoustic vibration and energy was extracted from the nanoparticles and released to the surrounding matrix due to the acoustic impedance mismatch. It was found that material properties including density, modulus of elasticity, and thermal conductivity played an important role in affecting the energy converting from the nanoparticles to the surrounding matrix.

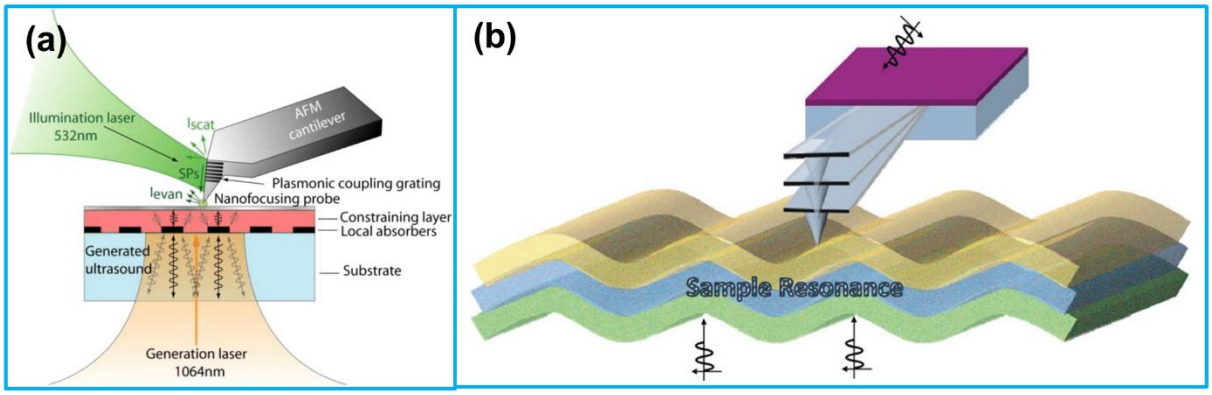

Figure 6. (a) Ultrasonic near-field optical microscopy. Reproduced with permission [99]. Copyright 2013, AIP Publishing. (b) Near-field thickness resonance acoustic microscopy. Reproduced with permission [30]. Copyright 2017, American Chemical Society.

3.2. Nanoacoustic manipulation

With advances in fields of nanoscience and nanotechnology such as micro/nano fabrication, materials engineering, biomedicine, manipulation of micro/nano objects including particles, droplets and cells, are required [113]. These manipulation functions consist of micro/nano objects orientation, concentration, sorting, trapping, assembly, etc. [113] To realize these manipulation functions, many different strategies have been developed by researchers, which are classified as optical [114,115], magnetic [116,117], electrical [118], mechanical [119], AFM [120], microfluidic [121], and acoustic methods [122,123]. Each technique has its potential shortcomings, but when compared to the optical, magnetic, or electrical strategies, acoustic-based methods have various recommending characteristics. For example, acoustic-based methods generally have no specific requirements of the manipulated sample properties, they can provide a wide variety of manipulation functions, they can be carried out using a relatively simple and compact device structures, etc. [124–126]

While researchers have utilized bulk acoustic waves to manipulate micro/nano particles and cells in microfluidic channels [127–132], the microchannel should have outstanding acoustic reflection properties for acoustic wave generation [133]. Therefore, for a microfluidic device which is commonly made of PDMS and has poor acoustic reflection, manipulation based on

bulk acoustic waves is not a wise option. In addition, it is not easy to integrate a bulk ultrasonic transducer into a microsystem [134]. A specific disadvantage for using bulk acoustic waves for this type of application is that the acoustic energy is spread throughout the device and is not readily confined to the interaction zone of interest. However, surface acoustic waves (SAWs) can be used to have great advantage since they propagate on the surface of an elastic medium and most of the energy is confined to the device surface. As a result, achieving the same acoustic effect, SAWs require less energy than bulk acoustic waves [135].

Rayleigh waves are the most recognized mode of SAWs which include both longitudinal and transverse motions that decay exponentially into the substrate [136]. While other modes of SAWs exist, such as Love, Scholte, Lamb, Leaky, and shear horizontal SAW, because most SAW-based lab-on-a-chip devices (i.e., miniaturized laboratories built on a chip) utilize Rayleigh waves, SAW here is used to specifically indicate Rayleigh-type SAWs.

3.2.1. Generation of SAWs

Typical SAW-based manipulation devices are interdigital transducers (IDTs) that are made of comb-shaped metal electrodes patterned on a piezoelectric substrate (**Figure 7a**). When an AC electrical signal oscillating at radio frequency is employed across the electrodes [135], the piezoelectric substrate strains in a way that generates acoustic waves propagating along the surface of it. The configuration of the electrodes on an IDT is the critical factor affecting the performance of the device. The characteristics of SAW can be changed by varying the spacing, number and aperture of the metal electrodes. The SAW wavelength is related to the IDT pitch size as $\lambda = 2d$. When SAWs propagate through a liquid medium, the acoustic energy will diffract into the liquid because of the acoustic velocity mismatch in the liquid and in the piezoelectric substrate, thus forming a leaky SAW that propagates on the interface of the liquid and substrate [137].

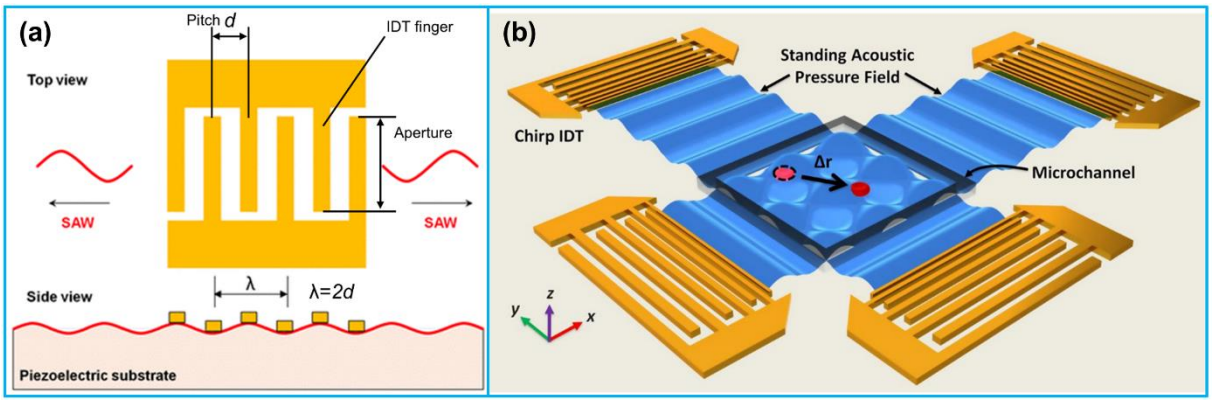

Figure 7. (a) The structure of a metallic IDT deposited on a piezoelectric substrate. Reproduced with permission [135]. Copyright 2013, The Royal Society of Chemistry. (b) A microfluidic device with orthogonal pairs of chirped IDTs for generating SSAW. Reproduced with permission [124]. Copyright 2012, National Academy of Sciences.

Materials popularly utilized for fabricating IDT include copper, aluminum, tungsten, gold, titanium, platinum, and platinum-based alloys [138]. The most widely used materials for fabricating piezoelectric substrate for SAW devices consist of quartz (SiO_2), $LiTaO_3$, and $LiNbO_3$ [139]. Thin films such as AlN, ZnO and PVDF can also be utilized in SAW-based microfluidic and lab-on-chip devices [140]. Others include GaAs, CdS, lithium tetraborate ($Li_2B_4O_7$), and langasite ($La_3Ga_5SiO_{14}$) [141]. The properties of the piezoelectric materials used for substrate are summarized in **Table 3**.

Table 3. Properties of the piezoelectric materials used for SAW device substrate.

Substrate material	SAW velocity (m/s)	Electromechanical coupling coefficient, *k* (%)	Dielectric constant	Temperature coefficient of frequency (ppm/°C)
ST-X Quartz [142]	3159.3	0.11	3.7	0
Y-Z $LiTaO_3$ [143]	3230	0.74	-	35
$LiTaO_3$ [144]	3301	0.64	52	18
Y-Z $LiNbO_3$ [142]	3487.7	4.80	-	94
$LiNbO_3$ [145]	3992	5.6	83	75
ZnO [146]	2645	1.8	10	15
(0001) AlN [147]	5607	0.30	8.5	19
(001)-<110> GaAs [148]	2864	0.07	12.9	35
(0, 138.5, 26.8) $La_3Ga_5SiO_{14}$ [149]	2734	0.34	18	0

3.2.2. Principle of operation

Using powerful micro/nanoscale SAW-based acoustofluidic (the fusion of acoustics and micro/nanofluidics) methods, actuation (such as atomizing, mixing, and driving) of fluids on the micro/nanoscale as well as manipulation (such as separation, merging, aligning, and sorting) of micro/nano objects have been realized in a frequency range of 10-1000 MHz [150]. Two different types of SAWs are broadly used in acoustofluidics, which are traveling surface acoustic wave (TSAW) and standing surface acoustic wave (SSAW) [135]. TSAW is generated from a single IDT. SSAW is produced while one TSAW with its reflected form comes together and interfere (**Figure 7b**). Similarly, a 2D SSAW can be formed if two sets of IDTs are positioned perpendicularly. TSAWs induce acoustic radiation forces and acoustic streaming within fluids, which are used for manipulation of micro/nanoobjects and actuation of fluids [150], such as microfluidic mixing, concentration, micro/nanoparticle patterning and transport. SSAWs are mainly employed for the manipulation modes, such as jetting, focusing, tweezing, and separation [151].

Because the objective here is to discuss the most recent advancement in manipulating nanosized objects using SAWs, a comprehensive examination of particles and droplets manipulation at the microscale is beyond the scope of this review. Readers who are interested in microscale acoustofluidics are advised to refer to a book titled "Microscale Acoustofluidics" [152]. Additionally, the readers can find the review on microscale acoustofluidics published by Friend et al. [153], Ding et al. [124,135], Yeo et al. [151], Destgeer et al. [150], and Fu et al. [140]

3.2.3. Travelling surface acoustic wave (TSAW) acoustofluidics

3.2.3.1. Atomization. Atomization, referring to the disintegration of bulk solids or liquids into fine particles or liquid droplets [135], has many practical applications including medicine,

internal combustion engines, and agriculture [154]. It has been reported that ultrasonic atomizer can be developed based on TSAW for a variety of applications [155], while the atomized particles are usually at the microscale. In 2008, Alvarez et al. [156] developed a 20 MHz SAW device for transdermal and gastrointestinal drug delivery, which could generate solid protein nanoparticles with a diameter range of 50-100 nm. Similarly, Friend et al. [157] developed a SAW device (resonant frequency 8.6 MHz) for the generation of polymeric nanoparticles for potential drug delivery applications. The device could rapidly produce nanoparticle assemblies ranging from 150 to 200 nm, which were composed of 5-10 nm fine nanoparticles.

3.2.3.2. Acoustic streaming and radiation forces. Collins et al. [158] demonstrated an acoustic streaming-based SAW device working at 633 MHz for filter-free manipulation of nanoparticles (**Figure 8a**). Contrary to other TSAW studies, the reported device could continuously focus nanoparticles using focused TSAW. Mao et al. [126] developed a SAW device that could generate a torsional vibration mode and acoustic streaming in a square glass capillary (**Figure 8b**). Nanoparticles could be enriched and focused within the glass capillary due to the combined effect of the acoustic radiation force and the hydrodynamic viscous force induced by the single vortex acoustic streaming. Ren et al. [159] fabricated an acoustofluidic device that could achieve both positive and negative rheotaxis of synthetic bimetallic micromotors with the assistance of combined acoustic force and chemical fuel (**Figure 8c**). The bimetallic microrods could be pushed along the bottom surface of a fluid channel by employing acoustic force alone. However, using chemical fuel (H_2O_2) alone, the microrods would orient themselves with their anode end against the flow with the existing of shear flow.

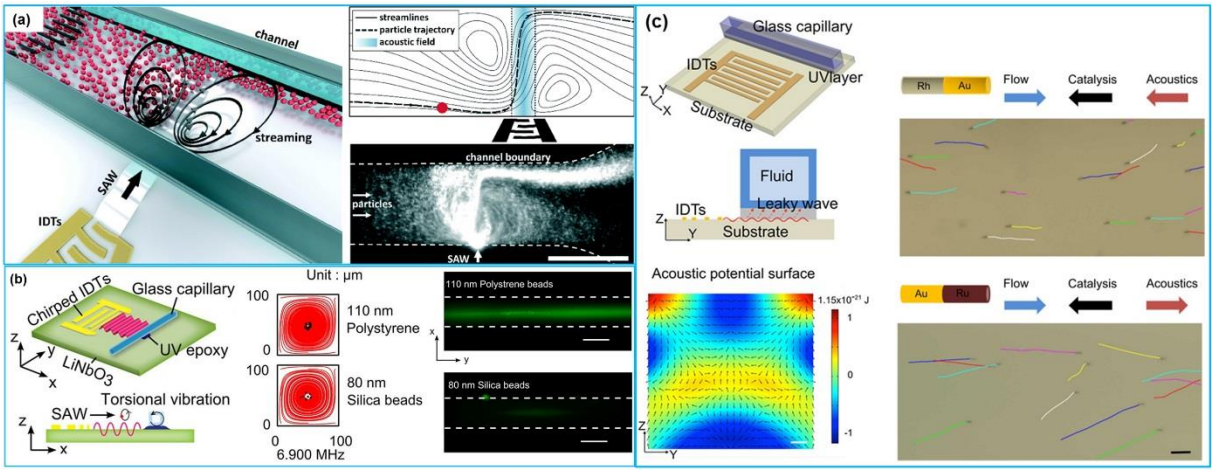

Figure 8. (a) Principle of SAW-based nanoparticle focusing. Reproduced with permission [158]. Copyright 2017, The Royal Society of Chemistry. (b) An acoustofluidic-based nanoparticle-enrichment device. Reproduced with permission [126]. Copyright 2017, American Chemical Society. (c) An acoustofluidic device for rheotaxis of synthetic bimetallic micromotors and illustration of its working mechanism. Reproduced with permission [159]. Copyright 2017, American Chemical Society.

3.2.3.3. Carbon nanotubes (CNTs) alignment. CNTs have attracted much attentions from the nanotechnology research field for their great mechanical strength and unique electrical properties in applications [160]. Nevertheless, it has proven challenging to align CNTs in large quantities for practical applications. TSAWs offer a promising solution for aligning of a large number of CNTs simultaneously. Strobl et al. [161] applied TSAWs to align multi-walled carbon nanotubes (MWNTs) 25-45° relative to the SAW field. Due to the piezoelectric field and the acoustic streaming generated by Rayleigh waves, the MWNTs were shifted and directly aligned with the piezoelectric field. Smorodin et al. [162] developed an approach to improve the CNTs alignment performance by first thiolating single-walled carbon nanotubes (SWNTs) and then placing them on a substrate with patterned gold electrodes. It was found that most of the SWNTs aligned 0-20° relative to the SAW field after applying SAWs across the device. The improvement was attributed to the alleviated acoustic streaming effect on the alignment after attaching the thiolated SWNTs to the gold electrodes. While investigations have successfully illustrated CNTs alignment using SAW-based devices, the requirement of piezoelectric substrate restricts their applications in microelectronics in which silicon

substrate are commonly utilized. To overcome this limitation, Seemann et al. [163] patterned gold contacts in a silicon substrate and made them close to a $LiNbO_3$ substrate which used to generated TSAWs. While TSAWs were applied to a CNT solution deposited between the two substrates, the alignment of CNTs on the silicone substrate was successfully achieved due to the combined piezoelectric field and acoustic streaming effects.

3.2.4. Standing surface acoustic wave (SSAW) acoustofluidics

A manipulation strategy based on SSAW was firstly reported by the Penn State Acoustofluidics Laboratory in 2009 [164]. This SSAW-based technology was based on a particle manipulation technology called "acoustic tweezers" [165]. Acoustic tweezers were the first technology to use SSAW to manipulate (pattern, focus, and separate) electronically insulating micro/nanoparticles or cells, but have since been applied to continuous flow applications [166–169]. **Figure 7b** shows a typical configuration of an acoustic tweezer device [135]. This standing wave field is coupled into the liquid in the microchannel, resulting in periodic pressure fluctuation in the liquid. Pressure fluctuation in the liquid gives rise to acoustic radiation forces that are applied on particles to position them at the pressure nodes or antinodes. The acoustic radiation force F_r is given by **Equation 3** [170]:

$$F_r = -\left(\frac{\pi p_0^2 V_p \beta_f}{2\lambda}\right)\phi(\beta,\rho)\sin(2kx) \quad (3)$$

$$\phi(\beta,\rho) = \frac{5\rho_p - 2\rho_f}{2\rho_p + \rho_f} - \frac{\beta_p}{\beta_f} \quad (4)$$

In **Equation 3** and **4**, p_0 is the acoustic pressure, V_p is the particle volume, λ is the wavelength of SAW, k is the wave vector, x is the distance from a pressure node point, ρ_p and ρ_f are the density of the particle and fluid, respectively. β_p and β_f are the compressibility of the particle and fluid, respectively. ϕ is the acoustic contrast factor, determining whether the particle will move to pressure node or to antinode in the SSAW field. If ϕ is positive, the particle will move towards pressure node; if ϕ is negative, it will move to antinode.

As the particle moves in the fluid, it is opposed by a Stokes drag force, which is given by **Equation 5**:

$$F_d = -6\pi\eta R_p(u_p - u_f) \quad (5)$$

Where η is the fluid viscosity, R_p is the particle radius, u_p and u_f are the velocity of particle and fluid, respectively. Other forces acting on the particle include gravity and buoyant forces, but these two forces are comparable in magnitude and opposite in direction. Using a SSAW-based approach, manipulation of nanoparticles in microfluidic channels as well as cell separation can be achieved. Examples include patterning nanoscale polystyrene beads [171], 1D and 2D alignment of nanowires [172], separation of nanoparticles in a flow (**Figure 9a-b**) [173], and isolation of ~ 100 nm exosomes from whole blood (**Figure 9c**) [174].

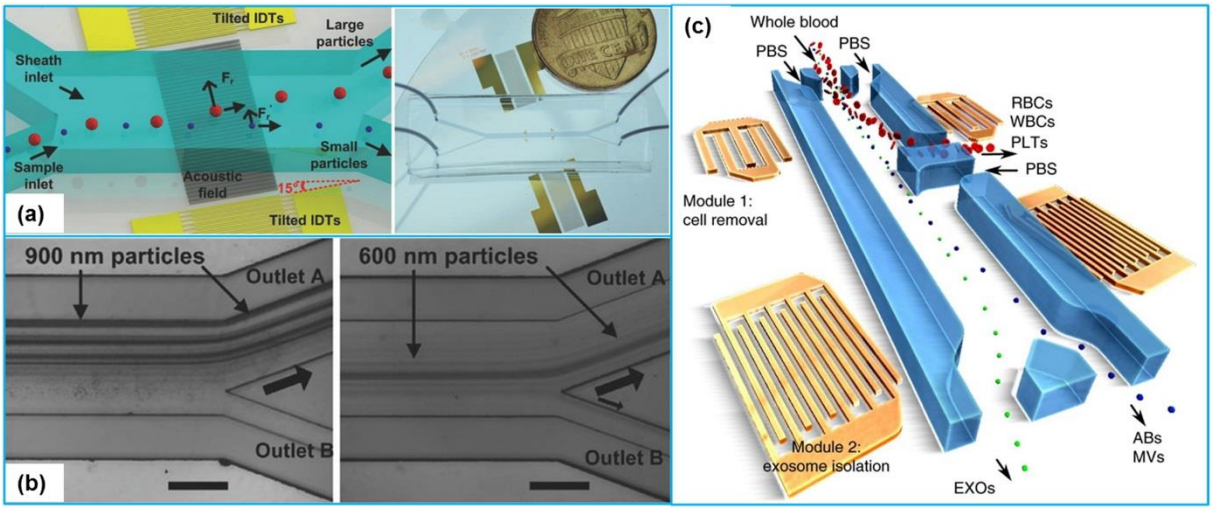

Figure 9. (a) Principle of the acoustic-based nanoparticle separation device. (b) A size-based filter generated by A tilted-angle SSAW acoustic field. (a) and (b) Reproduced with permission [173]. Copyright 2017, Wiley-VCH. (c) Schematic to show exosome isolation via standing-wave tweezers. Reproduced with permission [174]. Copyright 2017, National Academy of Sciences.

3.3. Nanoacoustic sensing

Over the past four decades, SAW devices have attracted increasing interest for sensor applications since the first SAW sensor was introduced by Wohltjen and Dessy in 1979 [175]. Since SAW devices are responsive to different types of perturbations on their surface, such as chemical, electrical, mechanical signals, it makes possible to use them as SAW sensors

[176,177]. The major advantages of SAW sensors involve compact size, superior response time, high sensitivity and low cost [178–180]. Additionally, they demonstrate outstanding linearity, selectivity and stability provided with appropriate design of sensing surfaces, IDTs and piezoelectric substrates [138,181].

3.3.1. Sensing principle

The SAW-based sensing depends on the variation of SAW propagation characteristics resulting from the interaction between SAWs and surface specimen [182]. The sensors based on SAW propagations are greatly sensitive to physical factors including pressure, stress, and temperature, as well as chemical and biological characteristics [179,183,184]. A SAW sensor is usually coated with a thin layer of selected material as sensing film such as metals or metal oxides (**Figure 10**) [185]. When the sensing layer exposes to the external molecules, the property of this layer such as mass, electrical or mechanical properties will be changed and accordingly the propagation of SAWs will be varied [186]. While many review articles have reported the SAW devices in chemical and biological sensing applications [179,183,185,187], none of the literature has reviewed the recent advances in nanoscale chemical and biological sensing.

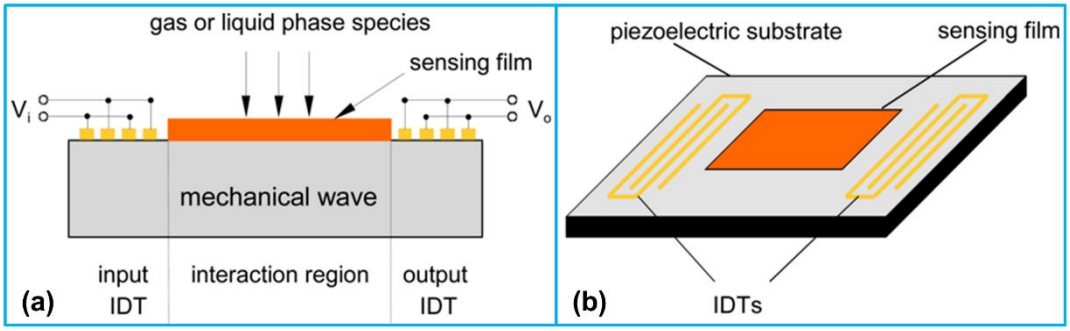

Figure 10. Schematic illustration of (a) structure and (b) IDT configuration for a SAW sensor. Reproduced with permission [188]. Copyright 2009, MDPI.

3.3.2. Chemical sensing

Over the past decade, sensing chemicals in gaseous phase has been reported by using SAW devices based on Rayleigh waves [138]. Due to its large surface area and unique electronic

properties, graphene has been adopted for fabricating SAW based chemical sensors. Arsat et al. [189] developed a 102 MHz SAW device for detecting H_2 and CO. The device was composed of 9 nm thick graphene-like nano-sheets deposited on the active area of 36° YX lithium tantalate ($LiTaO_3$) SAW transducer and 38 electrode pairs (IDT fingers) in both input and output IDTs. Raj et al. [190] developed a ZnO-coated one port SAW resonator for the detection of DMMP (dimethyl methyl phosphonate), a simulant of the chemical warfare agent Sarin at room temperature. The device worked at a center frequency of 433 MHz. With DMMP exposure, the frequency shift of the device was increased with the thickness of ZnO film. Luo et al. [191] reported a SAW sensor composed of nanocrystalline SnO_2 film for H_2S detection. The sensing principle of the device was based on the acoustoelectric effect due to the electrical conductivity variation of the SnO_2 film. The maximal response of the sensor (i.e., center frequency change) was 112.232 kHz when the sensor with a 275 nm thick SnO_2 film was operated at 120 °C.

3.3.3. Biosensing

A biosensor typically consists of a biologically active component (antibody or enzyme) confined on the surface of a transducer, which enables the detection of target component in a complex mixture [192]. Conventionally, the most widely used acoustic devices for biosensing are operated at thickness shear mode [193] that are classified as bulk acoustic wave devices and are found in quartz crystal microbalances (QCMs). However, biosensing based on SAW has been reported to be more sensitive than the typical QCM-based biosensors. Since the first SAW biosensor was successfully developed in 1987 [194], SAW devices have been widely employed as biosensors to discover proteins, viruses, DNA, and cells [195].

Lee et al. [196] reported a 200 MHz SH-SAW device as immunosensor for detecting cardiac markers including cardiac troponin (cTn), creatine kinase (CK), and myoglobin (Mb), in human serum (**Figure 11a**). Antibody and gold nanoparticle conjugation was utilized as

receptor, which was immobilized on the sensing area between two IDTs. They found that the propagation of SAWs was varied with the concentration of the conjugated antibodies. Baca et al. [197] developed a SAW biosensor for rapid detection of Ebola virus no need of sample processing and professional staff. Two different lanes consisting of antibodies were adopted on the surface of the biosensor: test lane with Ebola antibodies and reference lane with a control group (**Figure 11b**). The phase information of the SAWs was recorded and compared between these two lanes. It was found that there was a phase shift between these two lanes of antibodies. In addition, Cai et al. [198] utilized a 6.4 GHz SAW device working at third-order harmonic mode to detect DNA sequences. Due to the adopting of higher order mode, atomic sensing resolution could be achieved and single strands of DNA could be detected.

It is well known that ZnO has excellent piezoelectric properties and relatively high electromechanical coupling coefficient, which can be potentially integrated with a SAW device [199]. Moreover, ZnO nanostructures demonstrate both piezoelectric and semiconducting properties [200], which makes them as promising candidates for various applications. It has been reported that ZnO thin film is deposited on a silicone substrate to electroacoustically generate hypersonic waves in SAW devices [201]. Augustine et al. [202] reported a SAW biosensor for potentially detecting cell proliferation in a cell culture system. The biosensor was made by electrospinning P(VDF-TrFE) fibers with ZnO nanoparticles over the sensing area (**Figure 11c**). The insertion loss of the developed biosensor encompassed with ZnO nanoparticles was much less than that of the only P(VDF-TrFE) deposited device.

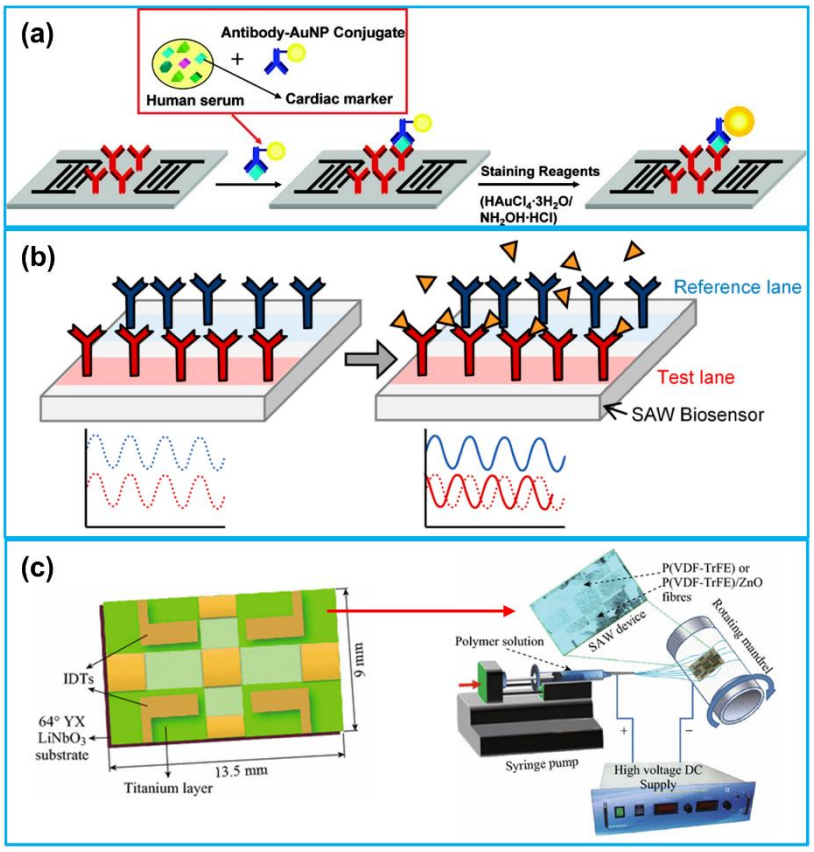

Figure 11. (a) Schematic of the sandwich immunoassay format utilized in combination with gold staining. Reproduced with permission [196]. Copyright 2011, American Chemical Society. (b) Principle of a SAW biosensor consisting of a test lane (red) and a reference lane (blue). Reproduced with permission [197]. Copyright 2015, MDPI. (c) Schematic of the SAW sensor composed of P(VDF-TrFE)/ZnO nanocomposites in the delay line area. Reproduced with permission [202]. Copyright 2016, Springer Nature.

3.3.4. Other nanoacoustic sensing

Besides SAW-based sensors, other types of acoustic sensors have also been reported. Gong et al. [203] developed a gold nanowire-based flexible pressure sensor which was fabricated by sandwiching gold nanowires between two thin PDMS sheets. The pressure sensor demonstrated low power consumption, high sensitivity, high stability, and fast response. The outstanding sensing properties along with the mechanical flexibility allowed the sensor to monitor heart rate (pulse) in real-time and detect tiny vibration forces from sound. Lang et al. [204] developed an acoustic sensor using PVDF nanofibers as a model polymer, which showed much higher sensitivity than the existing PVDF sensors. The developed sensor was especially sensitive to the sound waves in the low and middle frequency range, which made it

appropriate for loud noise monitoring. Recently, Peng et al. [49] reported an ultrasonic sensor composed of a flexible piezo-composite structure and silver nanowire-based stretchable electrodes for noninvasive and continuous blood pressure monitoring (**Figure 12a**). Compared with the measurement results using a commercial blood pressure monitor, the ultrasonic sensor demonstrated the capability to measure the blood pressure waveform accurately on a human's ulnar artery. Kim et al. [205] developed a stress sensing system consisting of a CSNP-PDMS composite-based laser ultrasound transmitter and an AlN piezoelectric receiver, placed in a semi-noncontact manner (**Figure 12b**). Subsurface longitudinal wave was generated by the transmitter and propagated parallel to the structural surface. The wave velocity would decrease linearly with the increase of the structural stress level according to the acoustoelastic effect.

More recently, for the first time, Shnaiderman et al. [206] developed a non-piezoelectric ultrasonic nanosensor (area 220 nm × 500 nm) with a dimension smaller than a blood cell for ultrasonic waves detection. Contrary to the commonly used piezoelectric sensors that the sensitivity is decreased with the reduction of the size, the submicrometer silicon waveguide–etalon detector (SWED) based on electro-optical technique can be miniaturized without sacrificing sensitivity. The SWED monitored the ultrasound-induced changes in light intensity propagating through the miniaturized photonic circuits, demonstrating an ultrabroad bandwidth of 230 MHz and a sensitivity orders of magnitude higher than that of piezoelectric sensors.

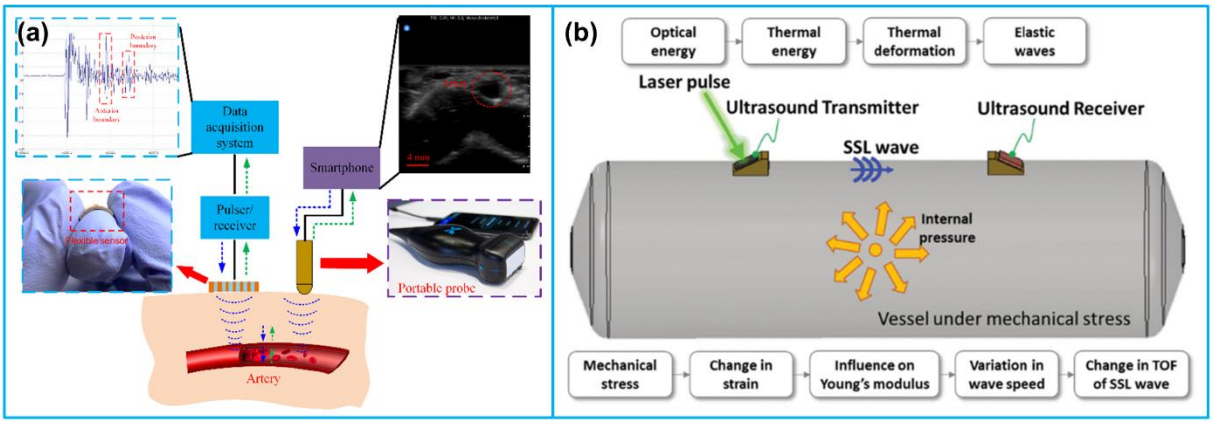

Figure 12. (a) Flexible ultrasonic sensor for blood pressure monitoring. Reproduced with permission [49]. Copyright 2021, IEEE. (b) Laser-generated ultrasound-based stress sensing. Reproduced with permission [205]. Copyright 2020, IEEE.

4. Conclusions and outlook

The field of nanoacoustics has been advancing remarkably over the past decade and continues to substantially expand its capabilities and refine its techniques. In this two-part review, for the first time, the recent progress in nanoacoustics was comprehensively presented. As part I of this two-part review, the recent advancement made in exploring nanomaterials and nanostructures for acoustics were reviewed including factors related to acoustic performance. Three different types of applications of nanoacoustics were summarized including material property characterization, nanomaterial/structure manipulation, and sensing, with special attention being paid to nanomaterials, nanostructures and nanodevice implementations. Despite the rapid progress and significant research achievements related to nanoacoustics, there are still many unsolved issues to be explored.

Compared with CB, CNTs, and CNFs, CSNPs produced higher photoacoustic conversion efficiencies due to their high surface area to volume ratio. While the CSNP approach has merits in terms of nanostructure, fabrication, and photoacoustic performance, there is still much to be explored about the performance limits including the maximum pressure output by high fluence excitation and the maximum peak negative pressure.

While acoustic nanomanipulation has demonstrated great potential for various applications including biomedicine and micro/nanofabrication, many issues remain to be explored in our understanding of the underlying principles of forming SAW inside microchannels. In addition, further investigations are necessary to expand our understanding of different phenomenon. The future development of acoustic nanomanipulation devices for practical application includes integrating devices for high precision and controllability.

Due to the inherent advantages of SAW-based sensing platforms, it is anticipated that the functionalization of SAW devices for increased selectivity will remain to be an active research area in the near future. Investigations focus on SAW-based sensing should continue exploration of novel sensing materials to advance performance levels and to broaden the applications. Moreover, one of the limitations of the current SAW-based sensors is that they require expensive electronic detection systems, such as network analyzers, to successfully record device behaviors. In the future, small, portable devices for data acquisition are needed that can be packaged into a highly integrated and cost-effective systems.

Declaration of competing interest

Xiaoning Jiang has a financial interest in SonoVascular, Inc., who licensed an intravascular sonothrombolysis technology from North Carolina State University.

Acknowledgments

The authors would like to acknowledge the financial support from the National Institutes of Health under the grants R01HL141967, R41HL154735, and R21EB027304; Office of Naval Research under the grant N00014-18-1-2538; and Department of Energy under the grant DE-NE0008708.

References

[1] K. Ng, Y. Liu, Therapeutic ultrasound: its application in drug delivery, Med. Res. Rev. 22 (2002) 204–223.

[2] R.C. Asher, Ultrasonic Sensors. Bristol and Philadelphia, (1997).

[3] V. Ciaravino, Biological Effects of Ultrasound: Mechanisms and Clinical Implications (NCRP Report No. 74), Med. Phys. 13 (1986) 424.

[4] K. Fellinger, J. Schmid, Klinik und Therapie des chronischen Gelenkrheumatismus, Verlag für Medizinische Wissenschaften, 1954.

[5] C.M. Rumack, D. Levine, Diagnostic ultrasound E-book, Elsevier Health Sciences, 2017.

[6] C. Peng, H.-W. Kim, T. Kim, X. Jiang, Blood volume flow measurement using a flexible ultrasound transducer (Conference Presentation), in: Heal. Monit. Struct. Biol. Syst. XIII, International Society for Optics and Photonics, 2019: p. 1097227.

[7] C. Peng, M. Chen, H.K. Sim, Y. Zhu, X. Jiang, Blood pressure measurement using a flexible piezo-composite ultrasonic transducer (Conference Presentation), in: Heal. Monit. Struct. Biol. Syst. IX, International Society for Optics and Photonics, 2020: p. 1138111.

[8] C. Peng, M. Chen, H.K. Sim, Y. Zhu, X. Jiang, A Flexible Piezo-Composite Ultrasound Blood Pressure Sensor with Silver Nanowire-based Stretchable Electrodes, in: 2020 IEEE 15th Int. Conf. Nano/Micro Eng. Mol. Syst., IEEE, 2020: pp. 143–146.

[9] Y. Zhuang, J. Li, Q. Hu, S. Han, W. Liu, C. Peng, Z. Li, L. Zhang, X. Wei, Z. Xu, Flexible composites with Ce-doped BaTiO3/P (VDF-TrFE) nanofibers for piezoelectric device, Compos. Sci. Technol. 200 (2020) 108386.

[10] S. Paliwal, S. Mitragotri, Ultrasound-induced cavitation: applications in drug and gene delivery, Expert Opin. Drug Deliv. 3 (2006) 713–726.

[11] S.B. Barnett, G.R. Ter Haar, M.C. Ziskin, H.-D. Rott, F.A. Duck, K. Maeda, International recommendations and guidelines for the safe use of diagnostic ultrasound in medicine, Ultrasound Med. Biol. 26 (2000) 355–366.

[12] D.L. Miller, N.B. Smith, M.R. Bailey, G.J. Czarnota, K. Hynynen, I.R.S. Makin, B.C. of the A.I. of U. in Medicine, Overview of therapeutic ultrasound applications and safety considerations, J. Ultrasound Med. 31 (2012) 623–634.

[13] X. Wang, Y. Gkanatsas, J. Palasubramaniam, J.D. Hohmann, Y.C. Chen, B. Lim, C.E. Hagemeyer, K. Peter, Thrombus-targeted theranostic microbubbles: a new technology towards concurrent rapid ultrasound diagnosis and bleeding-free fibrinolytic treatment of thrombosis, Theranostics. 6 (2016) 726.

[14] A.K.W. Wood, C.M. Sehgal, A review of low-intensity ultrasound for cancer therapy,

Ultrasound Med. Biol. 41 (2015) 905–928.

[15] V.F. Humphrey, Ultrasound and matter—Physical interactions, Prog. Biophys. Mol. Biol. 93 (2007) 195–211.

[16] C. Peng, S. Ravi, V.K. Patel, A.M. Momen, S. Moghaddam, Physics of direct-contact ultrasonic cloth drying process, Energy. 125 (2017). doi:10.1016/j.energy.2017.02.138.

[17] C. Peng, A.M. Momen, S. Moghaddam, An energy-efficient method for direct-contact ultrasonic cloth drying, Energy. 138 (2017). doi:10.1016/j.energy.2017.07.025.

[18] C. Peng, H. Lai, M.E. Orazem, S. Moghaddam, Microstructure of clay fabric in electrokinetic dewatering of phosphatic clay dispersions, Appl. Clay Sci. 158 (2018). doi:10.1016/j.clay.2018.03.020.

[19] C. Peng, S. Moghaddam, The Study of Fabric Drying Using Direct-Contact Ultrasonic Vibration, IntechOpen, 2019. doi:10.5772/intechopen.89424.

[20] C. Peng, Comment on the paper "Generation and reduction of bulk nanobubbles by ultrasonic irradiation" by Keiji Yasuda, Hodaka Matsushima, and Yoshiyuki Asakura, Chemical Engineering Science 195 (2019) 455–461, Chem. Eng. Sci. 207 (2019) 1364–1365.

[21] C. Peng, S. Moghaddam, Energy efficient piezoelectrically actuated transducer for direct-contact ultrasonic drying of fabrics, Dry. Technol. 38 (2020) 879–888.

[22] C. Peng, S. Moghaddam, Experimental Evaluation and Kinetic Analysis of Direct-Contact Ultrasonic Fabric Drying Process, J. Therm. Sci. Eng. Appl. 13 (2021).

[23] H.N. Banerjee, M. Verma, Application of nanotechnology in cancer, Technol. Cancer Res. Treat. 7 (2008) 149–154.

[24] A.G. Cuenca, H. Jiang, S.N. Hochwald, M. Delano, W.G. Cance, S.R. Grobmyer, Emerging implications of nanotechnology on cancer diagnostics and therapeutics, Cancer. 107 (2006) 459–466.

[25] O.C. Farokhzad, R. Langer, Nanomedicine: developing smarter therapeutic and diagnostic modalities, Adv. Drug Deliv. Rev. 58 (2006) 1456–1459.

[26] S. Nie, Y. Xing, G.J. Kim, J.W. Simons, Nanotechnology applications in cancer, Annu. Rev. Biomed. Eng. 9 (2007) 257–288.

[27] X. Wang, L. Yang, Z. Chen, D.M. Shin, Application of nanotechnology in cancer therapy and imaging, CA. Cancer J. Clin. 58 (2008) 97–110.

[28] J.A. Barreto, W. O'Malley, M. Kubeil, B. Graham, H. Stephan, L. Spiccia, Nanomaterials: applications in cancer imaging and therapy, Adv. Mater. 23 (2011)

H18–H40.

[29] J. Geng, W. Li, L.P. Smaga, N.R. Sottos, J. Chan, Damage-Responsive Microcapsules for Amplified Photoacoustic Detection of Microcracks in Polymers, Chem. Mater. 30 (2018) 2198–2202.

[30] G.S. Shekhawat, A.K. Srivastava, V.P. Dravid, O. Balogun, Thickness Resonance Acoustic Microscopy for Nanomechanical Subsurface Imaging, ACS Nano. 11 (2017) 6139–6145. doi:10.1021/acsnano.7b02170.

[31] X. Ding, Z. Peng, S.-C.S. Lin, M. Geri, S. Li, P. Li, Y. Chen, M. Dao, S. Suresh, T.J. Huang, Cell separation using tilted-angle standing surface acoustic waves, Proc. Natl. Acad. Sci. 111 (2014) 12992–12997.

[32] F.N. Diauudin, J.I.A. Rashid, V.F. Knight, W.M.Z.W. Yunus, K.K. Ong, N.A.M. Kasim, N.A. Halim, S.A.M. Noor, A review of current advances in the detection of organophosphorus chemical warfare agents based biosensor approaches, Sens. Bio-Sensing Res. 26 (2019) 100305.

[33] K. Siwawannapong, R. Zhang, H. Lei, Q. Jin, W. Tang, Z. Dong, R.-Y. Lai, Z. Liu, A. Kamkaew, L. Cheng, Ultra-small pyropheophorbide-a nanodots for near-infrared fluorescence/photoacoustic imaging-guided photodynamic therapy, Theranostics. 10 (2020) 62.

[34] B. Guo, J. Chen, N. Chen, E. Middha, S. Xu, Y. Pan, M. Wu, K. Li, C. Liu, B. Liu, High‐Resolution 3D NIR‐II Photoacoustic Imaging of Cerebral and Tumor Vasculatures Using Conjugated Polymer Nanoparticles as Contrast Agent, Adv. Mater. 31 (2019) 1808355.

[35] Y. Shen, Z. Pi, F. Yan, C.-K. Yeh, X. Zeng, X. Diao, Y. Hu, S. Chen, X. Chen, H. Zheng, Enhanced delivery of paclitaxel liposomes using focused ultrasound with microbubbles for treating nude mice bearing intracranial glioblastoma xenografts, Int. J. Nanomedicine. 12 (2017) 5613.

[36] X. Wu, Y. Suo, H. Shi, R. Liu, F. Wu, T. Wang, L. Ma, H. Liu, Z. Cheng, Deep-tissue Photothermal Therapy Using Laser Illumination at NIR-IIa Window, Nano-Micro Lett. 12 (2020) 38.

[37] X. Chen, J. Li, G. Zhang, Y. Shi, PZT nanoactive fiber composites for acoustic emission detection, Adv. Mater. 23 (2011) 3965–3969.

[38] B. Sun, X. Li, R. Zhao, H. Ji, J. Qiu, N. Zhang, D. He, C. Wang, Electrospun poly (vinylidene fluoride)-zinc oxide hierarchical composite fiber membrane as piezoelectric

acoustoelectric nanogenerator, J. Mater. Sci. 54 (2019) 2754–2762.

[39] X. Chen, S. Guo, J. Li, G. Zhang, M. Lu, Y. Shi, Flexible piezoelectric nanofiber composite membranes as high performance acoustic emission sensors, Sensors Actuators A Phys. 199 (2013) 372–378.

[40] C. Lang, J. Fang, H. Shao, X. Ding, T. Lin, High-sensitivity acoustic sensors from nanofibre webs, Nat. Commun. 7 (2016) 1–7. doi:10.1038/ncomms11108.

[41] Y. Shi, Piezoelectric Nanofibers and Their Applications in Energy Harvesting, (2019).

[42] T.R. Shrout, Z.P. Chang, N. Kim, S. Markgraf, Dielectric behavior of single crystals near the (1− X) Pb (Mg1/3Nb2/3) O3-(x) PbTiO3 morphotropic phase boundary, Ferroelectr. Lett. Sect. 12 (1990) 63–69.

[43] X. Zhao, B. Fang, H. Cao, Y. Guo, H. Luo, Dielectric and piezoelectric performance of PMN–PT single crystals with compositions around the MPB: influence of composition, poling field and crystal orientation, Mater. Sci. Eng. B. 96 (2002) 254–262.

[44] S. Zhang, F. Li, High performance ferroelectric relaxor-PbTiO3 single crystals: Status and perspective, J. Appl. Phys. 111 (2012) 2.

[45] W.-Y. Chang, W. Huang, A. Bagal, C.-H. Chang, J. Tian, P. Han, X. Jiang, Study on dielectric and piezoelectric properties of 0.7 Pb (Mg1/3Nb2/3) O3-0.3 PbTiO3 single crystal with nano-patterned composite electrode, J. Appl. Phys. 114 (2013) 114103.

[46] W.-Y. Chang, C.-C. Chung, Z. Yuan, C.-H. Chang, J. Tian, D. Viehland, J.-F. Li, J.L. Jones, X. Jiang, Patterned nano-domains in PMN-PT single crystals, Acta Mater. 143 (2018) 166–173.

[47] M. Gao, C. Luo, W.-Y. Chang, C.M. Leung, J. Tian, J. Li, X. Jiang, D. Viehland, Apparent phase stability and domain distribution of PMN-30PT single crystals with nanograted Au/MnOx electrodes, Acta Mater. 169 (2019) 28–35.

[48] C. Luo, W.-Y. Chang, M. Gao, C.-H. Chang, J. Li, D. Viehland, J. Tian, X. Jiang, Multi-layered domain morphology in relaxor single crystals with nano-patterned composite electrode, Acta Mater. 182 (2020) 10–17.

[49] C. Peng, M. Chen, H.K. Sim, Y. Zhu, X. Jiang, Noninvasive and Nonocclusive Blood Pressure Monitoring via a Flexible Piezo-Composite Ultrasonic Sensor, IEEE Sens. J. 21 (2020) 2642–2650.

[50] X. Jiang, T. Kim, Y. Zhu, Flexible Piezo-Composite Sensors and Transducers, (2020).

[51] T. Kim, Z. Cui, W.-Y. Chang, H.-W. Kim, Y. Zhu, X. Jiang, Flexible 1-3 Composite Ultrasound Transducers with Silver Nanowire-based Stretchable Electrodes, IEEE

Trans. Ind. Electron. (2019).

[52] C. Li, L. V. Wang, Photoacoustic tomography and sensing in biomedicine, Phys. Med. Biol. 54 (2010) 1–52. doi:10.1088/0031-9155/54/19/R01.Photoacoustic.

[53] D.A. Hutchins, Mechanisms of pulsed photoacoustic generation, Can. J. Phys. 64 (1986) 1247–1264.

[54] A.C. Tam, Applications of photoacoustic sensing techniques, Rev. Mod. Phys. 58 (1986) 381.

[55] R.M. White, Generation of Elastic Waves by Transient Elastic Heating, J. Appl. Phys. 34 (1963) 3559–3567. doi:10.1063/1.1729258.

[56] R.J. Dewhurst, D.A. Hutchins, S.B. Palmer, C.B. Scruby, Quantitative measurements of laser-generated acoustic waveforms, J. Appl. Phys. 53 (1982) 4064–4071.

[57] A. Korpel, R. Adler, B. Alpiner, Direct Observation of Optically Induced Generation and Amplication of Sound, Appl. Phys. Lett. 5 (1964) 86–88.

[58] P.H. Carr, Harmonic generation of microwave phonons by radiation pressure and by the phonon phonon interaction, IEEE Trans. Sonics Ultrason. 13 (1966) 103–108.

[59] X.L. Deán-Ben, S. Gottschalk, B. Mc Larney, S. Shoham, D. Razansky, Advanced optoacoustic methods for multiscale imaging of in vivo dynamics, Chem. Soc. Rev. 46 (2017) 2158–2198.

[60] J. Kim, H. Kim, W.-Y. Chang, W. Huang, X. Jiang, P.A. Dayton, Candle-Soot Carbon Nanoparticles in Photoacoustics: Advantages and Challenges for Laser Ultrasound Transmitters, IEEE Nanotechnol. Mag. 13 (2019) 13–28.

[61] G.C. Wetsel, Photothermal generation of thermoelastic waves in composite media, IEEE Trans. Ultrason. Ferroelectr. Freq. Control. 33 (1986) 450–461.

[62] F.A. McDonald, Practical quantitative theory of photoacoustic pulse generation, Appl. Phys. Lett. 54 (1989) 1504–1506.

[63] W. Chang, W. Huang, J. Kim, S. Li, X. Jiang, Candle soot nanoparticles-polydimethylsiloxane composites for laser ultrasound transducers, Appl. Phys. Lett. 107 (2015) 161903.

[64] Y. Hou, J.S. Kim, S. Ashkenazi, M. O'Donnell, L.J. Guo, Optical generation of high frequency ultrasound using a two dimensional array of gold nanoparticles, Proc. - IEEE Ultrason. Symp. 1 (2006) 401–404. doi:10.1109/ULTSYM.2006.113.

[65] T. Buma, M. Spisar, M.O. Donnell, A High-Frequency, 2-D Array Element Using Thermoelastic Expansion in PDMS, IEEE Trans. Ultrason. Ferroelectr. Freq. Control.

50 (2003) 1161–1176. doi:10.1109/TUFFC.2003.1235327.

[66] L. V Wang, Tutorial on photoacoustic microscopy and computed tomography, IEEE J. Sel. Top. Quantum Electron. 14 (2008) 171–179.

[67] R.J. Von Gutfeld, H.F. Budd, Laser-generated MHz elastic waves from metallic-liquid interfaces, Appl. Phys. Lett. 34 (1979) 617–619.

[68] T. Buma, M. Spisar, M. O'donnell, High-frequency ultrasound array element using thermoelastic expansion in an elastomeric film, Appl. Phys. Lett. 79 (2001) 548–550.

[69] B.Y. Hsieh, J. Kim, J. Zhu, S. Li, X. Zhang, X. Jiang, A laser ultrasound transducer using carbon nanofibers-polydimethylsiloxane composite thin film, Appl. Phys. Lett. 106 (2015) 1–5. doi:10.1063/1.4905659.

[70] Y. Hou, J.-S. Kim, S. Ashkenazi, M. O'Donnell, L.J. Guo, Optical generation of high frequency ultrasound using two-dimensional gold nanostructure, Appl. Phys. Lett. 89 (2006) 93901.

[71] N. Wu, Y. Tian, X. Zou, V. Silva, A. Chery, X. Wang, High-efficiency optical ultrasound generation using one-pot synthesized polydimethylsiloxane-gold nanoparticle nanocomposite, JOSA B. 29 (2012) 2016–2020.

[72] S. Hwan Lee, M. Park, J.J. Yoh, H. Song, E. Yun Jang, Y. Hyup Kim, S. Kang, Y. Seop Yoon, Reduced graphene oxide coated thin aluminum film as an optoacoustic transmitter for high pressure and high frequency ultrasound generation, Appl. Phys. Lett. 101 (2012) 241909.

[73] A.A. Karabutov, A.G. Kaptilniy, A.Y. Ivochkin, D.M. Ksenofontov, A.D. Trofimov, Optoacoustic study of laser-induced near-critical states of thin aluminum films, Moscow Univ. Phys. Bull. 68 (2013) 383–386.

[74] G. Yoo, Y. Park, P. Sang, H.W. Baac, J. Heo, High-frequency optoacoustic transmitter based on nanostructured germanium via metal-assisted chemical etching, Opt. Mater. Express. 6 (2016) 2567–2572.

[75] Y. Hou, S. Ashkenazi, S. Huang, M. O'Donnell, Improvements in optical generation of high-frequency ultrasound, IEEE Trans. Ultrason. Ferroelectr. Freq. Control. 54 (2007) 682–686.

[76] W. Huang, W.-Y. Chang, J. Kim, S. Li, S. Huang, X. Jiang, A novel laser ultrasound transducer using candle soot carbon nanoparticles, IEEE Trans. Nanotechnol. 15 (2016) 395–401.

[77] W.-Y. Chang, X.A. Zhang, J. Kim, W. Huang, A. Bagal, C.-H. Chang, T. Fang, H.F.

Wu, X. Jiang, Evaluation of photoacoustic transduction efficiency of candle soot nanocomposite transmitters, IEEE Trans. Nanotechnol. 17 (2018) 985–993.

[78] T. Kim, W.-Y. Chang, H. Kim, X. Jiang, Narrow band photoacoustic lamb wave generation for nondestructive testing using candle soot nanoparticle patches, Appl. Phys. Lett. 115 (2019) 102902.

[79] R.J. Colchester, C.A. Mosse, D.S. Bhachu, J.C. Bear, C.J. Carmalt, I.P. Parkin, B.E. Treeby, I. Papakonstantinou, A.E. Desjardins, Laser-generated ultrasound with optical fibres using functionalised carbon nanotube composite coatings, Appl. Phys. Lett. 104 (2014) 173502.

[80] B.-Y. Hsieh, J. Kim, J. Zhu, S. Li, X. Zhang, X. Jiang, A laser ultrasound transducer using carbon nanofibers–polydimethylsiloxane composite thin film, Appl. Phys. Lett. 106 (2015) 21902.

[81] J. Di, J. Kim, Q. Hu, X. Jiang, Z. Gu, Spatiotemporal drug delivery using laser-generated-focused ultrasound system, J. Control. Release. 220 (2015) 592–599. doi:10.1016/j.jconrel.2015.08.033.

[82] E.J. Alles, S. Noimark, E. Zhang, P.C. Beard, A.E. Desjardins, Pencil beam all-optical ultrasound imaging, Biomed. Opt. Express. 7 (2016) 3696–3704.

[83] H.W. Baac, J.G. Ok, A. Maxwell, K.-T. Lee, Y.-C. Chen, A.J. Hart, Z. Xu, E. Yoon, L.J. Guo, Carbon-nanotube optoacoustic lens for focused ultrasound generation and high-precision targeted therapy, Sci. Rep. 2 (2012) 989.

[84] H.W. Baac, T. Lee, L.J. Guo, Micro-ultrasonic cleaving of cell clusters by laser-generated focused ultrasound and its mechanisms, Biomed. Opt. Express. 4 (2013) 1442–1450.

[85] H.W. Baac, T. Lee, J.G. Ok, T. Hall, L. Jay Guo, Dual-frequency focused ultrasound using optoacoustic and piezoelectric transmitters for single-pulsed free-field cavitation in water, Appl. Phys. Lett. 103 (2013) 234103.

[86] T. Lee, W. Luo, Q. Li, H. Demirci, L.J. Guo, Laser‐Induced Focused Ultrasound for Cavitation Treatment: Toward High‐Precision Invisible Sonic Scalpel, Small. 13 (2017) 1701555.

[87] T. Lee, J.G. Ok, L.J. Guo, H.W. Baac, Low f-number photoacoustic lens for tight ultrasonic focusing and free-field micro-cavitation in water, Appl. Phys. Lett. 108 (2016) 104102.

[88] S. Noimark, R.J. Colchester, B.J. Blackburn, E.Z. Zhang, E.J. Alles, S. Ourselin, P.C. Beard, I. Papakonstantinou, I.P. Parkin, A.E. Desjardins, Carbon‐nanotube‐PDMS composite coatings on optical fibers for all‐optical ultrasound imaging, Adv. Funct. Mater. 26 (2016) 8390–8396.

[89] R.K. Poduval, S. Noimark, R.J. Colchester, T.J. Macdonald, I.P. Parkin, A.E. Desjardins, I. Papakonstantinou, Optical fiber ultrasound transmitter with electrospun carbon nanotube-polymer composite, Appl. Phys. Lett. 110 (2017) 223701.

[90] W. Chang, X.A. Zhang, J. Kim, W. Huang, A. Bagal, C. Chang, T. Fang, H.F. Wu, X. Jiang, Evaluation of Photoacoustic Transduction Efficiency of Candle Soot Nanocomposite Transmitters, IEEE Trans. Nanotechnol. 17 (2018) 985–993. doi:10.1109/TNANO.2018.2845703.

[91] Y. Li, Z. Guo, G. Li, S.-L. Chen, Miniature fiber-optic high-intensity focused ultrasound device using a candle soot nanoparticles-polydimethylsiloxane composites-coated photoacoustic lens, Opt. Express. 26 (2018) 21700–21711.

[92] H.K. Wickramasinghe, Scanning acoustic microscopy: a review, J. Microsc. 129 (1983) 63–73. doi:10.1016/0041-624X(93)90070-G.

[93] Z. Yu, S. Boseck, Scanning acoustic microscopy and its applications to material characterization, Rev. Mod. Phys. 67 (1995) 863.

[94] O. Balogun, G.D. Cole, R. Huber, D. Chinn, T.W. Murray, J.B. Spicer, High-spatial-resolution sub-surface imaging using a laser-based acoustic microscopy technique, IEEE Trans. Ultrason. Ferroelectr. Freq. Control. 58 (2011) 226–233. doi:10.1109/TUFFC.2011.1789.

[95] A. Briggs, Advances in acoustic microscopy, Springer Science & Business Media, 2013.

[96] F. Bertocci, A. Grandoni, T. Djuric-Rissner, Scanning Acoustic Microscopy (SAM): A Robust Method for Defect Detection during the Manufacturing Process of Ultrasound Probes for Medical Imaging, Sensors. 19 (2019) 4868.

[97] Y. Shan, H. Wang, The structure and function of cell membranes examined by atomic force microscopy and single-molecule force spectroscopy, Chem. Soc. Rev. 44 (2015) 3617–3638.

[98] R.J. da Fonseca, L. Ferdj‐Allah, G. Despaux, A. Boudour, L. Robert, J. Attal, Scanning Acoustic Microscopy-Recent Applications in Materials Science, Adv. Mater.

5 (1993) 508‑519.

[99] P. Ahn, Z. Zhang, C. Sun, O. Balogun, Ultrasonic near-field optical microscopy using a plasmonic nanofocusing probe, J. Appl. Phys. 113 (2013) 1–8. doi:10.1063/1.4810925.

[100] O. Kolosov, K. Yamanaka, Nonlinear detection of ultrasonic vibrations in an atomic force microscope, Jpn. J. Appl. Phys. 32 (1993) L1095.

[101] K. Yamanaka, H. Ogiso, O. Kolosov, Ultrasonic force microscopy for nanometer resolution subsurface imaging, Appl. Phys. Lett. 64 (1994) 178–180.

[102] E. Kester, U. Rabe, L. Presmanes, P. Tailhades, W. Arnold, Measurement of Young's modulus of nanocrystalline ferrites with spinel structures by atomic force acoustic microscopy, J. Phys. Chem. Solids. 61 (2000) 1275–1284.

[103] U. Rabe, S. Amelio, M. Kopycinska, S. Hirsekorn, M. Kempf, M. Göken, W. Arnold, Imaging and measurement of local mechanical material properties by atomic force acoustic microscopy, Surf. Interface Anal. An Int. J. Devoted to Dev. Appl. Tech. Anal. Surfaces, Interfaces Thin Film. 33 (2002) 65–70.

[104] S. Amelio, A. V Goldade, U. Rabe, V. Scherer, B. Bhushan, W. Arnold, Measurements of elastic properties of ultra-thin diamond-like carbon coatings using atomic force acoustic microscopy, Thin Solid Films. 392 (2001) 75–84.

[105] M. Prasad, M. Kopycinska, U. Rabe, W. Arnold, Measurement of Young's modulus of clay minerals using atomic force acoustic microscopy, Geophys. Res. Lett. 29 (2002) 13–1. doi:10.1029/2001gl014054.

[106] K. Yamanaka, H. Ogiso, O. Kolosov, Ultrasonic force microscopy for nanometer resolution subsurface imaging, Appl. Phys. Lett. 64 (1994) 178–180. doi:10.1063/1.111524.

[107] B.C. Daly, N.C.R. Holme, T. Buma, C. Branciard, T.B. Norris, D.M. Tennant, J.A. Taylor, J.E. Bower, S. Pau, Imaging nanostructures with coherent phonon pulses, Appl. Phys. Lett. 84 (2004) 5180–5182.

[108] C.J.K. Richardson, J.B. Spicer, Characterization of heat-treated tungsten thin films using picosecond duration thermoelastic transients, Opt. Lasers Eng. 40 (2003) 379–391.

[109] S. Ramanathan, D.G. Cahill, High-resolution picosecond acoustic microscopy for non-invasive characterization of buried interfaces, J. Mater. Res. 21 (2006) 1204–1208.

[110] K.-H. Lin, C.-T. Yu, S.-Z. Sun, H.-P. Chen, C.-C. Pan, J.-I. Chyi, S.-W. Huang, P.-C. Li, C.-K. Sun, Two-dimensional nanoultrasonic imaging by using acoustic nanowaves,

Appl. Phys. Lett. 89 (2006) 43106.

[111] P. Ahn, O. Balogun, Elastic characterization of nanoporous gold foams using laser based ultrasonics, Ultrasonics. 54 (2014) 795–800. doi:10.1016/j.ultras.2013.10.004.

[112] F.W. Zeng, J.B. Spicer, Nano-acoustic resonators for sensing near-particle environments in polymer matrix nanocomposites, in: 2017 IEEE 17th Int. Conf. Nanotechnology, NANO 2017, 2017: pp. 436–438. doi:10.1109/NANO.2017.8117414.

[113] J. Hu, Acoustic Micro/Nano Manipulations: An Editorial Review, Int. J. Radiol. 1 (2014) 1–3. doi:10.6051/j.issn.2313-3406.2014.01.3.

[114] A. Ashkin, Acceleration and trapping of particles by radiation pressure, Phys. Rev. Lett. 24 (1970) 156.

[115] A. Ashkin, Optical trapping and manipulation of neutral particles using lasers: a reprint volume with commentaries, World Scientific, 2006.

[116] M. Tanase, L.A. Bauer, A. Hultgren, D.M. Silevitch, L. Sun, D.H. Reich, P.C. Searson, G.J. Meyer, Magnetic alignment of fluorescent nanowires, Nano Lett. 1 (2001) 155–158.

[117] S.-W. Lee, M.-C. Jeong, J.-M. Myoung, G.-S. Chae, I.-J. Chung, Magnetic alignment of ZnO nanowires for optoelectronic device applications, Appl. Phys. Lett. 90 (2007) 133115.

[118] J. Castillo, M. Dimaki, W.E. Svendsen, Manipulation of biological samples using micro and nano techniques, Integr. Biol. 1 (2008) 30–42.

[119] K. Mølhave, T. Wich, A. Kortschack, P. Bøggild, Pick-and-place nanomanipulation using microfabricated grippers, Nanotechnology. 17 (2006) 2434.

[120] G. Sitters, D. Kamsma, G. Thalhammer, M. Ritsch-Marte, E.J.G. Peterman, G.J.L. Wuite, Acoustic force spectroscopy, Nat. Methods. 12 (2015) 47–50.

[121] J. Pihl, J. Sinclair, M. Karlsson, O. Orwar, Microfluidics for cell-based assays, Mater. Today. 8 (2005) 46–51.

[122] X. Chen, K.H. Lam, R. Chen, Z. Chen, X. Qian, J. Zhang, P. Yu, Q. Zhou, Acoustic levitation and manipulation by a high-frequency focused ring ultrasonic transducer, Appl. Phys. Lett. 114 (2019) 54103.

[123] J. Zhang, S. Yang, C. Chen, J.H. Hartman, P.-H. Huang, L. Wang, Z. Tian, P. Zhang, D. Faulkenberry, J.N. Meyer, Surface acoustic waves enable rotational manipulation of Caenorhabditis elegans, Lab Chip. 19 (2019) 984–992.

[124] X. Ding, S.S. Lin, B. Kiraly, H. Yue, S. Li, I. Chiang, J. Shi, S.J. Benkovic, T.J. Huang,

On-chip manipulation of single microparticles, cells, and organisms using surface acoustic waves, Proc. Natl. Acad. Sci. 109 (2012) 11105–11109. doi:10.1073/pnas.1209288109.

[125] Y. Qiu, H. Wang, C.E.M. Demore, D.A. Hughes, P. Glynne-Jones, S. Gebhardt, A. Bolhovitins, R. Poltarjonoks, K. Weijer, A. Schönecker, M. Hill, S. Cochran, Acoustic Devices for Particle and Cell Manipulation and Sensing, Sensors. 14 (2014) 14806–14838. doi:10.3390/s140814806.

[126] Z. Mao, P. Li, M. Wu, H. Bachman, N. Mesyngier, X. Guo, S. Liu, F. Costanzo, T.J. Huang, Enriching Nanoparticles via Acoustofluidics, ACS Nano. 11 (2017) 603–612. doi:10.1021/acsnano.6b06784.

[127] J. Greenhall, F. Guevara Vasquez, B. Raeymaekers, Continuous and unconstrained manipulation of micro-particles using phase-control of bulk acoustic waves, Appl. Phys. Lett. 103 (2013) 74103.

[128] M.D. Haslam, B. Raeymaekers, Aligning carbon nanotubes using bulk acoustic waves to reinforce polymer composites, Compos. Part B Eng. 60 (2014) 91–97.

[129] J. Greenhall, F. Guevara Vasquez, B. Raeymaekers, Dynamic behavior of microscale particles controlled by standing bulk acoustic waves, Appl. Phys. Lett. 105 (2014) 144105.

[130] S. Chaki, W. Harizi, G. Bourse, M. Ourak, Multi-technique approach for non destructive diagnostic of structural composite materials using bulk ultrasonic waves, guided waves, acoustic emission and infrared thermography, Compos. Part A Appl. Sci. Manuf. 78 (2015) 358–361.

[131] G.P. Gautam, Manipulation of Particles and Fluid Using Bulk Acoustic Waves in Microfluidics, (2019).

[132] Z. Hou, Z. Zhou, P. Liu, Y. Pei, Deformable oscillation of particles patterning by parametric bulk acoustic waves, Extrem. Mech. Lett. (2020) 100716.

[133] J. Shi, X. Mao, D. Ahmed, A. Colletti, T.J. Huang, Focusing microparticles in a microfluidic channel with standing surface acoustic waves (SSAW), Lab Chip. 8 (2008) 221–223.

[134] Z. Wang, J. Zhe, Recent advances in particle and droplet manipulation for lab-on-a-chip devices based on surface acoustic waves, Lab Chip. 11 (2011) 1280–1285. doi:10.1039/c0lc00527d.

[135] X. Ding, P. Li, S.S. Lin, Z.S. Stratton, N. Nama, F. Guo, D. Slotcavage, X. Mao, J. Shi,

F. Costanzo, T.J. Huang, Surface acoustic wave microfluidics, Lab Chip. 13 (2013) 3626–3649. doi:10.1039/c3lc50361e.

[136] M. Gedge, M. Hill, Acoustofluidics 17: Theory and applications of surface acoustic wave devices for particle manipulation, Lab Chip. 12 (2012) 2998–3007. doi:10.1039/c2lc40565b.

[137] J. Nam, H. Lim, S. Shin, Manipulation of microparticles using surface acoustic wave in microfluidic systems: a brief review, Korea-Australia Rheol. J. 23 (2011) 255–267. doi:10.1007/s13367-011-0031-5.

[138] J. Devkota, P.R. Ohodnicki, D.W. Greve, SAW sensors for chemical vapors and gases, Sensors (Switzerland). 17 (2017) 13–15. doi:10.3390/s17040801.

[139] W. Connacher, N. Zhang, A. Huang, J. Mei, S. Zhang, T. Gopesh, J. Friend, Micro/nano acoustofluidics: materials, phenomena, design, devices, and applications, Lab Chip. 18 (2018) 1952–1996. doi:10.1039/c8lc00112j.

[140] Y.Q. Fu, J.K. Luo, N.T. Nguyen, A.J. Walton, A.J. Flewitt, X.T. Zu, Y. Li, G. Mchale, A. Matthews, E. Iborra, H. Du, W.I. Milne, Advances in piezoelectric thin films for acoustic biosensors, acoustofluidics and lab-on-chip applications, Prog. Mater. Sci. 89 (2017) 31–91. doi:10.1016/j.pmatsci.2017.04.006.

[141] R.N. Thurston, A.D. Pierce, E.P. Papadakis, Reference for Modern Instrumentation, Techniques, and Technology: Ultrasonic Instruments and Devices I: Ultrasonic Instruments and Devices I, Academic Press, 1998.

[142] H. Wohltjen, Mechanism of operation and design considerations for surface acoustic wave device vapour sensors, Sensors and Actuators. 5 (1984) 307–325.

[143] A.J. Slobodnik, Surface acoustic waves and SAW materials, Proc. IEEE. 64 (1976) 581–595.

[144] S. V Biryukov, H. Schmidt, M. Weihnacht, Gyroscopic effect for SAW in common piezoelectric crystals, in: 2009 IEEE Int. Ultrason. Symp., IEEE, 2009: pp. 2133–2136.

[145] C.K. Campbell, Applications of surface acoustic and shallow bulk acoustic wave devices, Proc. IEEE. 77 (1989) 1453–1484.

[146] I. Ben Salah, M.H. Ben Ghozlen, Rayleigh waves in piezoelectric material, Phys. Procedia. 2 (2009) 1377–1383.

[147] C. Caliendo, Analysis of the acoustoelectric behavior of microwave frequency, temperature-compensated AlN-based multilayer coupling configurations, J. Appl. Phys. 104 (2008) 104509.

[148] A.J. Ricco, S.J. Martin, T.E. Zipperian, Surface acoustic wave gas sensor based on film conductivity changes, Sensors and Actuators. 8 (1985) 319–333.

[149] N. Naumenko, L. Solie, Optimal cuts of langasite, La/sub 3/Ga/sub 5/SiO/sub 14/for SAW devices, Ieee Trans. Ultrason. Ferroelectr. Freq. Control. 48 (2001) 530–537.

[150] G. Destgeer, H.J. Sung, Recent advances in microfluidic actuation and micro-object manipulation via surface acoustic waves, Lab Chip. 15 (2015) 2722–2738. doi:10.1039/C5LC00265F.

[151] L.Y. Yeo, J.R. Friend, Surface Acoustic Wave Microfluidics, Annu. Rev. Fluid Mech. 46 (2014) 379–406. doi:10.1146/annurev-fluid-010313-141418.

[152] T. Laurell, A. Lenshof, Microscale Acoustofluidics, Royal Society of Chemistry, 2014.

[153] J. Friend, L.Y. Yeo, Microscale acoustofluidics: Microfluidics driven via acoustics and ultrasonics, Rev. Mod. Phys. 83 (2011) 647. doi:10.1103/RevModPhys.83.647.

[154] A.H. Lefebvre, V.G. McDonell, Atomization and sprays, CRC press, 2017.

[155] M. Kurosawa, T. Watanabe, A. Futami, T. Higuchi, Surface acoustic wave atomizer, Sensors and Actuators-A-Physical Sensors. 50 (1995) 69–74.

[156] M. Alvarez, J. Friend, L.Y. Yeo, Rapid generation of protein aerosols and nanoparticles via surface acoustic wave atomization, Nanotechnology. 19 (2008) 455103.

[157] J.R. Friend, L.Y. Yeo, D.R. Arifin, A. Mechler, Evaporative self-assembly assisted synthesis of polymeric nanoparticles by surface acoustic wave atomization, Nanotechnology. 19 (2008) 145301.

[158] D.J. Collins, Z. Ma, J. Han, Y. Ai, Continuous micro-vortex-based nanoparticle manipulation via focused surface acoustic waves, Lab Chip. 17 (2017) 91–103. doi:10.1039/c6lc01142j.

[159] L. Ren, D. Zhou, Z. Mao, P. Xu, T.J. Huang, T.E. Mallouk, Rheotaxis of Bimetallic Micromotors Driven by Chemical–Acoustic Hybrid Power, ACS Nano. 11 (2017) 10591–10598. doi:10.1021/acsnano.7b06107.

[160] R.H. Baughman, A.A. Zakhidov, W.A. De Heer, Carbon nanotubes--the route toward applications, Science (80-.). 297 (2002) 787–792.

[161] C.J. Strobl, C. Schäflein, U. Beierlein, J. Ebbecke, A. Wixforth, Carbon nanotube alignment by surface acoustic waves, Appl. Phys. Lett. 85 (2004) 1427–1429.

[162] T. Smorodin, U. Beierlein, J. Ebbecke, A. Wixforth, Surface‐Acoustic‐Wave‐Enhanced Alignment of Thiolated Carbon Nanotubes on Gold Electrodes, Small. 1 (2005) 1188‐1190.

[163] K.M. Seemann, J. Ebbecke, A. Wixforth, Alignment of carbon nanotubes on pre-structured silicon by surface acoustic waves, Nanotechnology. 17 (2006) 4529.

[164] J. Shi, H. Huang, Z. Stratton, Y. Huang, T.J. Huang, Continuous particle separation in a microfluidic channel via standing surface acoustic waves (SSAW), Lab Chip. 9 (2009) 3354–3359.

[165] J. Shi, D. Ahmed, X. Mao, S.-C.S. Lin, A. Lawit, T.J. Huang, Acoustic tweezers: patterning cells and microparticles using standing surface acoustic waves (SSAW), Lab Chip. 9 (2009) 2890–2895.

[166] A. Ozcelik, J. Rufo, F. Guo, Y. Gu, P. Li, J. Lata, T.J. Huang, Acoustic tweezers for the life sciences, Nat. Methods. 15 (2018) 1021–1028.

[167] L. Meng, F. Cai, F. Li, W. Zhou, L. Niu, H. Zheng, Acoustic tweezers, J. Phys. D. Appl. Phys. 52 (2019) 273001.

[168] M. Baudoin, J.-L. Thomas, Acoustic tweezers for particle and fluid micromanipulation, Annu. Rev. Fluid Mech. 52 (2019).

[169] A. Marzo, B.W. Drinkwater, Holographic acoustic tweezers, Proc. Natl. Acad. Sci. 116 (2019) 84–89.

[170] L.P. Gor'kov, Forces acting on a small particle in an acoustic field within an ideal fluid, in: Dokl. Akad. Nauk, Russian Academy of Sciences, 1961: pp. 88–91.

[171] J. Shi, Y.B. Zheng, T.J. Huang, Surface Acoustic Wave-Driven Active Plasmonics based on Dynamic Patterning of Nanoparticles in Microfluidic Channels, in: IEEE 22nd Int. Conf. Micro Electro Mech. Syst., 2009: pp. 332–335.

[172] Y. Chen, X. Ding, S.S. Lin, S. Yang, P. Huang, N. Nama, Y. Zhao, A.A. Nawaz, F. Guo, L. Wang, T.J. Huang, Aligning Nanowires by Standing Surface Acoustic Waves, in: Int. MicroTAS 2012, 2012: pp. 1309–1311.

[173] M. Wu, Z. Mao, K. Chen, H. Bachman, Y. Chen, J. Rufo, L. Ren, P. Li, L. Wang, T.J. Huang, Acoustic Separation of Nanoparticles in Continuous Flow, Adv. Funct. Mater. 27 (2017) 1606039. doi:10.1002/adfm.201606039.

[174] M. Wu, Y. Ouyang, Z. Wang, R. Zhang, P.-H. Huang, C. Chen, H. Li, P. Li, D. Quinn, M. Dao, Isolation of exosomes from whole blood by integrating acoustics and microfluidics, Proc. Natl. Acad. Sci. 114 (2017) 10584–10589.

[175] H. Wohltjen, R. Dessy, Surface acoustic wave probe for chemical analysis. I. Introduction and instrument description, Anal. Chem. 51 (1979) 1458–1464.

[176] F.R.R. Teles, L.P. Fonseca, Trends in DNA biosensors, Talanta. 77 (2008) 606–623.

[177] Y.Q. Fu, J.K. Luo, N.T. Nguyen, A.J. Walton, A.J. Flewitt, X.T. Zu, Y. Li, G. McHale, A. Matthews, E. Iborra, H. Du, W.I. Milne, Advances in piezoelectric thin films for acoustic biosensors, acoustofluidics and lab-on-chip applications, Prog. Mater. Sci. 89 (2017) 31–91. doi:10.1016/j.pmatsci.2017.04.006.

[178] Z.P. Khlebarov, A.I. Stoyanova, D.I. Topalova, Surface acoustic wave gas sensors, Sensors Actuators B Chem. 8 (1992) 33–40.

[179] L. Bo, C. Xiao, C. Hualin, M.A. Mohammad, T. Xiangguang, T. Luqi, Y. Yi, R. Tianling, Surface acoustic wave devices for sensor applications, J. Semicond. 37 (2016) 21001.

[180] Z. Awang, Gas sensors: a review, Sens. Transducers. 168 (2014) 61–75.

[181] C. Caliendo, P. Verardi, E. Verona, A. D'Amico, C. Di Natale, G. Saggio, M. Serafini, R. Paolesse, S.E. Huq, Advances in SAW-based gas sensors, Smart Mater. Struct. 6 (1997) 689.

[182] S. Shiokawa, J. Kondoh, Surface acoustic wave sensors, Jpn. J. Appl. Phys. 43 (2004) 2799–2802.

[183] W.P. Jakubik, Surface acoustic wave-based gas sensors, Thin Solid Films. 520 (2011) 986–993.

[184] R.B. Priya, T. Venkatesan, G. Pandiyarajan, H.M. Pandya, A short review of saw sensors, J. Environ. Nanotechnol. 4 (2015) 15–22.

[185] A. Afzal, N. Iqbal, A. Mujahid, R. Schirhagl, Advanced vapor recognition materials for selective and fast responsive surface acoustic wave sensors: A review, Anal. Chim. Acta. 787 (2013) 36–49.

[186] J.D.N. Cheeke, Z. Wang, Acoustic wave gas sensors, Sensors Actuators B Chem. 59 (1999) 146–153.

[187] L.M. Dorozhkin, I.A. Rozanov, Acoustic wave chemical sensors for gases, J. Anal. Chem. 56 (2001) 399–416.

[188] M.I. Rocha-Gaso, C. March-Iborra, Á. Montoya-Baides, A. Arnau-Vives, Surface generated acoustic wave biosensors for the detection of pathogens: A review, Sensors. 9 (2009) 5740–5769. doi:10.3390/s9095740.

[189] R. Arsat, M. Breedon, M. Shafiei, P.G. Spizziri, S. Gilje, R.B. Kaner, K. Kalantar-zadeh, W. Wlodarski, Graphene-like nano-sheets for surface acoustic wave gas sensor applications, Chem. Phys. Lett. 467 (2009) 344–347. doi:10.1016/j.cplett.2008.11.039.

[190] V. Bhasker Raj, M. Tomar, A.T. Nimal, Y. Parmar, M.U. Sharma, V. Gupta, ZnO

surface acoustic wave sensor for the enhanced detection of DMMP, in: Solid State Phenom., Trans Tech Publ, 2012: pp. 69–72.

[191] W. Luo, Q. Fu, D. Zhou, J. Deng, H. Liu, G. Yan, A surface acoustic wave H2S gas sensor employing nanocrystalline SnO2 thin film, Sensors Actuators B Chem. 176 (2013) 746–752.

[192] A. Montoya, A. Ocampo, C. March, Fundamentals of piezoelectric immunosensors, in: Piezoelectric Transducers Appl., Springer, 2009: pp. 289–306.

[193] H. Yatsuda, T. Kogai, 3F-3 Liquid sensor using SAW and SH-SAW on quartz, in: 2006 IEEE Ultrason. Symp., IEEE, 2006: pp. 552–555.

[194] C.A. Flory, R.L. Baer, Surface transverse wave mode analysis and coupling to interdigital transducers, in: IEEE 1987 Ultrason. Symp., IEEE, 1987: pp. 313–318.

[195] J.W. Grate, G.C. Frye, Acoustic wave sensors, Sensors Updat. 2 (1996) 37–83.

[196] J. Lee, Y.-S. Choi, Y. Lee, H.J. Lee, J.N. Lee, S.K. Kim, K.Y. Han, E.C. Cho, J.C. Park, S.S. Lee, Sensitive and simultaneous detection of cardiac markers in human serum using surface acoustic wave immunosensor, Anal. Chem. 83 (2011) 8629–8635.

[197] J. Baca, V. Severns, D. Lovato, D. Branch, R. Larson, Rapid detection of Ebola virus with a reagent-free, point-of-care biosensor, Sensors. 15 (2015) 8605–8614.

[198] H.-L. Cai, Y. Yang, X. Chen, M.A. Mohammad, T.-X. Ye, C.-R. Guo, L.-T. Yi, C.-J. Zhou, J. Liu, T.-L. Ren, A third-order mode high frequency biosensor with atomic resolution, Biosens. Bioelectron. 71 (2015) 261–268.

[199] X.Y. Du, Y.Q. Fu, S.C. Tan, J.K. Luo, A.J. Flewitt, S. Maeng, S.H. Kim, Y.J. Choi, D.S. Lee, N.M. Park, ZnO film for application in surface acoustic wave device, in: J. Phys. Conf. Ser., IOP Publishing, 2007: p. 12035.

[200] A. Sirelkhatim, S. Mahmud, A. Seeni, N.H.M. Kaus, L.C. Ann, S.K.M. Bakhori, H. Hasan, D. Mohamad, Review on zinc oxide nanoparticles: antibacterial activity and toxicity mechanism, Nano-Micro Lett. 7 (2015) 219–242.

[201] L. Le Brizoual, J.K. Krueger, O. Elmazria, B. Vincent, L. Bouvot, M. Kolle, D. Rouxel, P. Alnot, Mapping of microwave-induced phonons by μ-Brillouin spectroscopy: hypersons in ZnO on silicon, J. Phys. D. Appl. Phys. 41 (2008) 105502.

[202] R. Augustine, F. Sarry, N. Kalarikkal, S. Thomas, L. Badie, D. Rouxel, Surface acoustic wave device with reduced insertion loss by electrospinning P (VDF–TrFE)/ZnO nanocomposites, Nano-Micro Lett. 8 (2016) 282–290.

[203] S. Gong, W. Schwalb, Y. Wang, Y. Chen, Y. Tang, J. Si, B. Shirinzadeh, W. Cheng, A

wearable and highly sensitive pressure sensor with ultrathin gold nanowires, Nat. Commun. 5 (2014) 3132.

[204] C. Lang, J. Fang, H. Shao, X. Ding, T. Lin, High-sensitivity acoustic sensors from nanofibre webs, Nat. Commun. 7 (2016) 11108.

[205] H. Kim, W.-Y. Chang, T. Kim, X. Jiang, Stress Sensing Method via Laser-Generated Ultrasound Wave Using Candle Soot Nanoparticle Composite, IEEE Trans. Ultrason. Ferroelectr. Freq. Control. (2020).

[206] R. Shnaiderman, G. Wissmeyer, O. Ülgen, Q. Mustafa, A. Chmyrov, V. Ntziachristos, A submicrometre silicon-on-insulator resonator for ultrasound detection, Nature. 585 (2020) 372–378.

Acoustics at the nanoscale (nanoacoustics): A comprehensive literature review.

Part II: Nanoacoustics for biomedical imaging and therapy

Chang Peng[a], Mengyue Chen[a], James B. Spicer[b], and Xiaoning Jiang[a,*]

[a] *Department of Mechanical and Aerospace Engineering, North Carolina State University, Raleigh, NC 27695, USA*

[b] *Department of Materials Science and Engineering, The Johns Hopkins University, 3400 North Charles Street, Baltimore, MD 21218, USA*

** Corresponding author: xjiang5@ncsu.edu (Xiaoning Jiang).*

Abstract

In the past decade, acoustics at the nanoscale (i.e., nanoacoustics) has evolved rapidly with continuous and substantial expansion of capabilities and refinement of techniques. Motivated by research innovations in the last decade, for the first time, recent advancements of acoustics-associated nanomaterials/nanostructures and nanodevices for different applications are outlined in this comprehensive review, which is written in two parts. As part II of this two-part review, this paper concentrates on nanoacoustics in biomedical imaging and therapy applications, including molecular ultrasound imaging, photoacoustic imaging, ultrasound-mediated drug delivery and therapy, and photoacoustic drug delivery and therapy. Firstly, the recent developments of nanosized ultrasound and photoacoustic contrast agents as well as their various imaging applications are examined. Secondly, different types of nanomaterials/nanostructures as nanocarriers for ultrasound and photoacoustic therapies are discussed. Finally, a discussion of challenges and future research directions are provided for nanoacoustics in medical imaging and therapy.

Keywords: acoustics, nanotechnology, nanoacoustics, nanomaterials, biomedical applications, imaging, therapy, photoacoustics, laser ultrasound, sonothrombolysis

Contents

1. Introduction 2
2. Nanoacoustics for biomedical imaging 3
2.1. Molecular ultrasound imaging 3
2.1.1. Contrast enhanced ultrasound imaging 4
2.1.2. Organic and inorganic nanosized UCAs 6
2.1.3. Biogenic gas vesicles 9
2.2. Photoacoustic (PA) imaging 11
2.2.1. Principle of PA imaging 11
2.2.2. Organic and inorganic nanosized contrast agents 12
3. Nanoacoustics for medical therapy 19
3.1. Ultrasonic drug delivery 19
3.1.1. Nanocarriers for ultrasonic drug delivery 20
3.2. Ultrasound therapy 25
3.2.1. Ultrasound-triggered therapy 25
3.2.2. Nanoparticle-mediated sonothrombolysis 27
3.3. Photoacoustic drug delivery and therapy 30
3.3.1. Organic nanocarriers 30
3.3.2. Inorganic nanocarriers 32
3.3.3. Laser-generated ultrasound-accelerated thrombolysis 36
4. Conclusions and outlook 37
Declaration of competing interest 38
Acknowledgments 38
References 39

1. Introduction

The breakthroughs and advances in nanotechnology have provided various nanoscaled materials and devices with extraordinary characteristics for ultrasound investigations [1–5]. In many ways, the combination of nanotechnology with ultrasonics has revolutionized conventional approaches to use ultrasound. The emergence of different nanomaterials for the

support of diagnosis and treatment of various types of diseases has attracted increasingly more attention in past decades and has now become an important field of medical ultrasound. Motivated by the research innovations over the last decade, this paper, as part II of the two-part review of nanoacoustics, will concentrate on the nanoacoustics in biomedical imaging and therapy fields, including molecular ultrasound imaging, photoacoustic imaging, ultrasound-mediated drug delivery and therapy, and photoacoustic drug delivery and therapy. In the following sections, the review proceeds as follows: in Section 2, different kinds of nanomaterials and nanostructures to be adopted as contrast agents for biomolecular ultrasound imaging and photoacoustic imaging applications will be examined in detail. In Section 3, various types of nanomaterials and nanostructures to be utilized as nanocarriers for ultrasound-mediated drug delivery and therapy as well as photoacoustic drug delivery and therapy applications will be reviewed. The last section (Section 4) provides a summary and outlook for the nanoacoustic research in these fields.

2. Nanoacoustics for biomedical imaging

2.1. Molecular ultrasound imaging

Ultrasound imaging has been a popular medical imaging technique for decades, and is now the second most implemented imaging modality in clinical practice after X-ray radiography [6]. It has been widely utilized by physicians in diverse fields, including obstetrics and gynecology (OB-GYN), cardiology, radiology, as well as gastroenterology [7–11]. Compared with other imaging modalities, such as computed tomography (CT), magnetic resonance imaging (MRI), and photoacoustic (PA) imaging, ultrasound imaging shows the advantages, such as lack of ionizing radiation, high resolution, and low cost [12].

Due to the different acoustic properties of tissues and organs, ultrasound images can be generated while ultrasonic waves propagates through them [13–15]. The generation of images by ultrasound is based on the pulse-echo principle. A short pulse of ultrasonic waves

generated by an ultrasonic transducer are transmitted into issues. A short time later, the echo pulses that are reflected from the tissue and organ interface are received by the same transducer or by a different transducer and are converted into electrical signals which are then utilized to generate a grayscale image displayed on the monitor, indicating the structure information. The depth of ultrasound image depends on the time between the transmitted pulse and the received echo. The echo amplitude is digitized and illustrated in the ultrasound image.

2.1.1. Contrast enhanced ultrasound imaging

Over the last few years, molecular ultrasound imaging, combining ultrasound technique with novel molecularly targeted contrast agents, has turned out to be a promising imaging technique for studying biological processes at the molecular level [16]. Microbubbles are by far the most commonly utilized ultrasound contrast agents (UCAs) owing to their widespread approval. They are composed of a gas core surrounded by a shell and usually 1-5 μm in size [17]. The gas core can generate a strong echogenic response which leads to a high contrast ratio on ultrasound images. The gas compositions usually applied in the gas core include air, nitrogen, and biologically-inert gases such as perfluoropropane, perfluorobutane, perfluorohexane, or sulfur hexafluoride (**Figure 1a**) [18]. The shell is utilized to prevent both gas leakage and stabilize microbubbles. The shell materials mainly consist of phospholipid, albumin and biocompatible polymers.

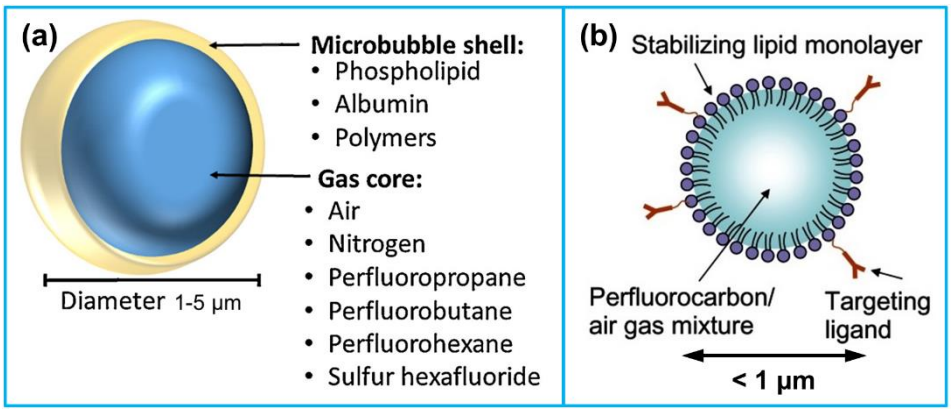

Figure 1. (a) Structure of a microbubble. Reproduced with permission [16]. Copyright 2015, Elsevier. (b) Composition of a nanosized ultrasound contrast agent. Reproduced with permission [19]. Copyright 2013, Dove Medical Press Ltd.

The bubble resonant frequency is the main parameter indicating the contrast efficiency. According to the small amplitude expansion of the Raleigh-Plesset equation, a nonlinear equation for describing oscillation of a spherical gas bubble in a liquid medium, the bubble resonant frequency is given by **Equation 1** [20]:

$$f_0 = \frac{1}{2\pi R_0}\sqrt{\frac{1}{\rho_L}\left[3\gamma P_0 + \frac{2(3\gamma-1)\sigma}{R_0} + \frac{4\chi}{R_0}\right]} \quad (1)$$

Where f_0 denotes the resonant frequency of a bubble, R_0 denotes the bubble radius, ρ_L denotes the density of surrounding liquid, γ denotes ratio of the specific heat of the gas inside the bubble, P_0 denotes the liquid pressure, σ denotes the surface tension at the gas-liquid interface, and χ denotes the shell elasticity.

While there has been numerous diagnostic applications in clinical radiology and cardiology using microbubbles combined with ultrasound, microbubbles cannot extravasate into the tissue and therefore cannot be utilized as extravascular contrast agents due to their relatively large size. In order to exploring the extravascular space, smaller, submicron UCAs have showed widespread interest, especially in the field of oncology [12]. Submicron UCAs are so small that can extravasate through the leaky cancerous vasculature into interstitium, which is promising for the clinical applications such as highlighting lesion locations and delivering a payload of drugs [21–23]. Nevertheless, according to **Equation 1**, the bubble size is inversely related with the bubble resonant frequency. The higher ultrasound frequency is required for acoustic signal detection in case of the smaller bubble size. Likewise, improving shell stiffness will also lead to a higher bubble resonant frequency.

In addition, reducing the bubble size into nanoscale will not only lower its echogenicity in ultrasound examination, but decrease its stability in solution as well. The bubble stability is closely related with the Laplace pressure [24], as given by **Equation 2**:

$$\Delta P = (P_b - P_a) = \frac{2\sigma}{R} \quad (2)$$

Where ΔP is the Laplace pressure, P_b is the total pressure in bubble, P_a is the ambient pressure outside of bubble. Reducing the bubble radius (R) will result in an increase of the Laplace pressure (ΔP), which will decrease the bubble stability. In order to increase the nanobubble stability, surfactants or lipids are usually bonded to the surface of nanobubbles to serve as elastic shells counteracting the effect of surface tension. Moreover, the choice of the gas core in a nanobubble is crucial to its stability as well. The application of a perfluorocarbon gas core rather than gas compositions commonly used in microbubbles, such as air, nitrogen and sulfur hexafluoride, can largely reduce the bubble dissolution time owing to its low solubility in the blood (**Figure 1b**).

2.1.2. Organic and inorganic nanosized UCAs

A variety of nanosized UCAs have been developed and reported by many researchers, which offers a paradigm shift of contrast enhanced ultrasound in both medical diagnostics and therapeutics [25–28]. Such agents are chemical-based agents that are produced by organic (**Figure 2a-c**) or inorganic materials (**Figure 2d**) [29]. The applications of these agents as ultrasound molecular imaging contrast agents will be examined, while many of them can also be utilized theranostic agents that provide the combination of diagnostics and therapeutics in a single nanoscale agent. The reported organic and inorganic nanosized UCAs and their applications are presented in **Table 1** and **Table 2**, respectively [29].

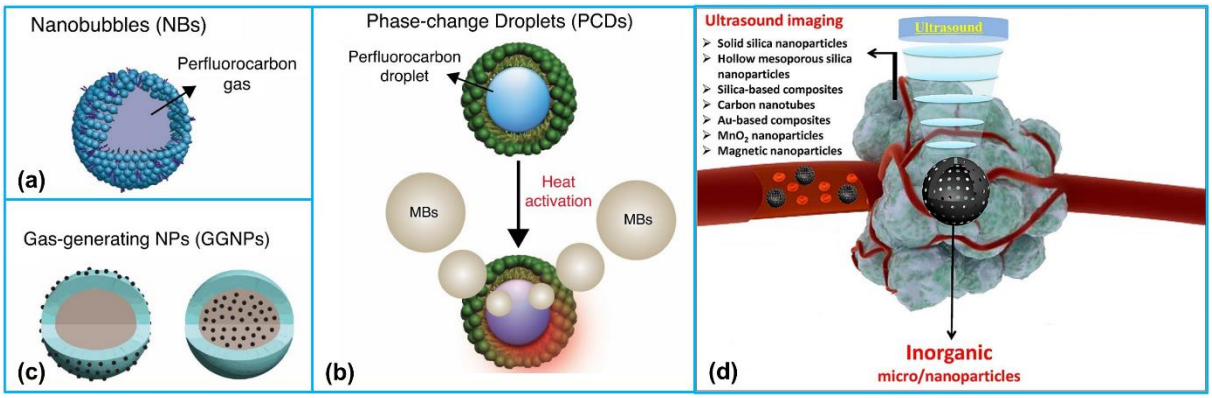

Figure 2. Schematic representation of organic and inorganic nanosized UCAs for ultrasound imaging. Organic UCAs: (a) nanobubbles, (b) phase-change droplets, and (c) gas-generating nanoparticles. (a)-(c) Reproduced with permission [29]. Copyright 2018, Elsevier. (d) The summary of inorganic nanoparticles. Reproduced with permission [30]. Copyright 2017, Elsevier.

Table 1. Summary of organic nanosized UCAs for ultrasound imaging applications.

Organic nano sized UCAs	Composition	Diameter	Cytotoxicity	Applications
Nanobubbles (NBs)	NB-affibody conjugates [31]	478.2 ± 29.7 nm	No distinct cytotoxicity	Molecular ultrasound imaging of tumor
	Anti-PSMA nanobody coated nanobubbles [32]	487.60 ± 33.55 nm	N/A	Prostate cancer-targeted imaging
	Herceptin-targeted nanobubbles [33]	613.0 ± 25.4 nm	Low cytotoxicity	Diagnosis and treatment of Her-2-positive breast cancers
	CA-125 antibody-conjugated nanobubbles [34]	74.6 ± 16.7 nm	No recognizable cytotoxicity	Diagnosis of ovarian cancer
	Crosslinked pluronic-lipid-perfluorocarbon nanobubbles [35]	95.2 ± 25.2 nm	N/A	Tumor detection
Phase-change nanodroplets	Liquid core of perfluorooctyl bromide liposome conjugated with folic acid and polyethylene glycol [36]	301 ± 10.8 nm	N/A	Diagnosis of folate receptor (FR)-overexpressing tumors
	Phase changeable perfluoropentane nanodroplets [37]	321 ± 67 nm	N/A	tumor-targeted ultrasound imaging
	Diatrizoic acid conjugated glycol chitosan nanoparticles [38]	454.9 ± 3.33 nm	Having potential toxicity	Tumor diagnosis
	Oleic-acid-coated Fe_3O_4 nanoparticles [39]	294 nm	No appreciable toxicity	Tumor imaging and therapy
	Liquid perfluorohexane core encapsulated by a fluorosurfactant polymer shell [40]	180 nm	N/A	Molecular ultrasound imaging of tumor
	Perfluorohexane and carbon nanoparticles encapsulated by PLGA [41]	435.9 ± 41.31 nm	Low cytotoxicity	Sentinel lymph nodes detection and therapy of lymph nodes
	Photosensitizer and perfluorocarbon coencapsulated by lipids [42]	200 nm	No significant cytotoxicity	Photodynamic therapy
	Perfluorohexane-loaded magnetic hollow iron oxide nanoparticles [43]	537.3 nm	No distinct cytotoxicity	Stimuli-responsive cancer theranostics

	Poly lactide-glycolide acid (PLGA) nanocapsules [44]	450 nm	Negligible cytotoxicity	Cancer theranostics
	Perfluorocarbons core and lipid shell [45]	132 ± 78 nm	Low cytotoxicity	Tumor therapy
Gas-generating nanoparticles	CO_2-generating carbonate copolymer nanoparticles [46]	290 ± 18 nm	No significant cytotoxicity	Tumor-targeted US imaging and US-triggered drug delivery
	H_2O_2-triggered CO_2-generating antioxidant poly(vanillin oxalate) [47]	~550 nm	Negligible cytotoxicity	Ultrasound imaging and therapy for hepatic ischemia/reperfusion treatment
	CO_2-generating nano-lipid carriers [48]	152.4 ± 0.6	No significant cytotoxicity	Temperature-controlled drug release and multimodal imaging
	Calcium carbonate loaded alginate nanocarrier [49]	~160 nm	No appreciable toxicity	In vivo tumor imaging
	CO_2-generating mesoporous calcium carbonate (MCC) nanoparticles [50]	~250 nm	No significant cytotoxicity	Ultrasound imaging-guided cancer therapy
	Calcium carbonate encapsulated by poly(d,l-lactide-co-glycolide) [51]	220 nm	No significant cytotoxicity	Ultrasound imaging and treating neuroblastoma
	Doxorubicin (DOX)-loaded calcium carbonate nanoparticles [52]	240.8 ± 8.1 nm	No appreciable toxicity	Theranostic agent for cancer treatment
	Superparamagnetic iron oxide particles @ glycol chitosan nanogel [53]	218 nm	No appreciable toxicity	Dual-modality US/MR imaging
	O_2-generating hybrid ICG-HANP/MnO2 nanocomplex [54]	239 ± 5.8 nm	No significant cytotoxicity	Ultrasound imaging-guided tumor photodynamic therapy

Table 2. Summary of inorganic nanosized UCAs for ultrasound imaging applications.

Inorganic nanoparticles	**Composition**	**Size**	**Cytotoxicity**	**Applications**
Silica NPs [55]	Solid spheres	330 nm in diameter	No acute toxicity	Targetable contrast agent for ultrasound imaging
Hollow silica NPs [56]	Surface PEGylated hollow silica microspheres	~1250 nm in diameter	Low cytotoxicity	Ultrasound contrast agents for imaging
Hollow hard porous silica NPs [57]	Hollow hard porous silica shell; filled with perfluorocarbon gas	2 μm in diameter; 10 nm thick porous silica shell	Low cytotoxicity	Tumor imaging
Mesoporous silica NPs [58]	Mesoporous structure	Pore diameter 2.4 nm; pore volume 0.98 cm^2.	Tumor-specific cytotoxicity	US-based breast cancer imaging
Mesoporous silica NPs [59]	Superhydrophobicity	Pore diameter < 1 nm	N/A	Targeting ultrasound imaging
Rattle-type mesoporous silica NPs [60]	Nanorattle hollow structure	NP diameter 420 nm; core diameter 260 nm	No evident toxicities	Intracellular ultrasound molecular imaging
Exosome-like silica NPs [61]	Concave mesoporous structure	140 nm in diameter	No detectable toxicity	Stem cells imaging and drug delivery
Fe-doped hollow silica nanoshells [62]	Ultrathin nanoshells with varying shell thicknesses and fused nanoflakes	2.4-22.8 nm in diameter; nanoflakes thicknesses 1.4-3.8 nm;	Minimal toxicity	Long-imaging capability for tumor
Au-PLGA NPs [63]	PLGA shell and perfluorohexane liquid core	200 nm in diameter	No detectable toxicity	Contrast-enhanced US imaging

Au-nanoshelled PLA nanocapsules [64]	Perfluorooctylbromide and superparamagnetic iron oxide nanoparticles co-loading	300.4 nm in diameter	No evident toxicity	Contrast imaging-guided photothermal therapy
MnO_2 NPs [54]	Catalytic property	180 nm in diameter	No significant cytotoxicity	Tumor photodynamic therapy
Albumin-MnO_2 NPs [65]	Polyelectrolyte–albumin complex and MnO2 nanoparticles	~50 nm in diameter	Low cytotoxicity	Treatment of cancer
CO_2-generating $CaCO_3$ NPs [52]	Doxorubicin-loaded calcium carbonate hybrid nanoparticles	Mean diameter 145.2 to 240.8 nm	No appreciable toxicity	US imaging and simultaneous therapy of tumors
Prussian Blue NPs [66]	Catalytic property	Mean diameter 126.7 nm	No acute toxicity	Contrast-enhanced US imaging
Hollow mesoporous Prussian Blue nanocubes [67]	Hollow mesoporous Prussian Blue shell and perfluoropentane core	500 nm	No observable toxicity	US imaging-guided tumor detection and therapy
Superparamagnetic hollow Fe_3O_4 NPs [43]	Perfluorohexane-encapsulated hollow nanoparticles	Average particle size 537.3 nm	No distinct cytotoxicity	Stimuli-responsive cancer theranostics
Multiwalled carbon nanotubes [68]	Oxidized and functionalized to make them biocompatible (ox-MWCNT-NH_3^+)	Diameter 20-30 nm; Mean length 400 nm	No detectable toxicity	Contrast-enhanced US imaging
Multiwalled carbon nanotubes [69]	Antibody modification	Mean length ~150 nm	Negligible cytotoxicity	Targeted US imaging of tumor

2.1.3. Biogenic gas vesicles

Besides chemical-based agents, genetically engineered protein-shelled nanoparticles, gas vesicles (GVs), have also illustrated remarkable imaging performance as molecular ultrasound contrast agents. GVs are hollow proteinaceous nanostructures with cylinder or spindle shapes, which are composed of a 2 nm-thick protein shell that encapsulates a hollow interior normally filled with air (**Figure 3a-b**) [70]. The shell of GVs has a highly hydrophobic inner surface, thereby water cannot pass through it and water vapor cannot condense inside [71]. However, ambient gases are able to freely diffuse into and out of GVs. In 2014, Shapiro et al. [72] first found that purified GVs from a kind of photosynthetic bacteria which were used to regulate buoyancy could scatter ultrasound waves and thus produce ultrasound contrast.

Because GVs are filled with gas, it was assumed that GVs could act as nanoscale contrast agents for ultrasound imaging. This hypothesis was then verified by using GVs purified from *Anabaena flos-aquae* and *halobacteria NRC-1* and ultrasound imaging in a gel phantom at 4.8, 8.6 and 17 MHz [72]. Following this pioneering finding, many studies about using GVs

as biomolecular contrast agents have been conducted, such as exploring their acoustic properties [73,74], engineering them through genetic and biochemical modulations [75,76], investigating the in vivo biodistribution as molecular contrast agents [77], using them as biomolecular tool for deep tissue imaging [78–80], imaging of microorganisms inside living animals (**Figure 3c-f**) [81], as well as more dedicated imaging of generic expression in mammalian cells [82].

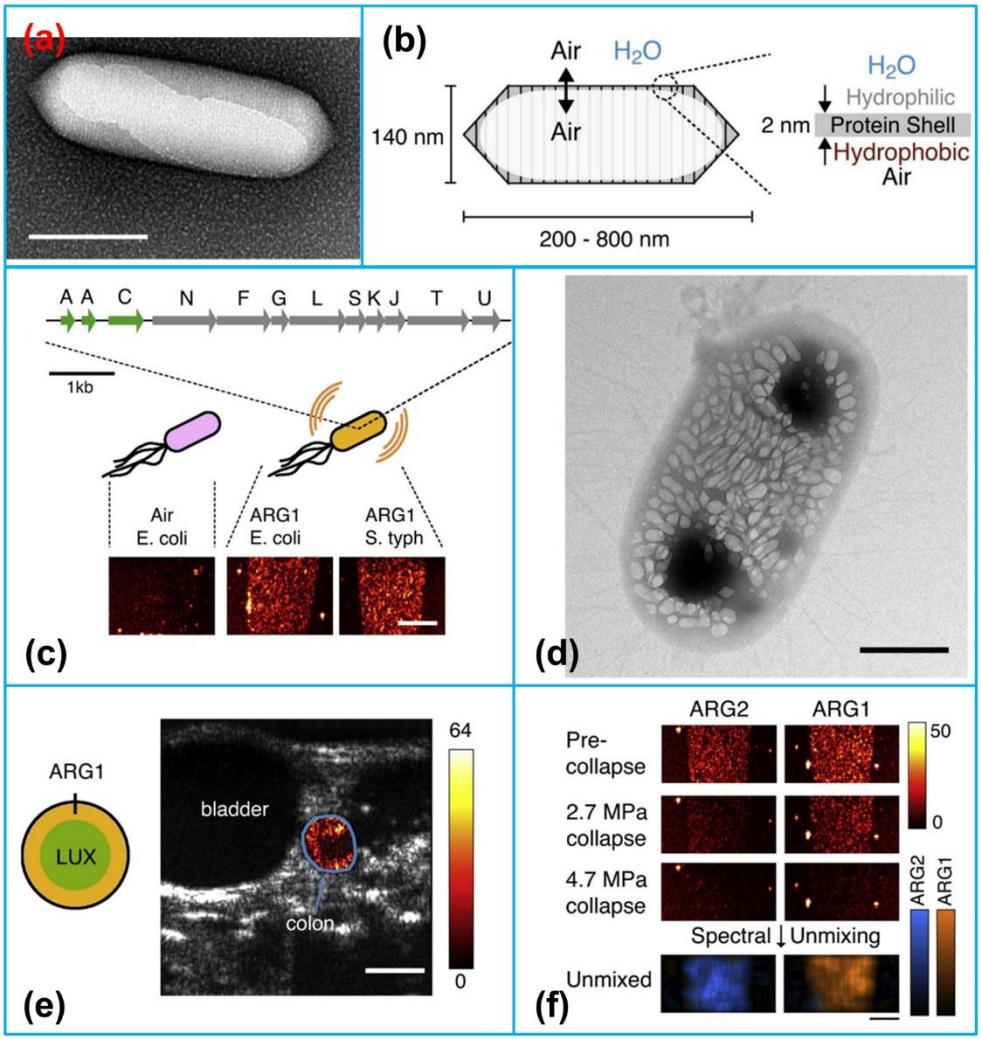

Figure 3. (a) Transmission electron microscopy (TEM) image of a gas vesicle (scale bars, 150 nm). (b) Composition of a gas vesicle. (c) Engineered gene, ARG1, comprising genes from A. flos-aquae (green) and B. megaterium (gray) to make the gas vesicles detectable by ultrasound in heterologous host. (d) TEM image of an E. coli Nissle 1917 cell expressing ARG1 (scale bar, 50 nm). (e) Ultrasound image of a live mouse with ARG1-expressing E. coli arranged in the colon (scale bar, 2.5 mm). (f) Ultrasound images of ARG1 and ARG2 before and after the application of two different collapse pressures. Reproduced with permission [83]. Copyright 2018, Elsevier.

2.2. Photoacoustic (PA) imaging

2.2.1. Principle of PA imaging

Photoacoustic (PA) imaging (also referred to as optoacoustic imaging) is an emerging multiscale functional, anatomical, and molecular imaging modality, having demonstrated great promise in preclinical researches and clinical applications [84]. PA imaging is based on photoacoustic effect that light absorbed by tissues is used to excite ultrasonic waves via thermoelastic expansion. In PA imaging, nanosecond duration laser pulse is delivered into the animal tissues (**Figure 4**). The absorption of short laser pulses by endogenous chromophores (such as hemoglobin and melanin) or exogenous contrast agents (such as small molecule dyes and carbon nanoparticles) is converted into thermal energy that results in transient thermoelastic expansion to generate acoustic waves in 3D space. The ultrasound waves can then be detected with an ultrasonic transducer or a transducer array surrounding the tissue or animal body. The detected ultrasonic waves are analyzed to reconstruct a photoacoustic image of tissue optical absorption [85].

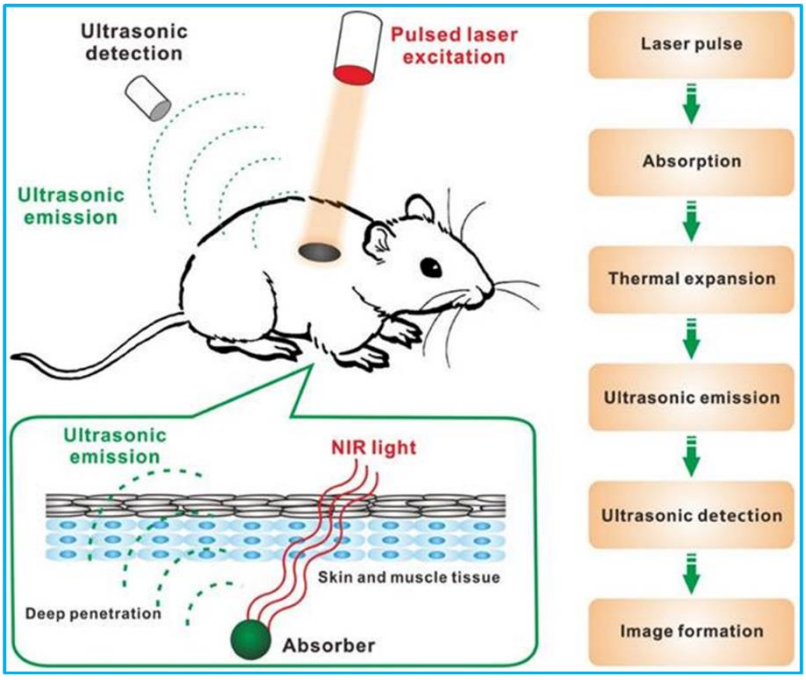

Figure 4. Schematic of working principle of PA imaging. Reproduced with permission [85]. Copyright 2016, Ivyspring International Publisher.

A PA imaging system mainly consists of an optical source for short laser pulse generation, an ultrasonic transducer array for acoustic wave detection, and a data acquisition (DAQ) system [86]. The pulse repetition frequency of the laser pulse and the time for ultrasonic signals detection are two major factors determining the PA imaging frame rate. Combining advantages from both optical and ultrasound imaging, PA imaging offers unique advantages over existing imaging modalities. First of all, PA imaging is free of ionizing radiation and noninvasive, thus it can be safely used in vivo. Secondly, it has higher resolution and deeper penetration depth (~ 4 cm in vivo and ~ 12 cm in vitro) compared to optical imaging techniques (~ 1 mm). Moreover, compared with other imaging modalities such as MRI and CT, PA imaging is much faster and less expensive. Other benefits include speckle free and label free [85,87–90]. With all these benefits, PA imaging has been found applications in diverse fields, including oncology, vascular biology, dermatology, neurology, ophthalmology, and cardiology [91–94].

2.2.2. Organic and inorganic nanosized contrast agents

Although PA imaging is able to penetrate deeper into tissue than other optical imaging methods, owing to the laser light scattering, the photoacoustic signal-to-noise ratio and light intensity attenuate exponentially with the increase of penetration depth, affecting the imaging contrast and resolution [85,95]. In order to enhance the PA imaging sensitivity and contrast, various oral or injectable chemicals, i.e., exogenous contrast agents, have been adopted to change the optical and acoustic properties of structures within the body [96]. Thus, the PA imaging contrast and resolution are reinforced with the assistance of exogenous contrast agents. In this section, the recent development of exogenous contrast agents that address biomedical applications and clinical practice will be examined. For the characteristics of endogenous chromophores and biomedical applications of PA imaging assisted with these chromophores, readers are referred to the references [97].

The exogenous PA contrast agents can be classified into organic and inorganic contrast agents according to their structures. A summary of recent reported PA organic and inorganic nanosized contrast agents is shown in **Table 3**. The highlights of different types of organic and inorganic nanosized contrast agents are presented in the following section. Various biomedical applications of PA imaging including bioimaging of tumors and biosensing of tumor microenvironments are summarized in **Table 4**.

Table 3. Organic and inorganic nanosized contrast agents reported in the literatures for PA imaging applications.

Organic nanomaterials	Small organic molecules	Cyanine-based dyes, croconine, naphthalocyanines, perylene-diimide (PDI), phthalocyanine, porphyrin, porphysome, squaraine
	Semiconducting polymer NPs	semiconducting polymers, PDI-based NPs, organic NPs, oligomers, chlorin dimers, polypyrrole, polylysine, natural humic-acid-based nanoagents
Inorganic nanomaterials	Metallic NPs	Gold NPs, gold NP assemblies, Prussian blue, copper neodecanoate NPs, Ag NPs, Pd nanosheets
	Transition metal chalcogenides/MXene-based NPs	CuS, Ag_2S, CuInS/ZnS, MoS_2, TiS_2, WS_2, CoS_2, ReS_2, Bi_2S_3, $MoSe_2$, Nb_2C, TaC, Ti_3C_2, S_2V
	Carbon-based NPs	Au coated SWCNTs, single-walled carbon nanotubes (SWCNTs)-Arg-Gly-Asp (RGD) conjugation, rGO loaded AuNR, rGO loaded AuNRVe, CNTR@AuNPs
	Others	Te nanosheets, B nanosheets, Cu-Ag_2S NPs, black-phosphorus quantum dots, black-phosphorus nanosheets, Fe@γ-Fe_2O_3@H-TiO_2 nanocomposites, MnO_x loaded Ti_3C_2

Table 4. Summary of PA imaging applications using different nanosized contrast agents.

Application	**Nanosized UCA**	**Features**	**Performance**
Deep tumor imaging [98]	Micelle enveloped PDI NPs	High PA imaging sensitivity, high photostability and biocompatibility	The NPs provided high PA imaging contrast for detection of deep brain tumor in living mice.
Brain tumor imaging [99]	Second NIR (NIR II) conjugated polymer NPs	High imaging contrast, high photostability and good biocompatibility	The NPs showed much weakened light attenuation, strong signal/background ratio, and large penetration depth for brain tumor imaging.
Brain vascular imaging [100]	Conjugated polymer nanoparticles (CPNs)	High photostability, exhibiting no toxicities both in vitro and in vivo	The NPs can greatly enhance PA signals for brain vascular imaging.
Deep brain glioma imaging [101]	MoS_2-ICG hybrid	High PA imaging sensitivity, enhanced photoacoustic conversion efficiency compared with ICG	Brain tumor at twofold deeper site beneath a mouse scalp was clearly identified by using the hybrid as contrast agent.
Mouse brain imaging [102]	ICG-containing porous Si NPs	ICG sealed within a rigid NP that can protect the ICG payload from thermal and photolytic degradation	The PA efficiency was increased 17-fold compared with free ICG.

Vessel atherosclerosis imaging [103]	ICG@PEG-Ag_2S nanoprobe	Long blood circulation, hemocompatibility, and no organ toxicity	Atherosclerotic plaques were imaged in a high contrast-enhanced manner.
Venous thrombosis imaging and antithrombotic therapy [104]	Thrombus-specific theranostic NPs	H_2O_2-triggered photoacoustic signal amplification	Photoacoustic contrast was greatly enhanced by using the NPs as contrast agent in a thrombosed vessel.
Venous thrombosis imaging [105]	cRGD peptide modified PDI NPs	High PA intensity, high photostability and biocompatibility, and excellent binding ability with GPIIb/IIIa	The PA contrast enhanced by the NPs provided effective information about the thrombus including the profile, size, and spatial distribution.
Sentinel lymph node (SLN) imaging [106]	Silica-coated gold nanoplates	High photothermal stability, and low cytotoxicity	Strong and sustained PA signals were obtained for SLN imaging in a mouse model.
Lymph node imaging in living mice [107]	Semiconducting polymer nanoparticles	High structural flexibility, high photostability, and narrow photoacoustic spectral profiles	They can not only be utilized for LN mapping but also for PA imaging of ROS.
Sentinel lymph node imaging [108]	Encapsulated conjugated oligomer NPs	Excellent photostability and biocompatibility, strong absorption in the NIR range	The NPs showed great potential for SLN imaging and photothermal therapy.
Detection of cancer-related matrix metalloproteinases [109]	Copper sulfide NPs	Strong absorbance in the NIR range, good photostability	The NPs could dramatically improve the tissue penetration depth for PA imaging.
Tumor hypoxia imaging [110]	Ratiometric hypoxia probe 1 (rHyP-1)	Strong NIR absorption, and deep penetration depth	The probe enabled high resolution hypoxia detection using PA imaging at centimeter depths.
Tumor pH imaging [111]	pH-responsive albumin-based nanoprobe	High biocompatibility, easy to operate, and depth independent accuracy	The nanoprobe was clinically adoptable for real-time pH imaging of the whole tumor.
pH imaging [112]	Semiconducting oligomer NPs	Ultrasmall size, high stability, and high pH sensitivity	The NPs allowed real-time PA imaging of pH in tumors in living mice.
Lithium detection [113]	Lithium ionophore	Monitoring therapeutic drug concentrations in vivo based on PA imaging	To track the concentrations of therapeutic drugs and improve disease management.
Methylmercury ($MeHg^+$) detection [114]	Liposome (LP) and cyanine dye (hCy7) nanoprobe	The hydrophobic hCy7 was encapsulated in the lipid layer of the liposome. High biocompatibility and negligible cytotoxicity	The nanoprobe can detect $MeHg^+$ in vivo by ratiometric photoacoustic bioimaging.

(1) Organic contrast agents. A typical representative of small organic molecules is cyanine-based dyes that are commonly utilized as PA imaging contrast agents as a result of their good photostability, high photoconversion efficiencies and negligible toxicity [115]. Kang et al. [102] reported a method to improve the PA response of indocyanine green (ICG), one of the commonly applied PA imaging agents, by encapsulating it in a porous silicon nanoparticle host. Because of the low thermal conductivity of the host, the PA generation efficiency of the

composite structure was increased 17-fold compared with free ICG (**Figure 5a**). Liu et al. [114] developed a ratiometric photoacoustic nanoprobe consisting of liposome and $MeHg^+$-responsive NIR cyanine dye for $MeHg^+$ detection in living subjects (**Figure 5b**). It was found that in the presence of $MeHg^+$, the ratiometric photoacoustic signal was increased remarkably. Chen et al. [111] fabricated a nanoprobe composed of human serum albumin (HSA) and NIR dye (BPO_x and IR825) nanocomplexes for sensing tumor microenvironment pH using ratiometric photoacoustic imaging (**Figure 5c**). The tumor microenvironment pH could be detected by using the nanoprobe in combination of ratiometric photoacoustic imaging, which was very useful for regulating the proliferation of cancer cells.

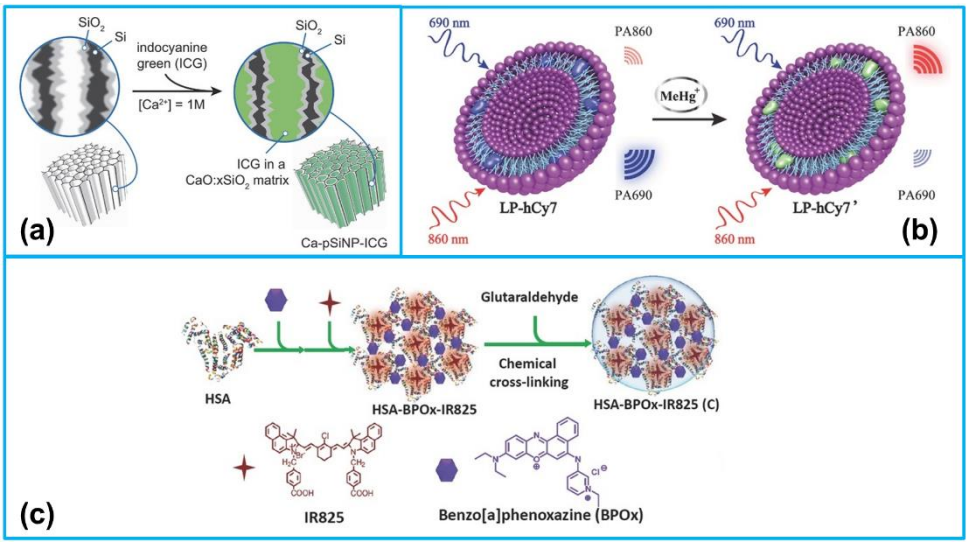

Figure 5. (a) Procedure used to simultaneously load and seal ICG into the pores of porous silicon nanoparticles (pSiNPs). Reproduced with permission [102]. Copyright 2018, Wiley-VCH. (b) Mechanism of ratiometric PA imaging of $MeHg^+$. Reproduced with permission [114]. Copyright 2017, Wiley-VCH. (c) The preparation process of C-HSA-BPOx-IR825. Reproduced with permission [111]. Copyright 2015, Wiley-VCH.

Besides, owing to their strong optical absorption and high photostability, semiconducting polymer nanoparticles (SPNs) have also been commonly adopted [115]. By encapsulating PDI into micelle, a kind of amphiphilic molecule, Fan et al. [98] developed a highly efficient PA imaging contrast agent, micelle-enveloped PDI, for imaging of deep brain tumors (**Figure 6a**). Their studies found that the organic NPs illustrated strong PA absorption in the NIR

range, and they could be utilized to detect brain tumors successfully in living mice. Following that, to diagnosis of early thrombus and monitoring thrombolysis, Cui et al. [105] developed cyclic Arg-Gly-Asp (cRGD) peptide modified PDI (cRGD-PDI) NPs as PA agents. The cRGD-PDI NPs showed strong PA imaging contrast and provided 4-folder greater PA intensity of early thrombus than the control group in a living mouse (**Figure 6b**). In another study, in order to achieve the combined PA and US imaging, Tang et al. [116] fabricated an organic semiconducting nanodroplet consisting of a PDI shell, a liquid perfluoropentane core and photosensitizers of $ZnF_{16}P_c$ molecules at the interface of the core-shell as PA and US dual-contrast agents (**Figure 6c**). The nanodroplets illustrated a high tumor accumulation in a living mouse due to their nanoscale size. Under a 671 nm laser irradiation, the nanodroplets could be effectively applied for dual-modal PA and US imaging-guided photothermal and photodynamic therapy.

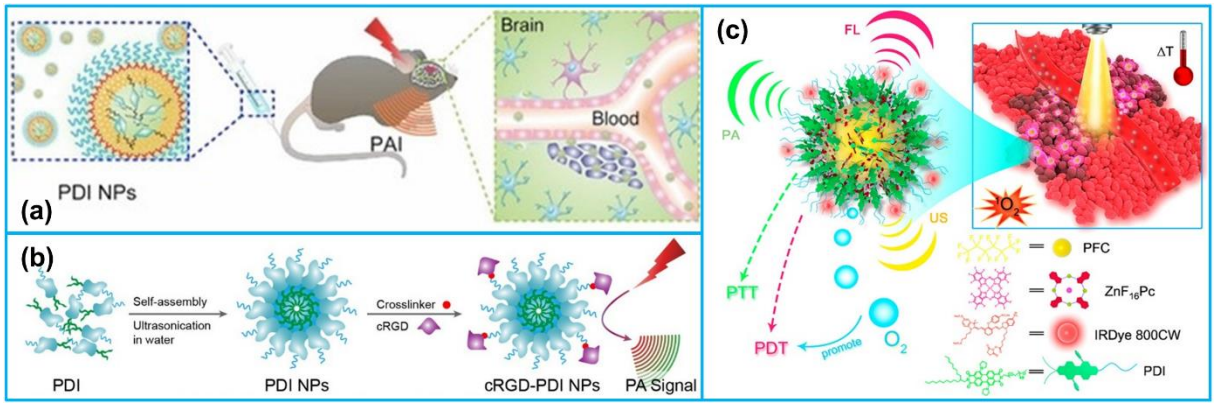

Figure 6. (a) PA imaging process of brain tumor in vivo by PDI NPs. Reproduced with permission [98]. Copyright 2015, Wiley-VCH. (b) The preparation of cRGD-PDI NPs. Reproduced with permission [105]. Copyright 2017, American Chemical Society. (c) IRDye800CW-labeled photosensitizer $ZnF_{16}P_c$-loaded PDI photoacoustic nanodroplet (PS-PDI-PAnD). Reproduced with permission [116]. Copyright 2018, American Chemical Society.

(2) Inorganic contrast agents. Metallic nanomaterials, especially gold nanoparticles (AuNPs), can achieve strong optical absorption via the localized surface plasmon resonance (LSPR) [85]. By synthesizing AuNPs with different morphologies, their optical absorption properties can be maximized in the NIR region. Other notable advantages of AuNPs include their

biocompatibility, high photothermal conversion efficiency, and good chemical inertness [117,118]. To date, different types of AuNPs have been reported including nanospheres [119–121], nanorods [122–125], nanoprisms [126–128], nanocages [129–131], nanostars [132–134], nanoplates [106,135,136], nanodisks [137–139], nanoshells [64,140–142], nanovesicles [123], nanotripods [143], nanowreaths [144], nanoflowers [145,146], and bipyramids and rhombic dodecahedra [147], as shown in **Figure 7**.

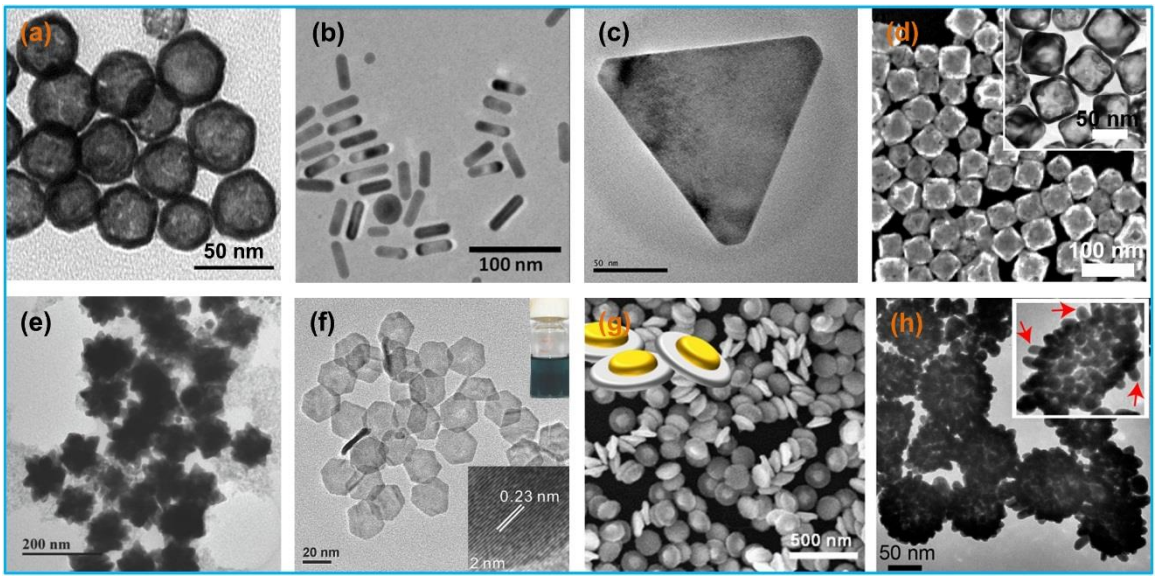

Figure 7. Microscopy photographs of different types of gold nanoparticles: (a) nanospheres, (b) nanorods, (c) nanoprisms, (d) nanocages, (e) nanostars, (f) nanoplates, (g) nanodisks, and (h) nanoshells. (a) Reproduced with permission [148]. Copyright 2009, Elsevier. (b) Reproduced with permission [149]. Copyright 2012, American Chemical Society. (c) Reproduced with permission [126]. Copyright 2015, American Chemical Society. (d) Reproduced with permission [131]. Copyright 2017, Elsevier. (e) Reproduced with permission [150]. Copyright 2018, Wiley-VCH. (f) Reproduced with permission [135]. Copyright 2014, Wiley-VCH. (g) Reproduced with permission [139]. Copyright 2017, American Chemical Society. (h) Reproduced with permission [142]. Copyright 2017, American Chemical Society.

Besides the gold nanocrystals, gold nanocrystal assemblies also show outstanding optical absorption properties in the NIR region. Bai et al. [151] fabricated a multifunctional nanocomposite combining imaging (PA imaging and MRI) and therapeutic functions for cancer cells imaging and photothermal therapy, which was composed of hollow gold nanospheres as cores and superparamagnetic iron oxide NPs as satellites. Song et al. [152] developed a plasmonic vesicular nanostructure comprising of amphiphilic gold nanocrystals

with polymer brush coatings. The nanocrystals imparted their remarkable properties to the assembly, and the strong interparticle plasmonic coupling caused collective properties different from those of the constitutive units. In another work, Deng et al. [153] developed a theranostic agent composed of comb-like amphipathic polymer template and DOX@gold nanomicelles for dual-modal imaging (CT and PA) and the combination of chemotherapy and photothermal therapy. Their studies in a mouse model demonstrated that the nanomicelles could be effectively used to detect tumors for CT and PA imaging simultaneously.

Carbon-based nanomaterials mainly consisting of CNTs [154–156] and graphene-based nanomaterials [157–161], have been widely adopted as contrast agents in PA imaging as well (**Figure 8a**). The major advantages of carbon-based nanomaterials are their broad absorbance band ranging from UV to NIR region as well as ease to integrate with various materials or compounds for multiple functions. De La Zerda et al. [162] synthesized a PA contrast agent based on SWNT conjugated with RGD peptides for PA imaging of tumors. According to the tumor detection in a living mouse, the PA signal of the tumor in the mouse injected with the contrast agents was eight times stronger than that of the control group. Kim et al. [163] reported gold-plated carbon nanotubes as contrast agents for PA imaging, which were composed of shortened SWNT core coated by a thin layer of gold. This novel hybrid plasmonic contrast agent, combined the advantages of gold and CNTs, presented a unique set of features. Song et al. [164] proposed a PA contrast agent fabricated by carbon nanotube ring (CNTR) template and AuNPs coating for imaging-guided cancer therapy (**Figure 8b**). Compared with CNTR and CNTR@AuNS, the CNTR@AuNP illustrated much stronger Raman and optical signals. Moon et al. [165] developed a PA imaging contrast agent rGO-AuNRs using an optically absorbing material rGO coated with gold nanorods (**Figure 8c**). The rGO-AuNRs demonstrated greatly enhanced PA signal intensity and photothermal efficiency, which was a promising nanomaterial for sensitive disease diagnosis and

photothermal therapy. In addition, Song et al. [166] fabricated a carbon-metal hybrid rGO-loaded plasmonic gold nanorod vesicle for dual chemo-photothermal therapy. The rGO was conjugated with DOX and the rGO-DOX conjugation was encapsulated in the AuNRVe to avoid direct interaction with the physiological environment.

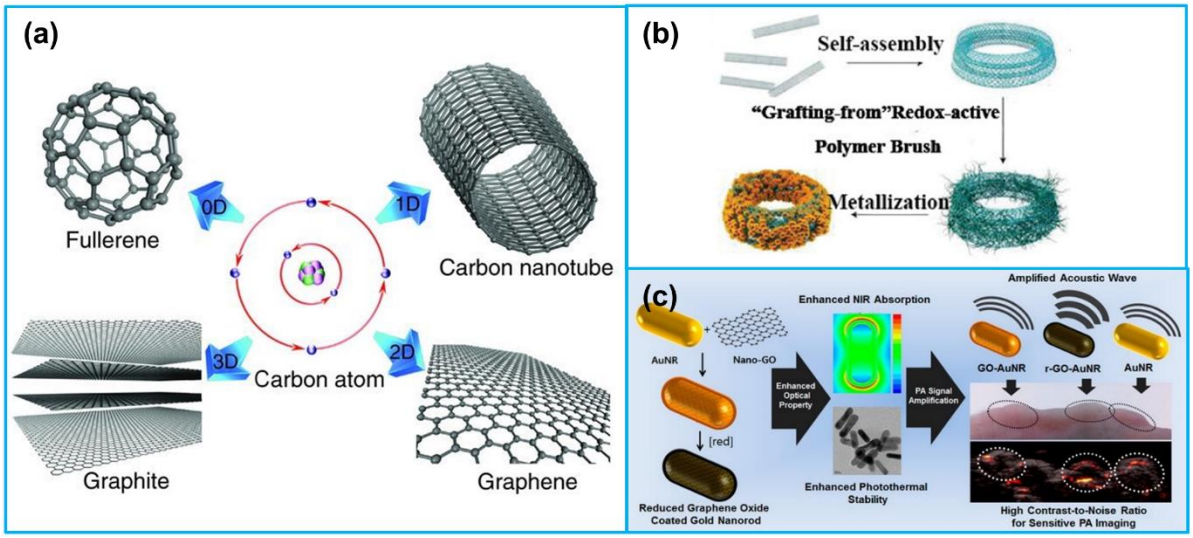

Figure 8. (a) Structures of 0D fullerene, 1D carbon nanotube, 2D graphene and 3D graphite formed by the carbon atoms. (b) Preparation of CNT ring Au nanoparticles (CNTR @ AuNPs). (c) Preparation and application of reduced graphene oxide Au nanorods (rGO-AuNRs). (a) Reproduced with permission [167]. Copyright 2011, Wiley-VCH. (b) Reproduced with permission [164]. Copyright 2016, American Chemical Society. (c) Reproduced with permission [165]. Copyright 2015, American Chemical Society.

3. Nanoacoustics for medical therapy

3.1. Ultrasonic drug delivery

Apart from diagnostic applications of ultrasound, therapeutic applications of ultrasound, such as ultrasound-mediated drug/gene delivery, has become an emerging topic of expanding interests. Starting from the mid-90s, many studies have reported that the exposure to ultrasound can temporarily enhance the cell membrane permeability (i.e., sonoporation), thus creating a physical channel for delivery of cell-impermeable drugs (**Figure 9**) [168]. The main benefit of delivery of therapeutics using ultrasound is that the drug delivery and release is spatially and temporally controlled in the target region, thus lowering the dosage use and the adverse side effects [169,170]. Different therapeutics including small-molecule drugs,

protein drugs, peptide drugs, and genetic drugs have been reported to be successfully delivered with the assistance of ultrasound waves [171–176].

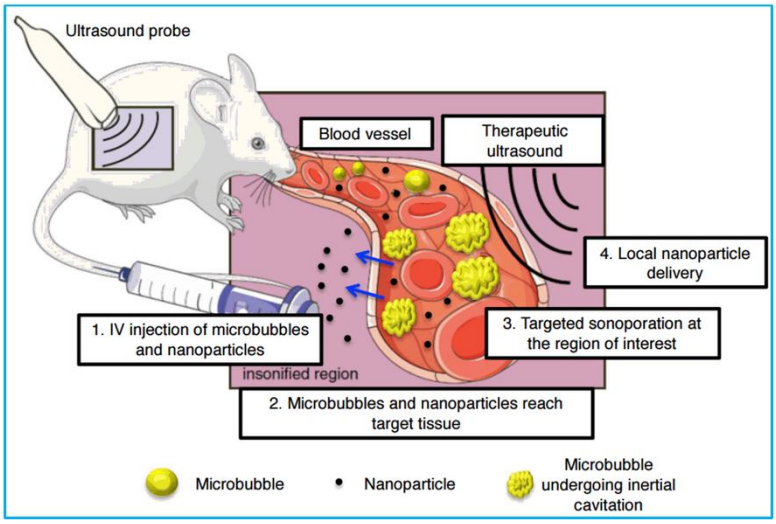

Figure 9. Schematic illustration of the mechanism of ultrasound-mediated nanoparticle delivery. Reproduced with permission [177]. Copyright 2017, Korean Society of Ultrasound in Medicine.

While microbubbles have been proved to be reliable tools for ultrasound-mediated therapeutic delivery, the key limitation of microbubbles is that the size of microbubbles is too large to penetrate into tumor tissues, thereby only confined their applications in blood circulation and cannot be effectively utilized for cancer therapy [23]. Various techniques have been devised for the use of nanosized bubbles/particles for delivery of therapeutics to targeted tissues [178]. Nanobubbles/particles, acted as delivery carriers, are able to deliver drugs precisely to the target tissues while maintaining efficiency. Moreover, combined with the visual and noninvasive features of ultrasound, the motion of drug nanocarriers can be tracked and the release of drugs from nanocarriers can be controlled by the ultrasound irradiation [179,180]. For all these reasons, the development of safe and efficient novel ultrasound-responsive therapeutic nanocarriers could greatly impact therapy strategies.

3.1.1. Nanocarriers for ultrasonic drug delivery

Recently, there have been various nanomaterials served as nanocarriers for delivery of anticancer drugs to tumor tissues [181–183], delivery of thrombolytics to break up or dissolve

blood clots [184–186], delivery gene to target tissues [187–190], as well as delivery insulin to regulate blood glucose level [191,192] (**Figure 10**). The recent development of different types of nanocarriers for ultrasonic drug delivery are highlighted in this section.

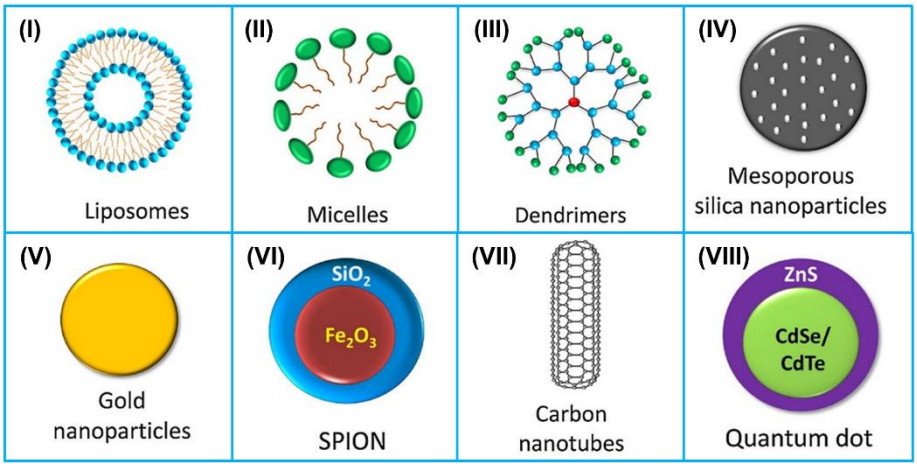

Figure 10. Schematic illustration of the 8 most reported nanocarriers: (I) liposomes, (II) micelles, (III) dendrimers, (IV) meso-porous silica nanoparticles (MSNs), (V) gold nanoparticles (AuNPs), (VI) super paramagnetic iron oxide nanoparticles (SPIONs), (VII) carbon nanotubes (CNTs), and (VIII) quantum dots (QDs). Reproduced with permission [193]. Copyright 2019, Elsevier.

(1) Liposomes. Liposomes, typically with a diameter of 100–200 nm, are composed of an aqueous core surrounded by a self-assembled lipid bilayer membrane. Due to their excellent biocompatibility and versatility, liposomes has become one of the most widely utilized nanocarriers for ultrasound-mediated drug delivery [194]. Marxer et al. [195] developed a long-circulating drug nanocarrier with three different lipid formulations for ultrasound-enhanced drug delivery. The physico-chemical properties of the developed lipid dispersions were compared with a commercially available contrast agent, which demonstrated adjustable properties including circulation stability, biocompatibility, and ultrasound reflectivity. In another study, Becker et al. [196] compared the sonothrombolytic efficacy of the three nanoscaled lipid formulations with the commercially available contrast agent for human blood clot under diagnostic ultrasound. Their results illustrated that the nanoscaled formulation of DSPC/PEG40S had the most significant clot weight reduction under the irradiation of

ultrasound at 1.4 MHz, even without thrombolytic drugs. Lattin et al. [197] reported an echogenic liposome that can release drugs from liposomes under ultrasound excitation. The developed liposomal drug nanocarrier was called an eLiposome (liposomes containing emulsion droplets), formed by using a lipid sheet folding technique. The eLiposome had an overall diameter of 800 nm and contained emulsion droplets 100-150 nm and 470 nm, respectively. Under ultrasound excitation, vapor phase was formed and expanded from the droplets, which would disrupt the liposomal membrane and lead to local drug release.

(2) Micelle. Micelle is typically spherical in shape, which is formed by a series of amphiphilic molecules that have a natural tendency to clump together. The hydrophobic drugs can be segregated in the hydrophobic core of micelle until they are released. Diaz de la Rosa et al. [198] investigated anticancer drug DOX release behavior from Pluronic P105 unstabilized and stabilized micelles. The in vitro experiments found that the drug release from unstabilized as well as stabilized micelles at ultrasound frequency < 90 kHz, while no drug was released from the micelles at ~500 kHz. This was mainly attributed to the different dynamics of oscillating bubbles under the different ultrasound excitations. Husseini et al. [199] fabricated DOX encapsulated Pluronic P105 micelles with a folic acid moiety to enhance the tumor cells targeting. They found that the percentage of drug release was improved with the rise of ultrasound power intensity under 70 kHz excitation. The maximum amount of DOX release was 14%, which was measured at an ultrasound intensity of 5.4 W/cm^2. Wu et al. [200] developed anticancer drug curcumin (Cur) encapsulated pluronic P123/F127 mixed micelles for site-specific sonochemotherapy. Under 1 MHz focused ultrasound excitation, the Cur-loaded micelles demonstrated tumor-targeting deposition, resulting from the ultrasound sonoporation. Moreover, the ultrasound-triggered Cur release from the Cur-loaded micelles was highly dependent on the ultrasound intensity.

(3) Polymeric nanoparticles. Polymeric nanoparticles mainly consist of nanocapsules, nanospheres, and polymersomes, which demonstrate the properties of enhanced encapsulation and controlled release of therapeutics [201]. Nestor et al. [202] fabricated air-filled nanocapsules with a biodegradable polymeric shell for tumor detection. The nanocapsules had a mean diameter of 370 nm and a spherical shape with smooth surfaces as well as a capsular morphology. The polymeric shell could potentially entrap drugs inside it, which made this kind of structure promising for theranostics agents. Yang et al. [203] reported a biodegradable nanocapsule that was filled with perfluorohexane and had the DOX-loaded PMAA as wall for achieving the ultrasound imaging and drug delivery functions. The developed nanocapsules could easily enter the tumor tissues due to their small and uniform size. Moreover, the filled perfluorohexane could be easily vaporized via ultrasound excitation, thus enhancing ultrasound imaging signals and ensuring imaging-guided drug delivery. Chen and Du [204] developed polymer vesicles that responded to both ultrasound and pH stimuli for drug entrapment and release. The size of the vesicles would become smaller under either ultrasound excitation or pH decrease. The encapsulated anticancer drugs could reach controllable release when exposed to ultrasound irradiation or pH variation.

(4) Nanobubbles. Nanobubbles are commonly adopted as theranostic agents due to their great imaging ability. Cavalli et al. [205] developed DNA-loaded chitosan nanobubbles which were composed of a perfluoropentane core and a chitosan shell as ultrasound-triggered gene delivery system. The plasmid DNA was loaded onto the chitosan shell, which was expected to have long circulation time and accumulate into tumor tissues easily. Based on the in vitro experiments, while in the absence of ultrasound, the nanobubble-bound plasmid DNA was not released at all, after one minute of 2.5 MHz ultrasound excitation, the release of plasmid DNA occurred. Yin et al. [206] developed siRNA-loaded nanobubbles which were fabricated by the negatively charged gas-cored liposomes and positively charged siRNA micelles for tumor

treatment. Under 1 MHz ultrasound irradiation, the siRNA micelles were effectively released from the nanobubbles in tumor tissue and delivered into cancer cells.

(5) Perfluorocarbons (PFCs). Rapoport et al. [207] reported paclitaxel (PTX)-loaded perfluoropentane (PFP) nanoemulsions that could effectively accumulate in tumor tissue and transformed into microbubbles in sonication. The ultrasound imaging properties and therapeutic efficacy of the nanoemulsions were experimentally verified in a mouse model. After injection of the drug-loaded nanoemulsions, tumors were significantly regressed after1 MHz ultrasound irradiation. In another study, Thakkar et al. [208] explored the effect of ultrasound irradiation on the penetration of drug-loaded nanoemulsions through vascular walls. Mouse carotid arteries were utilized as a blood vessel model. They found that under 1 MHz irradiation, the permeability of the arteries to the nanoemulsions was much more pronounced by using continuous ultrasound wave than that of pulsed ultrasound.

(6) Quantum dot. Based on the fact that ultrasound irradiation can enhance cell membrane permeability (sonoporation), Thein et al. [187] developed an ultrasonic micro-transducer array for cellular level controllable sonoporation that accelerates delivery of drugs or gene therapeutics to cells (**Figure 11**). The developed transducer array was composed of 3 × 3 arrays of PMN-PT transducers (each area 25 μm × 25 μm) with a central frequency of 30 MHz and lateral resolution of 18 μm for site-specific sonoporation. CdSe/ZnS quantum dots were utilized as nanocarriers to quantitatively evaluate the sonoporation degree of the human melanoma cells seeded on the surface of the transducer array. It was found that the cell membrane wound size and cellular uptake of quantum dots were increased linearly with the rise of ultrasound irradiation pressure.

Besides the nanocarriers reviewed above, other inorganic materials including mesoporous silica nanoparticles [209–214], Au nanocages [215–217], magnetic nanoparticles [218–220],

and carbon-based nanovehicles [69,221–224] have also been reported by researchers to be utilized as nanocarriers for ultrasound-mediated drug delivery.

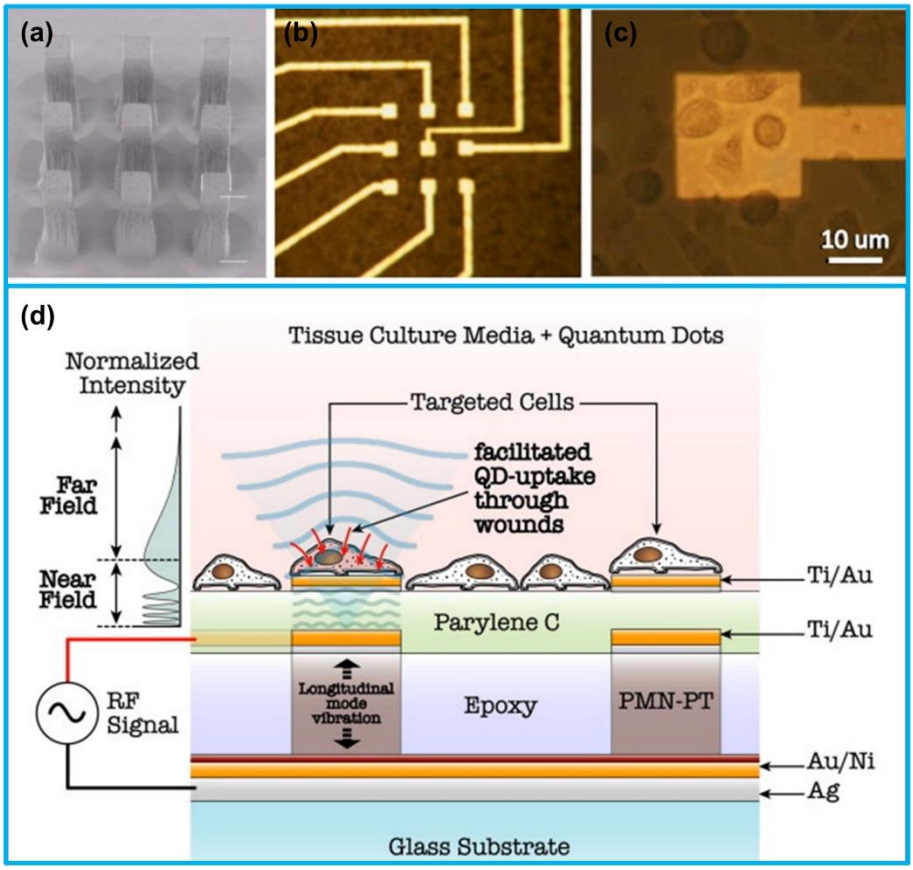

Figure 11. (a) SEM image of a 3 × 3 micro-transducer array (each area 25 μm × 25 μm). (b) Electrode above each micro-transducer. (c) Human melanoma cells above a micro-transducer. (d) Schematic illustration of ultrasound-mediated quantum dots (QDs) delivery at cellular level using the micro-transducer array. (a)-(d) Reproduced with permission [187]. Copyright 2011, Elsevier.

3.2. Ultrasound therapy

3.2.1. Ultrasound-triggered therapy

Ultrasound has long been employed in medicine for the treatment of many different pathologies, such as ultrasound-assisted liposuction, lithotripsy for kidney stone, and accelerating wound healing, mainly attributed to its advantages of safety to human tissues, low cost and deep tissue penetration capability [225]. Recently, high-intensity focused ultrasound (HIFU) has been served as a new noninvasive treatment technique for thermal ablation of local tumors [226]. Sonodynamic therapy (SDT) that is based on low-intensity

ultrasound and chemotherapeutic agents (known as sonosensitizer) has been reported by researchers to noninvasively eradiate solid tumors due to the ultrasound-induced cytotoxic effects [227]. Compared with the current major therapeutic techniques including chemotherapy and gene and cell therapy, ultrasound-triggered therapy is able to focalize at target tissues and reduce biotoxicity. In addition, better treatment could be achieved while combining the ultrasound method with conventional therapies [228].

Over the past few decades, the rapid development of nanomaterials and nanostructures not only advances ultrasound imaging by providing nanosized contrast agents with outstanding properties, but also accelerates ultrasound therapy with greatly enhanced therapeutic efficiency owing to their unique physiochemical properties, such as surface features, geometry, porosity, and composition [229]. Different nanoparticles can also potentially combine several imaging modalities and therapeutic functions into one nanoplatform to be utilized as multifunctional theranostic agents for imaging-guided synergistic therapy. Miscellaneous nanoparticles including organic nanomaterials and inorganic nanomaterials have been adopted in studies for treatment various diseases such as tumors, cardiovascular diseases, and central nervous system diseases [228].

While this section is focused on nanomaterials and nanostructures for ultrasound-triggered therapy applications, many recent published review articles have already covered this topic, especially the review about nanoparticles for ultrasound-triggered cancer therapy. Considering that several comprehensive reviews have summarized and discussed the emerging development of exploring organic and inorganic nanomaterials for ultrasound-triggered therapies, the same topic will not be reviewed again in this paper and the readers could refer to very recent reviews. Yang et al. [228] focused on the current applications of ultrasound-triggered therapy (2019). Zhou et al. [230] summarized the development of organic and inorganic nanoparticles for ultrasound-based cancer therapy (2020). Yang et al.

[231] reviewed the recent advance of 2D nanomaterials for ultrasound-triggered cancer therapy (2020). Fan et al. [232] comprehensively examined nanotechnology-mediated synergistic cancer therapy (2017). Xu et al. [233] focused on different nanoparticles in sonodynamic therapy (2016). Unga et al. [234] reviewed nanosized agents for ultrasound-induced cancer immunotherapy (2014).

3.2.2. Nanoparticle-mediated sonothrombolysis

While blood clot, or thrombus, helps human body stop bleeding when a person gets hurt, blood clots forming in veins or arteries are dangerous to human health. When blood clots form inside a vein or artery (i.e., thrombosis), they will reduce the blood flow past the clot or even totally block the blood flow. If the thrombosis forms in the legs, it causes deep vein thrombosis; if it is formed in the lung, life-threatening pulmonary embolism will be occurred; if the blood clots block the blood supply to the brain, ischemic strokes will happen [235]. Thrombolysis, known as thrombolytic therapy, is a treatment to dissolve blood clots that have blocked veins or arteries and pose potentially serious or life-threatening complications. Sonothrombolysis is an emerging technique that employs ultrasound waves to break down blood clots in vessels. The widely accepted mechanisms of sonothrombolysis are ultrasound-induced stable and inertial cavitation, microstreaming, microjetting and increased diffusion of therapeutics into the clots due to acoustic radiation force [236]. Conventionally, sonothrombolysis is usually adopted in combination with thrombolytic agents, such as tissue plasminogen activator (tPA) or microbubbles. However, the application of tPA will carry the risk of systemic hemorrhage in patients, and the use of microbubble is showed to be slow for treatment (usually several hours) and less effective for aged clots [237,238]. Nanodroplets, a generally applied ultrasound contrast agent that has a diameter of 100-300 nm, has been shown to be effective for sonothrombolysis [239]. Compared with microbubbles, the advantages of nanodroplets include their longer circulation time in blood

and deeper penetration into clots due to their smaller size. Recently, low-boiling-point (-2°C) lipid-shell perfluorocarbon phase-change nanodroplets were adopted by our group for sonothrombolysis based on the assumption that the smaller nanodroplets could permeate into a clot easier compared to microbubbles, thereby greater cavitation effects would be generated inside the clot and lysis rate would be improved [240]. The efficiency of the nanodroplets for sonothrombolysis was compared with that of microbubble-mediated sonothrombolysis. Under the same ultrasound excitation conditions (I_{SPTA} 0.384 W/cm^2, peak negative pressure 8.0 MPa), the nanodroplets-mediated treatment demonstrated a thrombolysis rate of 140% over the microbubble-mediated treatment. In another study, we conducted in-vitro study to compare the sonothrombolysis efficacy of nanodroplets on unretracted (< 24 hours old) and retracted (> 3 days old) blood blots with that of microbubbles [241]. The results illustrated that while the unretracted clot mass reduction was similar for both treatment conditions, the retracted clot mass reduction for the nanodroplet-mediated treatment was 1.6-fold over that of microbubble-mediated treatment. Under the treatment condition that tPA was combined with the nanodroplet-mediated sonothrombolysis for retracted clots, compared with control group (tPA + ultrasound), the nanodroplet-mediated sonothrombolysis with tPA illustrated greatly larger mass reduction (38% vs. 4%) [242].

Besides nanodroplets, magnetic microbubbles are also proved to be promising for sonothrombolysis. Magnetic microbubble (MMB), composed of a gas core and a shell of Fe_3O_4 nanoparticles, not only possesses the acoustic properties of a microbubble but also is sensitive to magnetic field excitation (**Figure 12c**) [243]. In our recent studies [244,245], MMBs were utilized in conjunction with an intravascular forward-looking ultrasound transducer (620 kHz) for MMBs-mediated sonothrombolysis (**Figure 12a**). We assumed that under a rotational magnetic field, the MMBs would be trapped and oscillated close to the target blood clot; the induced vortex-like microstreaming would enhance the cavitation effect

generated by sonication. Based on our in vitro studies, the mass reduction of MMBs-mediated sonothrombolysis for unretracted and retracted clot was 1.4-fold over that of microbubble-mediated sonothrombolysis. To achieve precise and controllable delivery of thrombolytic drugs, Wang et al. [186] synthesized a nanoparticle-shelled magnetic microbubble (MMB-SiO_2-tPA) for realizing the magnetic targeting under a magnetic field and ultrasound-triggered tPA release due to the microstreaming. The microbubble was composed of an air core and a shell of nanoparticles consisting of Fe_3O_4 nanoparticles and tPA-containing mesoporous silica nanoparticles (**Figure 12b**). Under a low-intensity ultrasound excitation, both the penetration depth of tPA into clot and thrombolysis efficacy were improved. Compared with conventional injection of tPA (0.03 mg/kg), the thrombus mass in a mouse model was reduced by 67.5% using the MMB-SiO_2-tPA treatment.

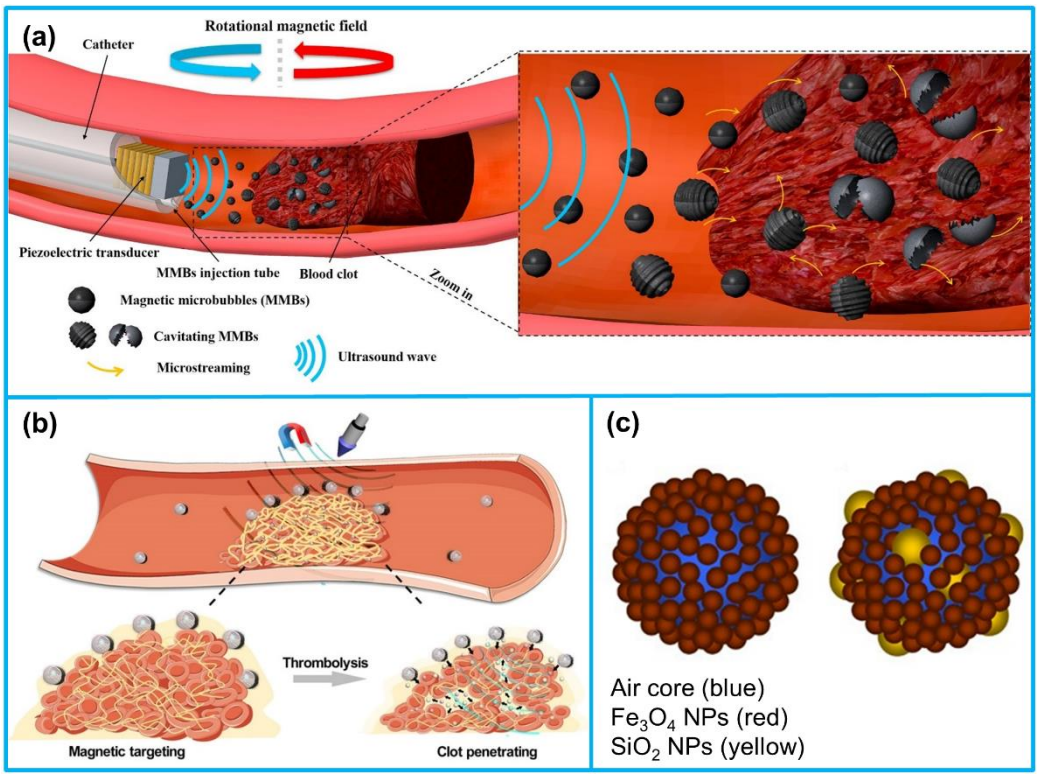

Figure 12. (a) Illustration of magnetic microbubbles (MMBs)-mediated sonothrombolysis. (b) Schematic view of SiO_2-tPA shelled MMBs for targeted tPA delivery and controlled release. (c) Composition of MMBs. (a) Reproduced with permission [245]. Copyright 2019, Elsevier. (b) Reproduced with permission [186]. Copyright 2020, American Association for the Advancement of Science. (c) Reproduced with permission [243]. Copyright 2016, Springer Nature.

3.3. Photoacoustic drug delivery and therapy

The PA imaging nanosized contrast agents have also been adopted by researchers as drug delivery vehicles since studies have found that the ultrasound irradiation generated by the PA effect could effectively accelerate the delivery and release of drugs in target tissues [246–248]. Furthermore, the local temperature rise of nanoparticles induced by the laser irradiation can cause thermal ablation and subsequent cancer cell death, i.e., photothermal therapy (PTT) [249]. The encapsulated drug release from nanocarriers can be promoted as well by the local heating generated in tumor tissues exposed to NIR laser irradiation [250,251].

3.3.1. Organic nanocarriers

Small molecular dyes and semiconducting polymer nanoparticles have also been commonly adopted for theranostic applications [252–258]. Gong et al. [259] reported a multifunctional nanomicelle fabricated by polyethylene glycol (PEG) coating and C18PMH conjugation for imaging-guided cancer therapy. Photosensitizer chlorin e6 (Ce6) was conjugated with C18PMH and photothermal agent IR825 was encapsulated into the nanomicelles. The resulted IR825@C18PMH-PEG-Ce6 nanomicelles could realize photoacoustic, fluorescence, and magnetic resonance triple modal imaging of tumors as well as combined photothermal and photodynamic therapy. Wang et al. [260] developed acid-switchable multifunctional nanomicelles for photothermal and chemotherapy of drug-resistant tumors. The nanomicelles were fabricated with PDPA-based polymeric matrix, which could cause dissociation of the nanostructures under acid condition. Photosensitizer Ce6 was conjugated with PDPA nanomicelles and DOX was loaded into the nanomicelles. The developed nanomicelles illustrated strong light absorption in the NIR region. Under NIR laser irradiation, the nanomicelles could effectively convert optical energy into local heat, which promoted PA imaging, drug penetration into tumor tissues as well as photothermal therapy. Cai et al. [261]

synthesized a diketopyrrolopyrrole (DPP)-triphenylamine (TPA) organic nanoagent for PA imaging-guided photodynamic/photothermal cancer therapy (**Figure 13a**). TPA, a commonly used donor, was conjugated with the DPP core to form a donor-acceptor- donor (D-A-D) structure. The nanoagent illustrated excellent NIR absorption, high photothermal conversion efficiency, and outstanding synergetic therapeutic effect due to the enhanced D-A-D structure of the DPP-TPA conjugation. Recently, Zhang et al. [262] developed electron donor-acceptor (D-A) conjugated semiconducting polymer nanoparticles (PPor-PEG NPs) for PA imaging-guided photothermal cancer therapy. The developed NPs could induce strong PA signals in tumor site for a long time, indicating the potential to be a long-term contrast agent. Additionally, the NPs showed a remarkedly high photothermal conversion efficiency 62.3%, the highest reported value among the reported polymer NPs.

Fan et al. [263] developed a novel multimodal imaging nanoplatform using ultra-small (~ 7.5 nm) water-soluble melanin nanoparticles (MNPs) (**Figure 13b**). The NPs not only demonstrated good photoacoustic properties for PA imaging but also illustrated natural binding ability with metal ions (Fe^{3+} and $^{64}Cu^{2+}$) for MRI and PET. Following that, Zhang et al. [264] developed a melanin nanoparticle-based nanosystem for PA imaging-guided chemotherapy. Anticancer drug, sorafenib (SRF), was bonded with melanin NPs to form a water-soluble nanoplatform, demonstrating great biocompatibility and PA property for imaging-guided therapy. The developed SRF-MNPs exhibited excellent tumor therapeutic effect after injection into the tail-vein of a living mice. Di et al. [248] recently developed an alginate sphere microgel encapsulated with DOX and CIF-loaded PLGA nanoparticles as a platform for laser ultrasound controlled drug delivery (**Figure 13c**). The drug release from the microgels was triggered by the laser generated pulsed ultrasound excitation that was transmitted from a laser-generated focused ultrasound transducer, made with a carbon black/PDMS-photoacoustic lens. Once the microgels were excited by the ultrasound waves,

cavitation effects were induced at the microgels, which accelerated the release of drugs from the nanoparticles.

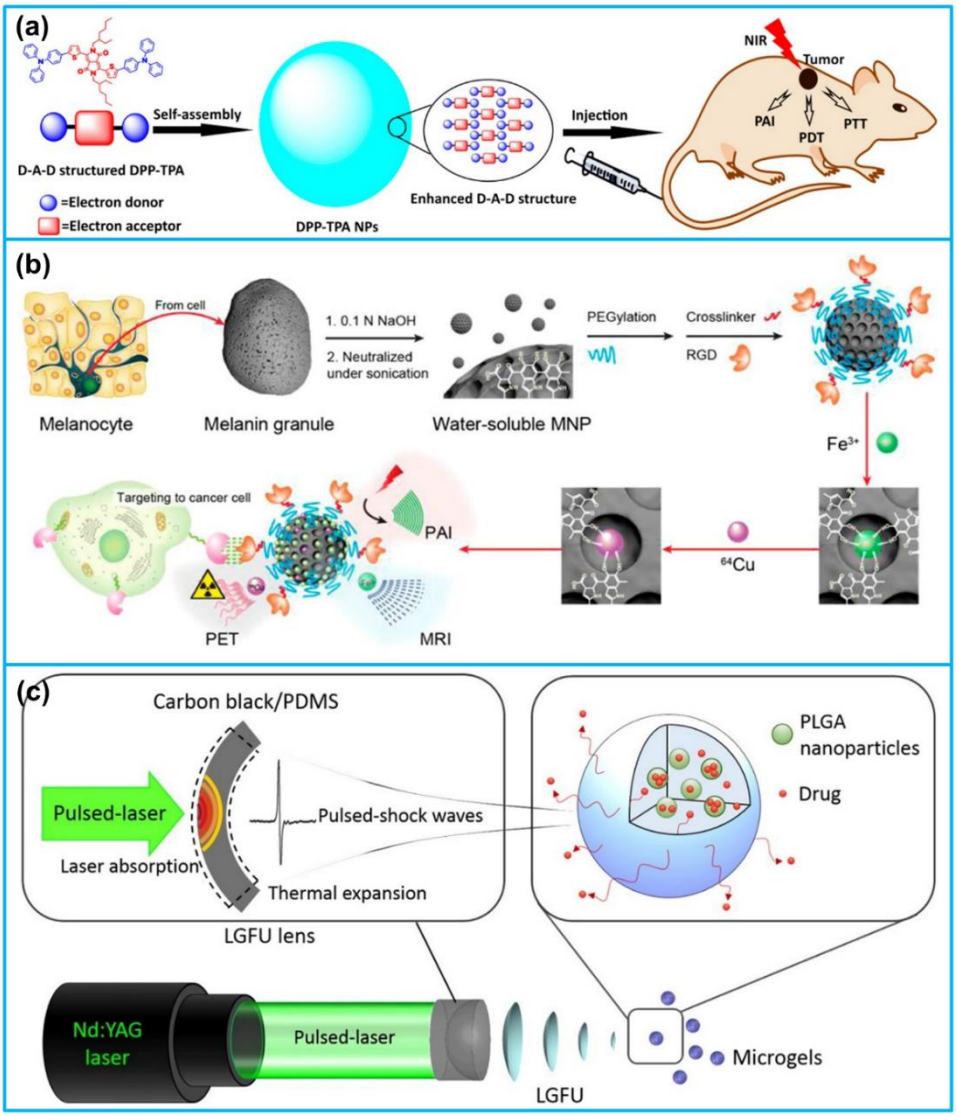

Figure 13. (a) D-A-D structured DPP-TPA NPs as theranostic agents for PA imaging-guided PDT/PTT. (b) Multimodality molecular imaging of MNPs. (c) Laser-generated-focused ultrasound-mediated drug delivery. (a) Reproduced with permission [261]. Copyright 2017, American Chemical Society. (b) Reproduced with permission [263]. Copyright 2014, American Chemical Society. (c) Reproduced with permission [248]. Copyright 2015, Elsevier.

3.3.2. Inorganic nanocarriers

(1) Metallic Nanomaterials. Numerous investigations have been demonstrated that metallic nanomaterials, especially AuNPs, can act as drug carriers for PA imaging-guided chemotherapy and PTT [215,265–267]. For instance, Wilson et al. [268] developed a photoacoustic nanodroplet composed of a liquid PFC core containing AuNRs and a bovine

serum albumin shell for combinational PA/ultrasound imaging and potential drug delivery. The nanodroplets could provide PA and ultrasound contrast improvement via the laser-induced vaporization of the liquid PFC nanodroplet and long duration thermal expansion of the AuNRs. Following that, Zhong et al. [269] designed a paclitaxel (PTX)-containing nanoparticle which was based on loading PTX and AuNRs into PFH nanodroplets for PA imaging-guided photothermal/chemo synergistic cancer therapy. Upon pulsed laser irradiation, the nanoparticle could be rapidly decomposed owing to PFH vaporization, resulting in fast drug release, which induced efficient apoptosis of cancer cells. Duan et al. [270] developed organic/inorganic nanohybrids consisting of AuNRs, quantum dots (QDs), mesoporous silica layer, and CD-PGEA for multimodal imaging-guided cancer therapy (**Figure 14a**). The AuNRs were integrated with QDs for combined PA, CT and fluorescent imaging. In addition, the high photothermal conversion efficiency of AuNRs facilitated them to be utilized for photothermal therapy. Antitumor drug, DOX, was loaded into the mesoporous structure of the silica layer and sealed by the CD-PGEA gatekeeper for both the drug and gene delivery.

Besides coating AuNRs with mesoporous silica, Huang et al. [271] synthesized a hollow-mesoporous nanocapsule consisting of AuNRs and iron oxide nanoparticles (IOs) for dual-modal PA imaging and MRI-guided synergistic photothermal/chemo tumor treatment (**Figure 14b**). The AuNRs was combined with the magnetic IOs via a yolk-shell structure, in which movable AuNRs were confined in the permeable IO nanoshells using silica templates. DOX was loaded into the mesoporous nanocapsule after the formation of the yolk-shell structure. Moon et al. [130] designed a new theranostic system composed of hollow nanostructured Au nanocages (AuNCs) and a phase-change material (PCM) (**Figure 14c**). Drugs were encapsulated into the PCM, and the PCM was functionalized as a gatekeeper to control the drug release corresponding to temperature rise. Two dyes used as drug models were loaded

into the PCM. Under HIFU irradiation, the PCM was melted and escaped from the interior of AuNCs, simultaneously releasing the encapsulated drugs.

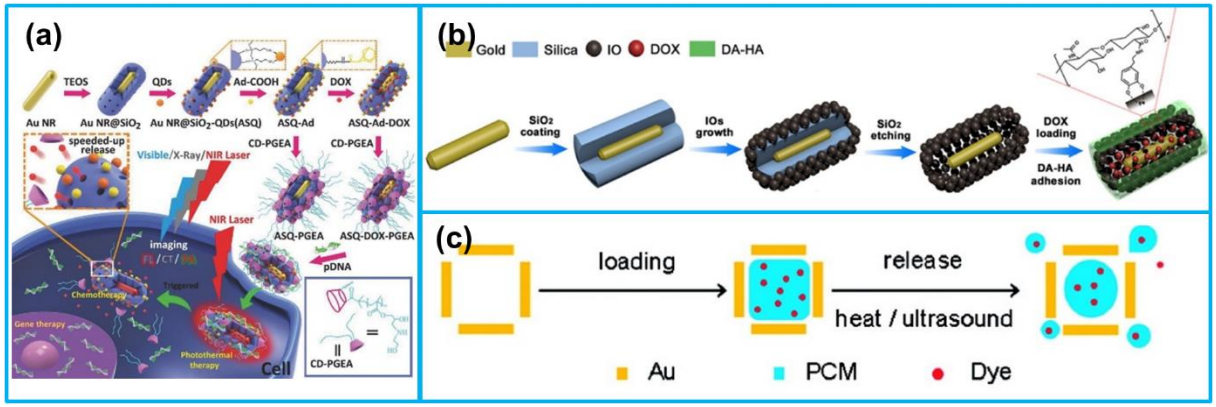

Figure 14. (a) Preparation processes of multimodal imaging-guided therapeutic platforms. (b) Preparation of GNR @ IOs-DOX nanocapsules. (c) Loading the hollow interior of an AuNC with a dye doped PCM and then releasing it from the AuNC. (a) Reproduced with permission [270]. Copyright 2016, Wiley-VCH. (b) Reproduced with permission [271]. Copyright 2016, American Chemical Society. (c) Reproduced with permission [130]. Copyright 2011, American Chemical Society.

Prussian blue, a clinical medicine approved by FDA, shows strong optical absorbance in the NIR region (650-900 nm) due to the charge transition between iron ions Fe^{2+} and Fe^{3+}. Recently, it has attracted interest for application in PA imaging and PTT [272–275]. Cai et al. [276] utilized hollow mesoporous Prussian blue NPs to develop a theranostic nanoplatform for ultrasound and PA dual-modal imaging-guided chemo-thermal cancer therapy. Anticancer drug, DOX, was loaded into the nanoparticles with relatively high loading capacity due to the mesoporous outer shell and big cavity. Since the drug loaded nanoparticles exhibited excellent photothermal conversion efficiency and high loading capacity, the Prussian blue-based nanoplatform opened a new avenue for chemo-thermal tumor therapy. Chen et al. [277] developed a dual-modal therapy platform fabricated by red blood cell membrane coated hollow mesoporous Prussian blue NPs for the combination of photothermal and chemotherapy. DOX was loaded into the NPs with a loading capacity up to 130%, resulting from the hollow mesoporous structure. Due to the photothermal effect, the DOX release from

the NPs was promoted by a NIR laser irradiation. In addition, the acidic tumor microenvironments could also accelerate the DOX release from the NPs.

Apart from metallic nanoparticles, transition metal-based nanomaterials have been reported as theranostic nanoagents for PA imaging-guided therapy as well. Bao et al. [278] synthesized hollow structure PEG-MoO_{3-x} nanospheres for PA imaging-guided chemo-photothermal cancer therapy. The hollow nanospheres had strong LSPR absorption in the NIR region, good biocompatibility, as well as high photothermal conversion efficiency. In addition, due to their large surface area and porous structure, anticancer drug could be loaded into them. Song et al. [279] synthesized polyacrylic acid functionalized Co_9Se_8 nanoplates for PA imaging and MRI-guided chemo-photothermal combinational cancer therapy. The nanoplates demonstrated strong NIR absorption spectrum, T_2 shortening effect, and good photothermal conversion efficiency. Moreover, due to the large surface area to mass ratio, the nanoplates could also act as drug nanocarriers for pH-responsive chemotherapy.

(2) Carbon-based nanomaterials. CNTs are also explored as drug delivery vehicles for cancer diagnostics and chemotherapies due to their unique properties. For example, Liu et al. [156] developed mesoporous silica (MS) coated SWNTs with polyethylene glycol (PEG) coating for imaging-guided cancer therapy. SWNTs provided strong contrast in both PA imaging and MRI. The PEG coating could improve the stability and solubility of the nanoparticles in a physiological environment. Anticancer drug, DOX, was loaded into the mesoporous structure of the synthesized SWNT@MS-PEG nanoparticle for chemotherapy. Using a low power of laser stimulation and a low dose of DOX, combined photothermal and chemotherapy of cancer tissues was achieved due to the accelerated nanoparticles penetration into cells and the light-triggered drug release.

rGO has an extremely high surface area and strong NIR absorption, and has very high potential to be utilized as a drug or gene delivery vehicle and as a photothermal agent for

cancer therapy [280]. For example, Song et al. [166] conjugated DOX with rGO first and then encapsulated of rGO-DOX conjugation in a gold nanorod vesicle (rGO-AuNRVe-DOX) for dual chemo-photothermal therapy. With a relatively low power density of laser irradiation (0.25 W/cm^2), the hybrid vesicle was disrupted and rGO-DOX and DOX was released from the vesicle due to the mild temperature rise in the tumor region with the vesicle injected. Moreover, the increased temperature also resulted in the improved intracellular uptake of DOX for chemotherapy.

3.3.3. Laser-generated ultrasound-accelerated thrombolysis

Due to its ability to generate high pressure and high frequency shock waves with tight focal spot, laser-generated ultrasound has recently been reported to be utilized for thrombolysis. Compared with existing thrombolysis techniques, the other advantages of laser-generated ultrasound includes its biocompatibility, low cost as well as high clot lysis rate. Kim et al. [281] firstly reported a laser-generated focused ultrasound (LGFU) transducer fabricated by a plano-concave glass lens coated with carbon black/PDMS thermoelastic layer. The transducer could generate shock waves with a central frequency of 14 MHz and peak negative pressure of ~ 12 MPa under a laser energy input of 20 mJ. Combined with 10^8/mL microbubble injection (100 μL/min for 30 min), 29% reduction of blood clot mass was achieved using the LGFU transducer for treatment. Following that, Wu et al. [282] developed a laser-generated ultrasound transducer consisting of candle soot nanoparticles-PDMS composite on an optical fiber for intravascular thrombolysis. It was showed that the fiber-optic laser ultrasound transducer had a central frequency of 6.8 MHz and peak negative pressure of 1.6 MPa under a laser fluence of 1.5 mJ/cm^2. Under the microbubble-mediated thrombolysis test, 32% reduction of blood clot mass was achieved. Most recently, Wu et al. [283] fabricated another fiber-optic laser ultrasound transducer, having the same structure as reported in [282]. The transducer had a central frequency and peak negative pressure of 5.8 MHz and 3.7 MPa,

respectively. At the same time of thrombolysis using the developed laser ultrasound transducer, the blood clot status was monitored using a 1064 nm laser source and a commercial linear array transducer based on PA imaging.

4. Conclusions and outlook

In this review, for the first time, the recent progress of nanoacoustics in biomedical imaging and therapy fields was comprehensively examined. The recent advancement made in exploring nanomaterials and nanostructures for biomedical ultrasound and photoacoustic imaging as well as ultrasound and photoacoustic therapies was reviewed in terms of nanomaterials, nanostructures and nanodevice implementations. Based on the literature survey, while many progresses have been made for translating basic scientific research outcomes into routine clinical applications, several obstacles hamper the advancement. Some recommendations for the development of nanoacoustics in biomedical imaging and therapy are outlined here.

Over the past decade, there's an increasing demand for miniaturized acoustic devices with the growing market shares of mobile devices and internet of things. While conventional piezoelectric acoustic devices currently still dominate the market, there has been extensive studies exploring capacitive micromachined ultrasonic transducers (CMUTs) and piezoelectric micromachined ultrasonic transducers (PMUTs) for various applications, especially for biomedical imaging and therapy. Compared with conventional piezoelectric transducers, one of the key benefits of CMUTs and PMUTs is their easy integration with integrated circuits. Other advantages include their batch production with submicron accuracy and uniformity, low power consumption and compact size.

Many reports focusing on nanosized contrast agents for ultrasound as well as photoacoustic imaging have appeared during the past few years, but the investigations about contrast agents are still largely confined to the research laboratory. While many different kinds of nanosized

contrast agent illustrate substantial advantages for imaging applications, the nanomaterials adopted usually possess shortcomings that need to be addressed, including relatively poor biocompatibility, requirements for large doses, low targeting efficiency, and difficulties in accurately quantifying agents. Clearly, many issues still exist and there remains a long road ahead for implementing nanosized contrast agents for clinical applications.

Ultrasound and photoacoustic-mediated drug delivery and therapy using various nanoparticles as drug delivery nanocarriers have demonstrated their great potentials for simultaneous biomedical imaging and synergistic chemotherapy and photoacoustic therapy. While the drug delivery systems fabricated by different nanoparticles are believed to be very promising for future therapeutics, especially oncotherapy, there still exist multiple challenges in the clinical translation of these nanoparticles. For example, although metallic NPs have been reported to have remarkable and tunable acoustic and optical properties, their long-term systemic cytotoxicity and biocompatibility have attracted much concerns from many researchers. In addition, in order to further advance ultrasound and photoacoustic-mediated therapeutic delivery strategies, developing a platform that can monitor the acoustic effect and quantify the drugs delivered into the target tissue in a real-time manner is considered to be very necessary and important. This is particularly crucial for tumor treatment since the tissue-related heterogeneity during drug delivery may bring about incomplete treatment and cancer recurrence.

Declaration of competing interest

Xiaoning Jiang has a financial interest in SonoVascular, Inc., who licensed an intravascular sonothrombolysis technology from North Carolina State University.

Acknowledgments

The authors would like to acknowledge the financial support from the National Institutes of Health under the grants R01HL141967, R41HL154735, and R21EB027304; Office of Naval

Research under the grant N00014-18-1-2538; and Department of Energy under the grant DE-NE0008708.

References

[1] A.G. Cuenca, H. Jiang, S.N. Hochwald, M. Delano, W.G. Cance, S.R. Grobmyer, Emerging implications of nanotechnology on cancer diagnostics and therapeutics, Cancer. 107 (2006) 459–466.

[2] O.C. Farokhzad, R. Langer, Nanomedicine: developing smarter therapeutic and diagnostic modalities, Adv. Drug Deliv. Rev. 58 (2006) 1456–1459.

[3] S. Nie, Y. Xing, G.J. Kim, J.W. Simons, Nanotechnology applications in cancer, Annu. Rev. Biomed. Eng. 9 (2007) 257–288.

[4] X. Wang, L. Yang, Z. Chen, D.M. Shin, Application of nanotechnology in cancer therapy and imaging, CA. Cancer J. Clin. 58 (2008) 97–110.

[5] J.A. Barreto, W. O'Malley, M. Kubeil, B. Graham, H. Stephan, L. Spiccia, Nanomaterials: applications in cancer imaging and therapy, Adv. Mater. 23 (2011) H18–H40.

[6] K.K. Shung, Diagnostic ultrasound: Past, present, and future, J Med Biol Eng. 31 (2011) 371–374.

[7] F. Kiessling, S. Fokong, J. Bzyl, W. Lederle, M. Palmowski, T. Lammers, Recent advances in molecular, multimodal and theranostic ultrasound imaging, Adv. Drug Deliv. Rev. 72 (2014) 15–27. doi:10.1016/j.addr.2013.11.013.

[8] Q. Cai, C. Peng, J.C. Prieto, A.J. Rosenbaum, J.S.A. Stringer, X. Jiang, A Low-Cost Camera-Based Ultrasound Probe Tracking System: Design and Prototype, in: 2019 IEEE Int. Ultrason. Symp., IEEE, 2019: pp. 997–999.

[9] Q. Cai, J. Lu, C. Peng, J.C. Prieto, A.J. Rosenbaum, J.S.A. Stringer, X. Jiang, Spatial Calibration for 3D Freehand Ultrasound via Independent General Motions, in: 2020 IEEE Int. Ultrason. Symp., IEEE, 2020: pp. 1–3.

[10] J. Hu, H. Kim, Q. Cai, C. Peng, M. Chen, J.C. Prieto, A.J. Rosenbaum, J.S.A. Stringer, X. Jiang, Fusion of Ultrasonic Tracking with an Inertial Measurement Unit for High-Accuracy 3D Space Localization, in: 2020 IEEE Int. Ultrason. Symp., IEEE, 2020: pp. 1–4.

[11] Q. Cai, C. Peng, J. Lu, J.C. Prieto, A.J. Rosenbaum, J.S.A. Stringer, X. Jiang, Performance Enhanced Ultrasound Probe Tracking with a Hemispherical Marker Rigid

Body, IEEE Trans. Ultrason. Ferroelectr. Freq. Control. (2021).

[12] R.H. Perera, C. Hernandez, H. Zhou, P. Kota, A. Burke, A.A. Exner, Ultrasound imaging beyond the vasculature with new generation contrast agents, Wiley Interdiscip. Rev. Nanomedicine Nanobiotechnology. 7 (2015) 593–608. doi:10.1002/wnan.1326.

[13] C. Peng, M. Chen, H. Wang, J. Shen, X. Jiang, Broadband Piezoelectric Transducers for Under-Display Ultrasonic Fingerprint Sensing Applications, IEEE Trans. Ind. Electron. (2020).

[14] C. Peng, M. Chen, H. Wang, J. Shen, X. Jiang, P (VDF TrFE) Thin Film Based Transducer for Under Display Ultrasonic Fingerprint Sensing Applications, IEEE Sens. J. (2020).

[15] C. Peng, M. Chen, X. Jiang, Under-Display Ultrasonic Fingerprint Recognition with Finger Vessel Imaging, IEEE Sens. J. (2021).

[16] L. Abou-Elkacem, S. V. Bachawal, J.K. Willmann, Ultrasound molecular imaging: Moving toward clinical translation, Eur. J. Radiol. 84 (2015) 1685–1693. doi:10.1016/j.ejrad.2015.03.016.

[17] N. Deshpande, A. Needles, J.K. Willmann, Molecular ultrasound imaging: current status and future directions, Clin. Radiol. 65 (2010) 567–581. doi:10.1016/j.crad.2010.02.013.

[18] A.L. Klibanov, Ligand-carrying gas-filled microbubbles: ultrasound contrast agents for targeted molecular imaging, Bioconjug. Chem. 16 (2005) 9–17.

[19] S. Ibsen, C.E. Schutt, S. Esener, Microbubble-mediated ultrasound therapy: a review of its potential in cancer treatment, Drug Des. Devel. Ther. 7 (2013) 375.

[20] N. de Jong, L. Hoff, T. Skotland, N. Bom, Absorption and scatter of encapsulated gas filled microspheres: theoretical considerations and some measurements, Ultrasonics. 30 (1992) 95–103.

[21] H. Wu, N.G. Rognin, T.M. Krupka, L. Solorio, H. Yoshiara, G. Guenette, C. Sanders, N. Kamiyama, A.A. Exner, Acoustic characterization and pharmacokinetic analyses of new nanobubble ultrasound contrast agents, Ultrasound Med. Biol. 39 (2013) 2137–2146.

[22] R.H. Perera, L. Solorio, H. Wu, M. Gangolli, E. Silverman, C. Hernandez, P.M. Peiris, A.-M. Broome, A.A. Exner, Nanobubble ultrasound contrast agents for enhanced delivery of thermal sensitizer to tumors undergoing radiofrequency ablation, Pharm. Res. 31 (2014) 1407–1417.

[23] Y. Wang, X. Li, Y. Zhou, P. Huang, Y. Xu, Preparation of nanobubbles for ultrasound imaging and intracelluar drug delivery, Int. J. Pharm. 384 (2010) 148–153.

[24] B.E. Oeffinger, M.A. Wheatley, Development and characterization of a nano-scale contrast agent, Ultrasonics. 42 (2004) 343–347.

[25] N. Güvener, L. Appold, F. de Lorenzi, S.K. Golombek, L.Y. Rizzo, T. Lammers, F. Kiessling, Recent advances in ultrasound-based diagnosis and therapy with micro-and nanometer-sized formulations, Methods. 130 (2017) 4–13.

[26] H. Tang, Y. Zheng, Y. Chen, Materials chemistry of nanoultrasonic biomedicine, Adv. Mater. 29 (2017) 1604105.

[27] E. Huynh, M.A. Rajora, G. Zheng, Multimodal micro, nano, and size conversion ultrasound agents for imaging and therapy, Wiley Interdiscip. Rev. Nanomedicine Nanobiotechnology. 8 (2016) 796–813.

[28] R.H. Perera, C. Hernandez, H. Zhou, P. Kota, A. Burke, A.A. Exner, Ultrasound imaging beyond the vasculature with new generation contrast agents, Wiley Interdiscip. Rev. Nanomedicine Nanobiotechnology. 7 (2015) 593–608.

[29] A. Zlitni, S.S. Gambhir, Molecular imaging agents for ultrasound, Curr. Opin. Chem. Biol. 45 (2018) 113–120. doi:10.1016/j.cbpa.2018.03.017.

[30] X. Qian, X. Han, Y. Chen, Insights into the unique functionality of inorganic micro/nanoparticles for versatile ultrasound theranostics, Biomaterials. 142 (2017) 13–30.

[31] H. Yang, W. Cai, L. Xu, X. Lv, Y. Qiao, P. Li, H. Wu, Y. Yang, L. Zhang, Y. Duan, Nanobubble–Affibody: Novel ultrasound contrast agents for targeted molecular ultrasound imaging of tumor, Biomaterials. 37 (2015) 279–288.

[32] X. Fan, L. Wang, Y. Guo, Z. Tu, L. Li, H. Tong, Y. Xu, R. Li, K. Fang, Ultrasonic nanobubbles carrying anti-PSMA nanobody: construction and application in prostate cancer-targeted imaging, PLoS One. 10 (2015) e0127419.

[33] Q. Jiang, S. Hao, X. Xiao, J. Yao, B. Ou, Z. Zhao, F. Liu, X. Pan, B. Luo, H. Zhi, Production and characterization of a novel long-acting Herceptin-targeted nanobubble contrast agent specific for Her-2-positive breast cancers, Breast Cancer. 23 (2016) 445–455.

[34] Y. Gao, C. Hernandez, H.-X. Yuan, J. Lilly, P. Kota, H. Zhou, H. Wu, A.A. Exner, Ultrasound molecular imaging of ovarian cancer with CA-125 targeted nanobubble contrast agents, Nanomedicine Nanotechnology, Biol. Med. 13 (2017) 2159–2168.

[35] R.H. Perera, H. Wu, P. Peiris, C. Hernandez, A. Burke, H. Zhang, A.A. Exner, Improving performance of nanoscale ultrasound contrast agents using N, N-diethylacrylamide stabilization, Nanomedicine Nanotechnology, Biol. Med. 13 (2017) 59–67.

[36] K. Li, Y. Liu, S. Zhang, Y. Xu, J. Jiang, F. Yin, Y. Hu, B. Han, S. Ge, L. Zhang, Folate receptor-targeted ultrasonic PFOB nanoparticles: Synthesis, characterization and application in tumor-targeted imaging, Int. J. Mol. Med. 39 (2017) 1505–1515.

[37] J. Liu, T. Shang, F. Wang, Y. Cao, L. Hao, J. Ren, H. Ran, Z. Wang, P. Li, Z. Du, Low-intensity focused ultrasound (LIFU)-induced acoustic droplet vaporization in phase-transition perfluoropentane nanodroplets modified by folate for ultrasound molecular imaging, Int. J. Nanomedicine. 12 (2017) 911.

[38] D. Choi, S. Jeon, D.G. You, W. Um, J.-Y. Kim, H.Y. Yoon, H. Chang, D.-E. Kim, J.H. Park, H. Kim, Iodinated echogenic glycol chitosan nanoparticles for X-ray CT/US dual imaging of tumor, Nanotheranostics. 2 (2018) 117.

[39] Y. Xu, C. Niu, S. An, S. Tang, P. Xiao, Q. Peng, L. Wang, Thermal-sensitive magnetic nanoparticles for dual-modal tumor imaging and therapy, RSC Adv. 7 (2017) 40791–40802.

[40] A.S. Hannah, G.P. Luke, S.Y. Emelianov, Blinking phase-change nanocapsules enable background-free ultrasound imaging, Theranostics. 6 (2016) 1866.

[41] L. Yang, J. Cheng, Y. Chen, S. Yu, F. Liu, Y. Sun, Y. Chen, H. Ran, Phase-transition nanodroplets for real-time photoacoustic/ultrasound dual-modality imaging and photothermal therapy of sentinel lymph node in breast cancer, Sci. Rep. 7 (2017) 45213.

[42] Y. Cheng, H. Cheng, C. Jiang, X. Qiu, K. Wang, W. Huan, A. Yuan, J. Wu, Y. Hu, Perfluorocarbon nanoparticles enhance reactive oxygen levels and tumour growth inhibition in photodynamic therapy, Nat. Commun. 6 (2015) 1–8.

[43] Y. Zhou, R. Wang, Z. Teng, Z. Wang, B. Hu, M. Kolios, H. Chen, N. Zhang, Y. Wang, P. Li, Magnetic nanoparticle-promoted droplet vaporization for in vivo stimuli-responsive cancer theranostics, NPG Asia Mater. 8 (2016) e313–e313.

[44] K. Zhang, P. Li, H. Chen, X. Bo, X. Li, H. Xu, Continuous cavitation designed for enhancing radiofrequency ablation via a special radiofrequency solidoid vaporization process, ACS Nano. 10 (2016) 2549–2558.

[45] J. Xu, Y. Chen, L. Deng, J. Liu, Y. Cao, P. Li, H. Ran, Y. Zheng, Z. Wang,

Microwave-activated nanodroplet vaporization for highly efficient tumor ablation with real-time monitoring performance, Biomaterials. 106 (2016) 264–275.

[46] H.S. Min, S. Son, D.G. You, T.W. Lee, J. Lee, S. Lee, J.Y. Yhee, J. Lee, M.H. Han, J.H. Park, Chemical gas-generating nanoparticles for tumor-targeted ultrasound imaging and ultrasound-triggered drug delivery, Biomaterials. 108 (2016) 57–70.

[47] C. Kang, W. Cho, M. Park, J. Kim, S. Park, D. Shin, C. Song, D. Lee, H2O2-triggered bubble generating antioxidant polymeric nanoparticles as ischemia/reperfusion targeted nanotheranostics, Biomaterials. 85 (2016) 195–203.

[48] N. Zhang, J. Li, R. Hou, J. Zhang, P. Wang, X. Liu, Z. Zhang, Bubble-generating nano-lipid carriers for ultrasound/CT imaging-guided efficient tumor therapy, Int. J. Pharm. 534 (2017) 251–262.

[49] M. Kim, J.H. Lee, S.E. Kim, S.S. Kang, G. Tae, Nanosized ultrasound enhanced-contrast agent for in vivo tumor imaging via intravenous injection, ACS Appl. Mater. Interfaces. 8 (2016) 8409–8418.

[50] Q. Feng, W. Zhang, X. Yang, Y. Li, Y. Hao, H. Zhang, L. Hou, Z. Zhang, pH/Ultrasound Dual-Responsive Gas Generator for Ultrasound Imaging-Guided Therapeutic Inertial Cavitation and Sonodynamic Therapy, Adv. Healthc. Mater. 7 (2018) 1700957.

[51] J. Lee, H.-S. Min, D.G. You, K. Kim, I.C. Kwon, T. Rhim, K.Y. Lee, Theranostic gas-generating nanoparticles for targeted ultrasound imaging and treatment of neuroblastoma, J. Control. Release. 223 (2016) 197–206.

[52] K.H. Min, H.S. Min, H.J. Lee, D.J. Park, J.Y. Yhee, K. Kim, I.C. Kwon, S.Y. Jeong, O.F. Silvestre, X. Chen, pH-controlled gas-generating mineralized nanoparticles: a theranostic agent for ultrasound imaging and therapy of cancers, ACS Nano. 9 (2015) 134–145.

[53] X. Wang, D. Niu, P. Li, Q. Wu, X. Bo, B. Liu, S. Bao, T. Su, H. Xu, Q. Wang, Dual-enzyme-loaded multifunctional hybrid nanogel system for pathological responsive ultrasound imaging and T 2-weighted magnetic resonance imaging, ACS Nano. 9 (2015) 5646–5656.

[54] S. Gao, G. Wang, Z. Qin, X. Wang, G. Zhao, Q. Ma, L. Zhu, Oxygen-generating hybrid nanoparticles to enhance fluorescent/photoacoustic/ultrasound imaging guided tumor photodynamic therapy, Biomaterials. 112 (2017) 324–335.

[55] S. Casciaro, F. Conversano, A. Ragusa, M.A. Malvindi, R. Franchini, A. Greco, T.

Pellegrino, G. Gigli, Optimal enhancement configuration of silica nanoparticles for ultrasound imaging and automatic detection at conventional diagnostic frequencies, Invest. Radiol. 45 (2010) 715–724.

[56] H. Hu, H. Zhou, J. Du, Z. Wang, L. An, H. Yang, F. Li, H. Wu, S. Yang, Biocompatiable hollow silica microspheres as novel ultrasound contrast agents for in vivo imaging, J. Mater. Chem. 21 (2011) 6576–6583.

[57] H.P. Martinez, Y. Kono, S.L. Blair, S. Sandoval, J. Wang-Rodriguez, R.F. Mattrey, A.C. Kummel, W.C. Trogler, Hard shell gas-filled contrast enhancement particles for colour Doppler ultrasound imaging of tumors, Medchemcomm. 1 (2010) 266–270.

[58] A. Milgroom, M. Intrator, K. Madhavan, L. Mazzaro, R. Shandas, B. Liu, D. Park, Mesoporous silica nanoparticles as a breast-cancer targeting ultrasound contrast agent, Colloids Surfaces B Biointerfaces. 116 (2014) 652–657.

[59] Q. Jin, C.-Y. Lin, S.-T. Kang, Y.-C. Chang, H. Zheng, C.-M. Yang, C.-K. Yeh, Superhydrophobic silica nanoparticles as ultrasound contrast agents, Ultrason. Sonochem. 36 (2017) 262–269.

[60] K. Zhang, H. Chen, X. Guo, D. Zhang, Y. Zheng, H. Zheng, J. Shi, Double-scattering/reflection in a single nanoparticle for intensified ultrasound imaging, Sci. Rep. 5 (2015) 1–11.

[61] F. Chen, M. Ma, J. Wang, F. Wang, S.-X. Chern, E.R. Zhao, A. Jhunjhunwala, S. Darmadi, H. Chen, J. V Jokerst, Exosome-like silica nanoparticles: a novel ultrasound contrast agent for stem cell imaging, Nanoscale. 9 (2017) 402–411.

[62] A. Liberman, J. Wang, N. Lu, R.D. Viveros, C.A. Allen, R.F. Mattrey, S.L. Blair, W.C. Trogler, M.J. Kim, A.C. Kummel, Mechanically tunable hollow silica ultrathin nanoshells for ultrasound contrast agents, Adv. Funct. Mater. 25 (2015) 4049–4057.

[63] Y. Sun, Y. Wang, C. Niu, E.M. Strohm, Y. Zheng, H. Ran, R. Huang, D. Zhou, Y. Gong, Z. Wang, Laser-activatible PLGA microparticles for image-guided cancer therapy in vivo, Adv. Funct. Mater. 24 (2014) 7674–7680.

[64] H. Ke, J. Wang, S. Tong, Y. Jin, S. Wang, E. Qu, G. Bao, Z. Dai, Gold nanoshelled liquid perfluorocarbon magnetic nanocapsules: a nanotheranostic platform for bimodal ultrasound/magnetic resonance imaging guided photothermal tumor ablation, Theranostics. 4 (2014) 12.

[65] P. Prasad, C.R. Gordijo, A.Z. Abbasi, A. Maeda, A. Ip, A.M. Rauth, R.S. DaCosta, X.Y. Wu, Multifunctional albumin–MnO2 nanoparticles modulate solid tumor

microenvironment by attenuating hypoxia, acidosis, vascular endothelial growth factor and enhance radiation response, ACS Nano. 8 (2014) 3202–3212.

[66] F. Yang, S. Hu, Y. Zhang, X. Cai, Y. Huang, F. Wang, S. Wen, G. Teng, N. Gu, A Hydrogen Peroxide-Responsive O2 Nanogenerator for Ultrasound and Magnetic-Resonance Dual Modality Imaging, Adv. Mater. 24 (2012) 5205–5211.

[67] X. Jia, X. Cai, Y. Chen, S. Wang, H. Xu, K. Zhang, M. Ma, H. Wu, J. Shi, H. Chen, Perfluoropentane-encapsulated hollow mesoporous prussian blue nanocubes for activated ultrasound imaging and photothermal therapy of cancer, ACS Appl. Mater. Interfaces. 7 (2015) 4579–4588.

[68] L.G. Delogu, G. Vidili, E. Venturelli, C. Ménard-Moyon, M.A. Zoroddu, G. Pilo, P. Nicolussi, C. Ligios, D. Bedognetti, F. Sgarrella, Functionalized multiwalled carbon nanotubes as ultrasound contrast agents, Proc. Natl. Acad. Sci. 109 (2012) 16612–16617.

[69] H. Wu, H. Shi, H. Zhang, X. Wang, Y. Yang, C. Yu, C. Hao, J. Du, H. Hu, S. Yang, Prostate stem cell antigen antibody-conjugated multiwalled carbon nanotubes for targeted ultrasound imaging and drug delivery, Biomaterials. 35 (2014) 5369–5380.

[70] A.E. Walsby, Gas vesicles, Microbiol. Mol. Biol. Rev. 58 (1994) 94–144.

[71] F. Pfeifer, Distribution, formation and regulation of gas vesicles, Nat. Rev. Microbiol. 10 (2012) 705.

[72] M.G. Shapiro, P.W. Goodwill, A. Neogy, M. Yin, F.S. Foster, D. V Schaffer, S.M. Conolly, Biogenic gas nanostructures as ultrasonic molecular reporters, Nat. Nanotechnol. 9 (2014) 311.

[73] E. Cherin, J.M. Melis, R.W. Bourdeau, M. Yin, D.M. Kochmann, F.S. Foster, M.G. Shapiro, Acoustic behavior of Halobacterium salinarum gas vesicles in the high-frequency range: experiments and modeling, Ultrasound Med. Biol. 43 (2017) 1016–1030.

[74] S. Zhang, A. Huang, A. Bar-Zion, J. Wang, O.V. Mena, M.G. Shapiro, J. Friend, The Vibration Behavior of Sub-Micrometer Gas Vesicles in Response to Acoustic Excitation Determined via Laser Doppler Vibrometry, Adv. Funct. Mater. 30 (2020) 2000239.

[75] A. Lakshmanan, A. Farhadi, S.P. Nety, A. Lee-Gosselin, R.W. Bourdeau, D. Maresca, M.G. Shapiro, Molecular engineering of acoustic protein nanostructures, ACS Nano. 10 (2016) 7314–7322.

[76] A. Lakshmanan, G.J. Lu, A. Farhadi, S.P. Nety, M. Kunth, A. Lee-Gosselin, D. Maresca, R.W. Bourdeau, M. Yin, J. Yan, Preparation of biogenic gas vesicle nanostructures for use as contrast agents for ultrasound and MRI, Nat. Protoc. 12 (2017) 2050.

[77] J. Le Floc'h, A. Zlitni, H.A. Bilton, M. Yin, A. Farhadi, N.R. Janzen, M.G. Shapiro, J.F. Valliant, F.S. Foster, In vivo Biodistribution of Radiolabeled Acoustic Protein Nanostructures, Mol. Imaging Biol. 20 (2018) 230–239.

[78] D. Maresca, A. Lakshmanan, A. Lee-Gosselin, J.M. Melis, Y.-L. Ni, R.W. Bourdeau, D.M. Kochmann, M.G. Shapiro, Nonlinear ultrasound imaging of nanoscale acoustic biomolecules, Appl. Phys. Lett. 110 (2017) 73704.

[79] J. Yan, M. Yin, F.S. Foster, C.E.M. Démoré, Tumor contrast imaging with gas vesicles by circumventing the reticuloendothelial system, Ultrasound Med. Biol. 46 (2020) 359–368.

[80] G.J. Lu, L. Chou, D. Malounda, A.K. Patel, D.S. Welsbie, D.L. Chao, T. Ramalingam, M.G. Shapiro, Genetically encodable contrast agents for optical coherence tomography, ACS Nano. (2020).

[81] R.W. Bourdeau, A. Lee-Gosselin, A. Lakshmanan, A. Farhadi, S.R. Kumar, S.P. Nety, M.G. Shapiro, Acoustic reporter genes for noninvasive imaging of microorganisms in mammalian hosts, Nature. 553 (2018) 86.

[82] A. Farhadi, G.H. Ho, D.P. Sawyer, R.W. Bourdeau, M.G. Shapiro, Ultrasound imaging of gene expression in mammalian cells, Science (80-.). 365 (2019) 1469–1475.

[83] G.J. Lu, A. Farhadi, A. Mukherjee, M.G. Shapiro, Proteins, air and water: reporter genes for ultrasound and magnetic resonance imaging, Curr. Opin. Chem. Biol. 45 (2018) 57–63. doi:10.1016/j.cbpa.2018.02.011.

[84] D. Wu, L. Huang, M.S. Jiang, H. Jiang, Contrast agents for photoacoustic and thermoacoustic imaging: a review, Int. J. Mol. Sci. 15 (2014) 23616–23639.

[85] S. Wang, J. Lin, T. Wang, X. Chen, P. Huang, Recent advances in photoacoustic imaging for deep-tissue biomedical applications, Theranostics. 6 (2016) 2394.

[86] S. Gargiulo, S. Albanese, M. Mancini, State-of-the-Art preclinical photoacoustic imaging in oncology: recent advances in cancer theranostics, Contrast Media Mol. Imaging. 2019 (2019).

[87] S.W. Yoo, D. Jung, J.-J. Min, H. Kim, C. Lee, Biodegradable contrast agents for photoacoustic imaging, Appl. Sci. 8 (2018) 1567.

[88] Y. Zhang, M. Jeon, L.J. Rich, H. Hong, J. Geng, Y. Zhang, S. Shi, T.E. Barnhart, P. Alexandridis, J.D. Huizinga, Non-invasive multimodal functional imaging of the intestine with frozen micellar naphthalocyanines, Nat. Nanotechnol. 9 (2014) 631.

[89] D. Lee, C. Lee, S. Kim, Q. Zhou, J. Kim, C. Kim, In vivo near infrared virtual intraoperative surgical photoacoustic optical coherence tomography, Sci. Rep. 6 (2016) 35176.

[90] K. Park, J.Y. Kim, C. Lee, S. Jeon, G. Lim, C. Kim, Handheld photoacoustic microscopy probe, Sci. Rep. 7 (2017) 1–15.

[91] S. Hu, L. V Wang, Neurovascular photoacoustic tomography, Front. Neuroenergetics. 2 (2010) 10.

[92] J. Yao, K.I. Maslov, Y. Zhang, Y. Xia, L. V Wang, Label-free oxygen-metabolic photoacoustic microscopy in vivo, J. Biomed. Opt. 16 (2011) 76003.

[93] C. Zhang, L. V Wang, Y.-J. Cheng, J. Chen, S.A. Wickline, Label-free photoacoustic microscopy of myocardial sheet architecture, J. Biomed. Opt. 17 (2012) 60506.

[94] Y. Zhou, W. Xing, K.I. Maslov, L.A. Cornelius, L. V Wang, Handheld photoacoustic microscopy to detect melanoma depth in vivo, Opt. Lett. 39 (2014) 4731–4734.

[95] L. V Wang, Multiscale photoacoustic microscopy and computed tomography, Nat. Photonics. 3 (2009) 503.

[96] M. Xu, L. V. Wang, Photoacoustic imaging in biomedicine, Rev. Sci. Instrum. 77 (2006) 041101. doi:10.1063/1.2195024.

[97] J. Weber, P.C. Beard, S.E. Bohndiek, Contrast agents for molecular photoacoustic imaging, Nat. Methods. 13 (2016) 639–650.

[98] Q. Fan, K. Cheng, Z. Yang, R. Zhang, M. Yang, X. Hu, X. Ma, L. Bu, X. Lu, X. Xiong, Perylene-diimide-based nanoparticles as highly efficient photoacoustic agents for deep brain tumor imaging in living mice, Adv. Mater. 27 (2015) 843–847.

[99] M.F. Kircher, A. De La Zerda, J. V Jokerst, C.L. Zavaleta, P.J. Kempen, E. Mittra, K. Pitter, R. Huang, C. Campos, F. Habte, A brain tumor molecular imaging strategy using a new triple-modality MRI-photoacoustic-Raman nanoparticle, Nat. Med. 18 (2012) 829–834.

[100] J. Liu, X. Cai, H. Pan, A. Bandla, C.K. Chuan, S. Wang, N. Thakor, L. Liao, B. Liu, Molecular engineering of photoacoustic performance by chalcogenide variation in conjugated polymer nanoparticles for brain vascular imaging, Small. 14 (2018) 1703732.

[101] C. Liu, J. Chen, Y. Zhu, X. Gong, R. Zheng, N. Chen, D. Chen, H. Yan, P. Zhang, H. Zheng, Highly sensitive MoS 2–indocyanine green hybrid for photoacoustic imaging of orthotopic brain glioma at deep site, Nano-Micro Lett. 10 (2018) 48.

[102] J. Kang, D. Kim, J. Wang, Y. Han, J.M. Zuidema, A. Hariri, J. Park, J. V Jokerst, M.J. Sailor, Enhanced performance of a molecular photoacoustic imaging agent by encapsulation in mesoporous silicon nanoparticles, Adv. Mater. 30 (2018) 1800512.

[103] C. Wu, Y. Zhang, Z. Li, C. Li, Q. Wang, A novel photoacoustic nanoprobe of ICG@ PEG-Ag 2 S for atherosclerosis targeting and imaging in vivo, Nanoscale. 8 (2016) 12531–12539.

[104] E. Jung, C. Kang, J. Lee, D. Yoo, D.W. Hwang, D. Kim, S.-C. Park, S.K. Lim, C. Song, D. Lee, Molecularly engineered theranostic nanoparticles for thrombosed vessels: H2O2-activatable contrast-enhanced photoacoustic imaging and antithrombotic therapy, ACS Nano. 12 (2018) 392–401.

[105] C. Cui, Z. Yang, X. Hu, J. Wu, K. Shou, H. Ma, C. Jian, Y. Zhao, B. Qi, X. Hu, Organic semiconducting nanoparticles as efficient photoacoustic agents for lightening early thrombus and monitoring thrombolysis in living mice, ACS Nano. 11 (2017) 3298–3310.

[106] G.P. Luke, A. Bashyam, K.A. Homan, S. Makhija, Y.-S. Chen, S.Y. Emelianov, Silica-coated gold nanoplates as stable photoacoustic contrast agents for sentinel lymph node imaging, Nanotechnology. 24 (2013) 455101.

[107] K. Pu, A.J. Shuhendler, J. V Jokerst, J. Mei, S.S. Gambhir, Z. Bao, J. Rao, Semiconducting polymer nanoparticles as photoacoustic molecular imaging probes in living mice, Nat. Nanotechnol. 9 (2014) 233.

[108] X. Cai, X. Liu, L. Liao, A. Bandla, J.M. Ling, Y. Liu, N. Thakor, G.C. Bazan, B. Liu, Encapsulated conjugated oligomer nanoparticles for real-time photoacoustic sentinel lymph node imaging and targeted photothermal therapy, Small. 12 (2016) 4873–4880.

[109] D.Y. Santiesteban, D.S. Dumani, D. Profili, S.Y. Emelianov, Copper sulfide perfluorocarbon nanodroplets as clinically relevant photoacoustic/ultrasound imaging agents, Nano Lett. 17 (2017) 5984–5989.

[110] H.J. Knox, T.W. Kim, Z. Zhu, J. Chan, Photophysical tuning of N-oxide-based probes enables ratiometric photoacoustic imaging of tumor hypoxia, ACS Chem. Biol. 13 (2018) 1838–1843.

[111] Q. Chen, X. Liu, J. Chen, J. Zeng, Z. Cheng, Z. Liu, A self-assembled albumin-based

nanoprobe for in vivo ratiometric photoacoustic pH imaging, Adv. Mater. 27 (2015) 6820–6827.

[112] Q. Miao, Y. Lyu, D. Ding, K. Pu, Semiconducting oligomer nanoparticles as an activatable photoacoustic probe with amplified brightness for in vivo imaging of pH, Adv. Mater. 28 (2016) 3662–3668.

[113] K.J. Cash, C. Li, J. Xia, L. V Wang, H.A. Clark, Optical drug monitoring: photoacoustic imaging of nanosensors to monitor therapeutic lithium in vivo, ACS Nano. 9 (2015) 1692–1698.

[114] Y. Liu, S. Wang, Y. Ma, J. Lin, H. Wang, Y. Gu, X. Chen, P. Huang, Ratiometric photoacoustic molecular imaging for methylmercury detection in living subjects, Adv. Mater. 29 (2017) 1606129.

[115] Q. Fu, R. Zhu, J. Song, H. Yang, X. Chen, Photoacoustic imaging: contrast agents and their biomedical applications, Adv. Mater. 31 (2019) 1805875.

[116] W. Tang, Z. Yang, S. Wang, Z. Wang, J. Song, G. Yu, W. Fan, Y. Dai, J. Wang, L. Shan, Organic semiconducting photoacoustic nanodroplets for laser-activatable ultrasound imaging and combinational cancer therapy, ACS Nano. 12 (2018) 2610–2622.

[117] E. Petryayeva, U.J. Krull, Localized surface plasmon resonance: Nanostructures, bioassays and biosensing—A review, Anal. Chim. Acta. 706 (2011) 8–24.

[118] J. Cao, T. Sun, K.T. V Grattan, Gold nanorod-based localized surface plasmon resonance biosensors: A review, Sensors Actuators B Chem. 195 (2014) 332–351.

[119] W. Lu, M.P. Melancon, C. Xiong, Q. Huang, A. Elliott, S. Song, R. Zhang, L.G. Flores, J.G. Gelovani, L. V Wang, Effects of photoacoustic imaging and photothermal ablation therapy mediated by targeted hollow gold nanospheres in an orthotopic mouse xenograft model of glioma, Cancer Res. 71 (2011) 6116–6121.

[120] C. Wei, M. Lombardo, K. Larson-Smith, I. Pelivanov, C. Perez, J. Xia, T. Matula, D. Pozzo, M. O'Donnell, Nonlinear contrast enhancement in photoacoustic molecular imaging with gold nanosphere encapsulated nanoemulsions, Appl. Phys. Lett. 104 (2014) 33701.

[121] A. Prost, F. Poisson, E. Bossy, Photoacoustic generation by a gold nanosphere: From linear to nonlinear thermoelastics in the long-pulse illumination regime, Phys. Rev. B. 92 (2015) 115450.

[122] P.-J. Chen, S.-H. Hu, C.-T. Fan, M.-L. Li, Y.-Y. Chen, S.-Y. Chen, D.-M. Liu, A novel

multifunctional nano-platform with enhanced anti-cancer and photoacoustic imaging modalities using gold-nanorod-filled silica nanobeads, Chem. Commun. 49 (2013) 892–894.

[123] J. Song, X. Yang, O. Jacobson, P. Huang, X. Sun, L. Lin, X. Yan, G. Niu, Q. Ma, X. Chen, Ultrasmall gold nanorod vesicles with enhanced tumor accumulation and fast excretion from the body for cancer therapy, Adv. Mater. 27 (2015) 4910–4917.

[124] J. Zhong, L. Wen, S. Yang, L. Xiang, Q. Chen, D. Xing, Imaging-guided high-efficient photoacoustic tumor therapy with targeting gold nanorods, Nanomedicine Nanotechnology, Biol. Med. 11 (2015) 1499–1509.

[125] N. Yan, X. Wang, L. Lin, T. Song, P. Sun, H. Tian, H. Liang, X. Chen, Gold Nanorods Electrostatically Binding Nucleic Acid Probe for In Vivo MicroRNA Amplified Detection and Photoacoustic Imaging-Guided Photothermal Therapy, Adv. Funct. Mater. 28 (2018) 1800490.

[126] M. Pérez-Hernández, P. del Pino, S.G. Mitchell, M. Moros, G. Stepien, B. Pelaz, W.J. Parak, E.M. Gálvez, J. Pardo, J.M. de la Fuente, Dissecting the molecular mechanism of apoptosis during photothermal therapy using gold nanoprisms, ACS Nano. 9 (2015) 52–61.

[127] C. Bao, J. Conde, F. Pan, C. Li, C. Zhang, F. Tian, S. Liang, M. Jesus, D. Cui, Gold nanoprisms as a hybrid in vivo cancer theranostic platform for in situ photoacoustic imaging, angiography, and localized hyperthermia, Nano Res. 9 (2016) 1043–1056.

[128] C. Bao, N. Beziere, P. del Pino, B. Pelaz, G. Estrada, F. Tian, V. Ntziachristos, J.M. de la Fuente, D. Cui, Gold nanoprisms as optoacoustic signal nanoamplifiers for in vivo bioimaging of gastrointestinal cancers, Small. 9 (2013) 68–74.

[129] C. Kim, E.C. Cho, J. Chen, K.H. Song, L. Au, C. Favazza, Q. Zhang, C.M. Cobley, F. Gao, Y. Xia, In vivo molecular photoacoustic tomography of melanomas targeted by bioconjugated gold nanocages, ACS Nano. 4 (2010) 4559–4564.

[130] G.D. Moon, S.-W. Choi, X. Cai, W. Li, E.C. Cho, U. Jeong, L. V Wang, Y. Xia, A new theranostic system based on gold nanocages and phase-change materials with unique features for photoacoustic imaging and controlled release, J. Am. Chem. Soc. 133 (2011) 4762–4765.

[131] R. Liang, J. Xie, J. Li, K. Wang, L. Liu, Y. Gao, M. Hussain, G. Shen, J. Zhu, J. Tao, Liposomes-coated gold nanocages with antigens and adjuvants targeted delivery to dendritic cells for enhancing antitumor immune response, Biomaterials. 149 (2017) 41–

50.

[132] J. An, X.-Q. Yang, K. Cheng, X.-L. Song, L. Zhang, C. Li, X.-S. Zhang, Y. Xuan, Y.-Y. Song, B.-Y. Fang, In Vivo Computed Tomography/Photoacoustic Imaging and NIR-Triggered Chemo–Photothermal Combined Therapy Based on a Gold Nanostar-, Mesoporous Silica-, and Thermosensitive Liposome-Composited Nanoprobe, ACS Appl. Mater. Interfaces. 9 (2017) 41748–41759.

[133] X. Li, L. Xing, K. Zheng, P. Wei, L. Du, M. Shen, X. Shi, Formation of gold nanostar-coated hollow mesoporous silica for tumor multimodality imaging and photothermal therapy, ACS Appl. Mater. Interfaces. 9 (2017) 5817–5827.

[134] V. Raghavan, C. O'Flatharta, R. Dwyer, A. Breathnach, H. Zafar, P. Dockery, A. Wheatley, I. Keogh, M. Leahy, M. Olivo, Dual plasmonic gold nanostars for photoacoustic imaging and photothermal therapy, Nanomedicine. 12 (2017) 457–471.

[135] M. Chen, S. Tang, Z. Guo, X. Wang, S. Mo, X. Huang, G. Liu, N. Zheng, Core–Shell Pd@ Au Nanoplates as Theranostic Agents for In-Vivo Photoacoustic Imaging, CT Imaging, and Photothermal Therapy, Adv. Mater. 26 (2014) 8210–8216.

[136] M. Morsin, M. Mat Salleh, A. Ali Umar, M.Z. Sahdan, Gold nanoplates for a localized surface plasmon resonance-based boric acid sensor, Sensors. 17 (2017) 947.

[137] Q. Yu, P. Guan, D. Qin, G. Golden, P.M. Wallace, Inverted size-dependence of surface-enhanced Raman scattering on gold nanohole and nanodisk arrays, Nano Lett. 8 (2008) 1923–1928.

[138] I. Zoric, M. Zach, B. Kasemo, C. Langhammer, Gold, platinum, and aluminum nanodisk plasmons: material independence, subradiance, and damping mechanisms, ACS Nano. 5 (2011) 2535–2546.

[139] J.-S. Wi, J. Park, H. Kang, D. Jung, S.-W. Lee, T.G. Lee, Stacked gold nanodisks for bimodal photoacoustic and optical coherence imaging, ACS Nano. 11 (2017) 6225–6232.

[140] J. Zhao, M. Wallace, M.P. Melancon, Cancer theranostics with gold nanoshells, Nanomedicine. 9 (2014) 2041–2057.

[141] V. Weber, A. Feis, C. Gellini, R. Pilot, P.R. Salvi, R. Signorini, Far-and near-field properties of gold nanoshells studied by photoacoustic and surface-enhanced Raman spectroscopies, Phys. Chem. Chem. Phys. 17 (2015) 21190–21197.

[142] J. Song, X. Yang, Z. Yang, L. Lin, Y. Liu, Z. Zhou, Z. Shen, G. Yu, Y. Dai, O. Jacobson, Rational design of branched nanoporous gold nanoshells with enhanced

physico-optical properties for optical imaging and cancer therapy, ACS Nano. 11 (2017) 6102–6113.

[143] K. Cheng, S.-R. Kothapalli, H. Liu, A.L. Koh, J. V Jokerst, H. Jiang, M. Yang, J. Li, J. Levi, J.C. Wu, Construction and validation of nano gold tripods for molecular imaging of living subjects, J. Am. Chem. Soc. 136 (2014) 3560–3571.

[144] Y. Liu, Z. Yang, X. Huang, G. Yu, S. Wang, Z. Zhou, Z. Shen, W. Fan, Y. Liu, M. Davisson, Glutathione-responsive self-assembled magnetic gold nanowreath for enhanced tumor imaging and imaging-guided photothermal therapy, ACS Nano. 12 (2018) 8129–8137.

[145] P. Huang, O. Pandoli, X. Wang, Z. Wang, Z. Li, C. Zhang, F. Chen, J. Lin, D. Cui, X. Chen, Chiral guanosine 5′-monophosphate-capped gold nanoflowers: Controllable synthesis, characterization, surface-enhanced Raman scattering activity, cellular imaging and photothermal therapy, Nano Res. 5 (2012) 630–639.

[146] P. Huang, P. Rong, J. Lin, W. Li, X. Yan, M.G. Zhang, L. Nie, G. Niu, J. Lu, W. Wang, Triphase interface synthesis of plasmonic gold bellflowers as near-infrared light mediated acoustic and thermal theranostics, J. Am. Chem. Soc. 136 (2014) 8307–8313.

[147] M.L. Personick, M.R. Langille, J. Zhang, N. Harris, G.C. Schatz, C.A. Mirkin, Synthesis and isolation of {110}-faceted gold bipyramids and rhombic dodecahedra, J. Am. Chem. Soc. 133 (2011) 6170–6173.

[148] W. Lu, Q. Huang, G. Ku, X. Wen, M. Zhou, D. Guzatov, P. Brecht, R. Su, A. Oraevsky, L. V Wang, Photoacoustic imaging of living mouse brain vasculature using hollow gold nanospheres, Biomaterials. 31 (2010) 2617–2626.

[149] J. V Jokerst, A.J. Cole, D. Van de Sompel, S.S. Gambhir, Gold nanorods for ovarian cancer detection with photoacoustic imaging and resection guidance via Raman imaging in living mice, ACS Nano. 6 (2012) 10366–10377.

[150] W. Wang, C. Hao, M. Sun, L. Xu, C. Xu, H. Kuang, Spiky Fe3O4@ Au supraparticles for multimodal in vivo imaging, Adv. Funct. Mater. 28 (2018) 1800310.

[151] L.-Y. Bai, X.-Q. Yang, J. An, L. Zhang, K. Zhao, M.-Y. Qin, B.-Y. Fang, C. Li, Y. Xuan, X.-S. Zhang, Multifunctional magnetic-hollow gold nanospheres for bimodal cancer cell imaging and photothermal therapy, Nanotechnology. 26 (2015) 315701.

[152] J. Song, L. Cheng, A. Liu, J. Yin, M. Kuang, H. Duan, Plasmonic vesicles of amphiphilic gold nanocrystals: self-assembly and external-stimuli-triggered destruction, J. Am. Chem. Soc. 133 (2011) 10760–10763.

[153] H. Deng, F. Dai, G. Ma, X. Zhang, Theranostic gold nanomicelles made from biocompatible comb-like polymers for thermochemotherapy and multifunctional imaging with rapid clearance, Adv. Mater. 27 (2015) 3645–3653.

[154] L. Meng, X. Zhang, Q. Lu, Z. Fei, P.J. Dyson, Single walled carbon nanotubes as drug delivery vehicles: targeting doxorubicin to tumors, Biomaterials. 33 (2012) 1689–1698.

[155] H. Gong, R. Peng, Z. Liu, Carbon nanotubes for biomedical imaging: the recent advances, Adv. Drug Deliv. Rev. 65 (2013) 1951–1963.

[156] J. Liu, C. Wang, X. Wang, X. Wang, L. Cheng, Y. Li, Z. Liu, Mesoporous silica coated single-walled carbon nanotubes as a multifunctional light-responsive platform for cancer combination therapy, Adv. Funct. Mater. 25 (2015) 384–392.

[157] G. Lalwani, X. Cai, L. Nie, L. V Wang, B. Sitharaman, Graphene-based contrast agents for photoacoustic and thermoacoustic tomography, Photoacoustics. 1 (2013) 62–67.

[158] Y. Chen, C. Tan, H. Zhang, L. Wang, Two-dimensional graphene analogues for biomedical applications, Chem. Soc. Rev. 44 (2015) 2681–2701.

[159] D. Hu, J. Zhang, G. Gao, Z. Sheng, H. Cui, L. Cai, Indocyanine green-loaded polydopamine-reduced graphene oxide nanocomposites with amplifying photoacoustic and photothermal effects for cancer theranostics, Theranostics. 6 (2016) 1043.

[160] Y. Toumia, F. Domenici, S. Orlanducci, F. Mura, D. Grishenkov, P. Trochet, S. Lacerenza, F. Bordi, G. Paradossi, Graphene meets microbubbles: A superior contrast agent for photoacoustic imaging, ACS Appl. Mater. Interfaces. 8 (2016) 16465–16475.

[161] F. Yang, W. Song, C. Zhang, C. Min, H. Fang, L. Du, P. Wu, W. Zheng, C. Li, S. Zhu, Broadband graphene-based photoacoustic microscopy with high sensitivity, Nanoscale. 10 (2018) 8606–8614.

[162] A. De La Zerda, C. Zavaleta, S. Keren, S. Vaithilingam, S. Bodapati, Z. Liu, J. Levi, B.R. Smith, T.-J. Ma, O. Oralkan, Carbon nanotubes as photoacoustic molecular imaging agents in living mice, Nat. Nanotechnol. 3 (2008) 557.

[163] J.-W. Kim, E.I. Galanzha, E. V Shashkov, H.-M. Moon, V.P. Zharov, Golden carbon nanotubes as multimodal photoacoustic and photothermal high-contrast molecular agents, Nat. Nanotechnol. 4 (2009) 688.

[164] J. Song, F. Wang, X. Yang, B. Ning, M.G. Harp, S.H. Culp, S. Hu, P. Huang, L. Nie, J. Chen, Gold nanoparticle coated carbon nanotube ring with enhanced raman scattering and photothermal conversion property for theranostic applications, J. Am. Chem. Soc. 138 (2016) 7005–7015.

[165] H. Moon, D. Kumar, H. Kim, C. Sim, J.-H. Chang, J.-M. Kim, H. Kim, D.-K. Lim, Amplified photoacoustic performance and enhanced photothermal stability of reduced graphene oxide coated gold nanorods for sensitive photoacoustic imaging, ACS Nano. 9 (2015) 2711–2719.

[166] J. Song, X. Yang, O. Jacobson, L. Lin, P. Huang, G. Niu, Q. Ma, X. Chen, Sequential drug release and enhanced photothermal and photoacoustic effect of hybrid reduced graphene oxide-loaded ultrasmall gold nanorod vesicles for cancer therapy, ACS Nano. 9 (2015) 9199–9209.

[167] C. Biswas, Y.H. Lee, Graphene versus carbon nanotubes in electronic devices, Adv. Funct. Mater. 21 (2011) 3806–3826.

[168] I. Lentacker, I. De Cock, R. Deckers, S.C. De Smedt, C.T.W. Moonen, Understanding ultrasound induced sonoporation: Definitions and underlying mechanisms, Adv. Drug Deliv. Rev. 72 (2014) 49–64. doi:10.1016/j.addr.2013.11.008.

[169] T.-Y. Wang, K. E Wilson, S. Machtaler, J. K Willmann, Ultrasound and microbubble guided drug delivery: mechanistic understanding and clinical implications, Curr. Pharm. Biotechnol. 14 (2013) 743–752.

[170] S.M. Chowdhury, T.-Y. Wang, S. Bachawal, R. Devulapally, J.W. Choe, L.A. Elkacem, B.K. Yakub, D.S. Wang, L. Tian, R. Paulmurugan, Ultrasound-guided therapeutic modulation of hepatocellular carcinoma using complementary microRNAs, J. Control. Release. 238 (2016) 272–280.

[171] H. Dewitte, K. Vanderperren, H. Haers, E. Stock, L. Duchateau, M. Hesta, J.H. Saunders, S.C. De Smedt, I. Lentacker, Theranostic mRNA-loaded microbubbles in the lymphatics of dogs: implications for drug delivery, Theranostics. 5 (2015) 97.

[172] X. Xie, W. Lin, H. Liu, J. Deng, Y. Chen, H. Liu, X. Fu, Y. Yang, Ultrasound-responsive nanobubbles contained with peptide–camptothecin conjugates for targeted drug delivery, Drug Deliv. 23 (2016) 2756–2764.

[173] C.M. Schoellhammer, G.Y. Lauwers, J.A. Goettel, M.A. Oberli, C. Cleveland, J.Y. Park, D. Minahan, Y. Chen, D.G. Anderson, A. Jaklenec, Ultrasound-mediated delivery of RNA to colonic mucosa of live mice, Gastroenterology. 152 (2017) 1151–1160.

[174] N.M. Salkho, R.Z. Turki, O. Guessoum, A.M. Martins, R.F. Vitor, G.A. Husseini, Liposomes as a promising ultrasound-triggered drug delivery system in cancer treatment, Curr. Mol. Med. 17 (2017) 668–688.

[175] C.A. Sennoga, E. Kanbar, L. Auboire, P.-A. Dujardin, D. Fouan, J.-M. Escoffre, A. Bouakaz, Microbubble-mediated ultrasound drug-delivery and therapeutic monitoring, Expert Opin. Drug Deliv. 14 (2017) 1031–1043.

[176] X. Li, Z. Sui, X. Li, W. Xu, Q. Guo, J. Sun, F. Jing, Perfluorooctylbromide nanoparticles for ultrasound imaging and drug delivery, Int. J. Nanomedicine. 13 (2018) 3053.

[177] S. Mullick Chowdhury, T. Lee, J.K. Willmann, Ultrasound-guided drug delivery in cancer, Ultrasonography. 36 (2017) 171–184. doi:10.14366/usg.17021.

[178] I. Brigger, C. Dubernet, P. Couvreur, Nanoparticles in cancer therapy and diagnosis, Adv. Drug Deliv. Rev. 64 (2012) 24–36.

[179] H. Hasanzadeh, M. Mokhtari-Dizaji, S.Z. Bathaie, Z.M. Hassan, Effect of local dual frequency sonication on drug distribution from polymeric nanomicelles, Ultrason. Sonochem. 18 (2011) 1165–1171.

[180] S.R. Sirsi, C. Fung, S. Garg, M.Y. Tianning, P.A. Mountford, M.A. Borden, Lung surfactant microbubbles increase lipophilic drug payload for ultrasound-targeted delivery, Theranostics. 3 (2013) 409.

[181] J. Chen, S. Ratnayaka, A. Alford, V. Kozlovskaya, F. Liu, B. Xue, K. Hoyt, E. Kharlampieva, Theranostic multilayer capsules for ultrasound imaging and guided drug delivery, ACS Nano. 11 (2017) 3135–3146.

[182] A. Jain, A. Tiwari, A. Verma, S.K. Jain, Ultrasound-based triggered drug delivery to tumors, Drug Deliv. Transl. Res. 8 (2018) 150–164. doi:10.1007/s13346-017-0448-6.

[183] Y. Cao, Y. Chen, T. Yu, Y. Guo, F. Liu, Y. Yao, P. Li, D. Wang, Z. Wang, Y. Chen, Drug release from phase-changeable nanodroplets triggered by low-intensity focused ultrasound, Theranostics. 8 (2018) 1327.

[184] H. Jin, H. Tan, L. Zhao, W. Sun, L. Zhu, Y. Sun, H. Hao, H. Xing, L. Liu, X. Qu, Ultrasound-triggered thrombolysis using urokinase-loaded nanogels, Int. J. Pharm. 434 (2012) 384–390.

[185] J. Kim, R. DeRuiter, P. Durham, J. Tsuruta, L. Goel, X. Jiang, Z. Xu, P.A. Dayton, Perfluorocarbon nanodroplets versus microbubbles in cavitation-enhanced sonothrombolysis of retracted clots, J. Acoust. Soc. Am. 146 (2019) 2775.

[186] S. Wang, X. Guo, W. Xiu, Y. Liu, L. Ren, H. Xiao, F. Yang, Y. Gao, C. Xu, L. Wang, Accelerating thrombolysis using a precision and clot-penetrating drug delivery strategy by nanoparticle-shelled microbubbles, Sci. Adv. 6 (2020) eaaz8204.

[187] M. Thein, A. Cheng, P. Khanna, C. Zhang, E.-J. Park, D. Ahmed, C.J. Goodrich, F. Asphahani, F. Wu, N.B. Smith, Site-specific sonoporation of human melanoma cells at the cellular level using high lateral-resolution ultrasonic micro-transducer arrays, Biosens. Bioelectron. 27 (2011) 25–33.

[188] M. Figueiredo, R. Esenaliev, PLGA nanoparticles for ultrasound-mediated gene delivery to solid tumors, J. Drug Deliv. 2012 (2012).

[189] Q.-L. Zhou, Z.-Y. Chen, Y.-X. Wang, F. Yang, Y. Lin, Y.-Y. Liao, Ultrasound-mediated local drug and gene delivery using nanocarriers, Biomed Res. Int. 2014 (2014).

[190] Y. Negishi, Y. Endo-Takahashi, K. Maruyama, Gene delivery systems by the combination of lipid bubbles and ultrasound, Drug Discov. Ther. (2016).

[191] J. Di, J. Price, X. Gu, X. Jiang, Y. Jing, Z. Gu, Ultrasound-triggered regulation of blood glucose levels using injectable nano-network, Adv. Healthc. Mater. 3 (2014) 811–816.

[192] J. Di, J. Yu, Q. Wang, S. Yao, D. Suo, Y. Ye, M. Pless, Y. Zhu, Y. Jing, Z. Gu, Ultrasound-triggered noninvasive regulation of blood glucose levels using microgels integrated with insulin nanocapsules, Nano Res. 10 (2017) 1393–1402.

[193] S. Hossen, M.K. Hossain, M.K. Basher, M.N.H. Mia, M.T. Rahman, M.J. Uddin, Smart nanocarrier-based drug delivery systems for cancer therapy and toxicity studies: A review, J. Adv. Res. 15 (2019) 1–18. doi:10.1016/j.jare.2018.06.005.

[194] T.M. Allen, P.R. Cullis, Liposomal drug delivery systems: from concept to clinical applications, Adv. Drug Deliv. Rev. 65 (2013) 36–48.

[195] E.E.J. Marxer, J. Brüßler, A. Becker, J. Schümmelfeder, R. Schubert, C. Nimsky, U. Bakowsky, Development and characterization of new nanoscaled ultrasound active lipid dispersions as contrast agents, Eur. J. Pharm. Biopharm. 77 (2011) 430–437.

[196] A. Becker, E. Marxer, J. Brüßler, A.S. Hoormann, D. Kuhnt, U. Bakowsky, C. Nimsky, Ultrasound active nanoscaled lipid formulations for thrombus lysis, Eur. J. Pharm. Biopharm. 77 (2011) 424–429.

[197] J.R. Lattin, W.G. Pitt, D.M. Belnap, G.A. Husseini, Ultrasound-induced calcein release from eLiposomes, Ultrasound Med. Biol. 38 (2012) 2163–2173.

[198] M.A.D. de la Rosa, G.A. Husseini, W.G. Pitt, Comparing microbubble cavitation at 500 kHz and 70 kHz related to micellar drug delivery using ultrasound, Ultrasonics. 53 (2013) 377–386.

[199] G.A. Husseini, D. Velluto, L. Kherbeck, W.G. Pitt, J.A. Hubbell, D.A. Christensen,

Investigating the acoustic release of doxorubicin from targeted micelles, Colloids Surfaces B Biointerfaces. 101 (2013) 153–155.

[200] P. Wu, Y. Jia, F. Qu, Y. Sun, P. Wang, K. Zhang, C. Xu, Q. Liu, X. Wang, Ultrasound-responsive polymeric micelles for sonoporation-assisted site-specific therapeutic action, ACS Appl. Mater. Interfaces. 9 (2017) 25706–25716.

[201] C. Sanson, O. Diou, J. Thevenot, E. Ibarboure, A. Soum, A. Brûlet, S. Miraux, E. Thiaudière, S. Tan, A. Brisson, Doxorubicin loaded magnetic polymersomes: theranostic nanocarriers for MR imaging and magneto-chemotherapy, ACS Nano. 5 (2011) 1122–1140.

[202] M.-M. Néstor, N.-P.E. Kei, N.-A.M. Guadalupe, M.-E.S. Elisa, G.-Q. Adriana, Q.-G. David, Preparation and in vitro evaluation of poly (D, L-lactide-co-glycolide) air-filled nanocapsules as a contrast agent for ultrasound imaging, Ultrasonics. 51 (2011) 839–845.

[203] P. Yang, D. Li, S. Jin, J. Ding, J. Guo, W. Shi, C. Wang, Stimuli-responsive biodegradable poly (methacrylic acid) based nanocapsules for ultrasound traced and triggered drug delivery system, Biomaterials. 35 (2014) 2079–2088.

[204] W. Chen, J. Du, Ultrasound and pH dually responsive polymer vesicles for anticancer drug delivery, Sci. Rep. 3 (2013) 2162.

[205] R. Cavalli, A. Bisazza, M. Trotta, M. Argenziano, A. Civra, M. Donalisio, D. Lembo, New chitosan nanobubbles for ultrasound-mediated gene delivery: preparation and in vitro characterization, Int. J. Nanomedicine. 7 (2012) 3309.

[206] T. Yin, P. Wang, J. Li, R. Zheng, B. Zheng, D. Cheng, R. Li, J. Lai, X. Shuai, Ultrasound-sensitive siRNA-loaded nanobubbles formed by hetero-assembly of polymeric micelles and liposomes and their therapeutic effect in gliomas, Biomaterials. 34 (2013) 4532–4543.

[207] N.Y. Rapoport, A.M. Kennedy, J.E. Shea, C.L. Scaife, K.-H. Nam, Controlled and targeted tumor chemotherapy by ultrasound-activated nanoemulsions/microbubbles, J. Control. Release. 138 (2009) 268–276.

[208] D. Thakkar, R. Gupta, K. Monson, N. Rapoport, Effect of ultrasound on the permeability of vascular wall to nano-emulsion droplets, Ultrasound Med. Biol. 39 (2013) 1804–1811.

[209] J.L. Paris, M.V. Cabañas, M. Manzano, M. Vallet-Regí, Polymer-grafted mesoporous silica nanoparticles as ultrasound-responsive drug carriers, ACS Nano. 9 (2015)

11023–11033.

[210] J.L. Paris, C. Mannaris, M.V. Cabañas, R. Carlisle, M. Manzano, M. Vallet-Regí, C.C. Coussios, Ultrasound-mediated cavitation-enhanced extravasation of mesoporous silica nanoparticles for controlled-release drug delivery, Chem. Eng. J. 340 (2018) 2–8.

[211] T.S. Anirudhan, A.S. Nair, Temperature and ultrasound sensitive gatekeepers for the controlled release of chemotherapeutic drugs from mesoporous silica nanoparticles, J. Mater. Chem. B. 6 (2018) 428–439.

[212] J.L. Paris, M. Manzano, M.V. Cabañas, M. Vallet-Regí, Mesoporous silica nanoparticles engineered for ultrasound-induced uptake by cancer cells, Nanoscale. 10 (2018) 6402–6408.

[213] X. Li, Z. Wang, H. Xia, Ultrasound Reversible Response Nanocarrier Based on Sodium Alginate Modified Mesoporous Silica Nanoparticles, Front. Chem. 7 (2019) 59.

[214] M. Manzano, M. Vallet-Regí, Ultrasound responsive mesoporous silica nanoparticles for biomedical applications, Chem. Commun. 55 (2019) 2731–2740.

[215] Y. Xia, W. Li, C.M. Cobley, J. Chen, X. Xia, Q. Zhang, M. Yang, E.C. Cho, P.K. Brown, Gold nanocages: from synthesis to theranostic applications, Acc. Chem. Res. 44 (2011) 914–924.

[216] X. Xia, Y. Xia, Gold nanocages as multifunctional materials for nanomedicine, Front. Phys. 9 (2014) 378–384.

[217] P.S. Zangabad, M. Karimi, F. Mehdizadeh, H. Malekzad, A. Ghasemi, S. Bahrami, H. Zare, M. Moghoofei, A. Hekmatmanesh, M.R. Hamblin, Nanocaged platforms: modification, drug delivery and nanotoxicity. Opening synthetic cages to release the tiger, Nanoscale. 9 (2017) 1356–1392.

[218] H.-W. Yang, M.-Y. Hua, H.-L. Liu, C.-Y. Huang, K.-C. Wei, Potential of magnetic nanoparticles for targeted drug delivery, Nanotechnol. Sci. Appl. 5 (2012) 73.

[219] V. V Mody, A. Cox, S. Shah, A. Singh, W. Bevins, H. Parihar, Magnetic nanoparticle drug delivery systems for targeting tumor, Appl. Nanosci. 4 (2014) 385–392.

[220] J.Y. Lee, C. Crake, B. Teo, D. Carugo, M. de Saint Victor, A. Seth, E. Stride, Ultrasound-Enhanced siRNA Delivery Using Magnetic Nanoparticle-Loaded Chitosan-Deoxycholic Acid Nanodroplets, Adv. Healthc. Mater. 6 (2017) 1601246.

[221] D. Chen, C.A. Dougherty, K. Zhu, H. Hong, Theranostic applications of carbon nanomaterials in cancer: Focus on imaging and cargo delivery, J. Control. Release. 210

(2015) 230–245.

[222] A. Al Faraj, A.P. Shaik, A.S. Shaik, Magnetic single-walled carbon nanotubes as efficient drug delivery nanocarriers in breast cancer murine model: noninvasive monitoring using diffusion-weighted magnetic resonance imaging as sensitive imaging biomarker, Int. J. Nanomedicine. 10 (2015) 157.

[223] S. Beg, M. Rahman, A. Jain, S. Saini, M.S. Hasnain, S. Swain, S. Imam, I. Kazmi, S. Akhter, Emergence in the functionalized carbon nanotubes as smart nanocarriers for drug delivery applications, in: Fullerens, Graphenes Nanotub., Elsevier, 2018: pp. 105–133.

[224] J. Kaur, G.S. Gill, K. Jeet, Applications of carbon nanotubes in drug delivery: a comprehensive review, in: Charact. Biol. Nanomater. Drug Deliv., Elsevier, 2019: pp. 113–135.

[225] D.L. Miller, N.B. Smith, M.R. Bailey, G.J. Czarnota, K. Hynynen, I.R.S. Makin, Overview of Therapeutic Ultrasound Applications and Safety Considerations, J. Ultrasound Med. 31 (2012) 623–634. doi:10.7863/jum.2012.31.4.623.

[226] T. Liu, N. Zhang, Z. Wang, M. Wu, Y. Chen, M. Ma, H. Chen, J. Shi, Endogenous catalytic generation of O2 bubbles for in situ ultrasound-guided high intensity focused ultrasound ablation, ACS Nano. 11 (2017) 9093–9102.

[227] X. Qian, Y. Zheng, Y. Chen, Micro/nanoparticle-augmented sonodynamic therapy (SDT): Breaking the depth shallow of photoactivation, Adv. Mater. 28 (2016) 8097–8129.

[228] C. Yang, Y. Li, M. Du, Z. Chen, Recent advances in ultrasound-triggered therapy, J. Drug Target. 27 (2019) 33–50.

[229] J. Shi, P.W. Kantoff, R. Wooster, O.C. Farokhzad, Cancer nanomedicine: progress, challenges and opportunities, Nat. Rev. Cancer. 17 (2017) 20.

[230] L.-Q. Zhou, P. Li, X.-W. Cui, C.F. Dietrich, Ultrasound nanotheranostics in fighting cancer: Advances and prospects, Cancer Lett. 470 (2020) 204–219.

[231] W. Yang, Q. Lyu, J. Zhao, L. Cao, Y. Hao, H. Zhang, Recent advance in near-infrared/ultrasound-sensitive 2D-nanomaterials for cancer therapeutics, Sci. China Mater. (2020) 1–32.

[232] W. Fan, B. Yung, P. Huang, X. Chen, Nanotechnology for multimodal synergistic cancer therapy, Chem. Rev. 117 (2017) 13566–13638.

[233] H. Xu, X. Zhang, R. Han, P. Yang, H. Ma, Y. Song, Z. Lu, W. Yin, X. Wu, H. Wang,

Nanoparticles in sonodynamic therapy: state of the art review, RSC Adv. 6 (2016) 50697–50705.

[234] J. Unga, M. Hashida, Ultrasound induced cancer immunotherapy, Adv. Drug Deliv. Rev. 72 (2014) 144–153.

[235] S.Z. Goldhaber, H. Bounameaux, Pulmonary embolism and deep vein thrombosis, Lancet. 379 (2012) 1835–1846.

[236] L. Goel, X. Jiang, Advances in Sonothrombolysis Techniques Using Piezoelectric Transducers, Sensors. 20 (2020) 1288.

[237] J. Kim, B.D. Lindsey, W.-Y. Chang, X. Dai, J.M. Stavas, P.A. Dayton, X. Jiang, Intravascular forward-looking ultrasound transducers for microbubble-mediated sonothrombolysis, Sci. Rep. 7 (2017) 1–10.

[238] X. Zhang, G.E. Owens, C.A. Cain, H.S. Gurm, J. Macoskey, Z. Xu, Histotripsy thrombolysis on retracted clots, Ultrasound Med. Biol. 42 (2016) 1903–1918.

[239] L. Goel, H. Wu, B. Zhang, J. Kim, P.A. Dayton, Z. Xu, X. Jiang, Nanodroplet-Mediated Intravascular Sonothrombolysis: Cavitation Study, in: 2020 IEEE 20th Int. Conf. Nanotechnol., IEEE, 2020: pp. 185–188.

[240] J. Kim, R.M. DeRuiter, L. Goel, Z. Xu, X. Jiang, P.A. Dayton, A Comparison of Sonothrombolysis in Aged Clots between Low-Boiling-Point Phase-Change Nanodroplets and Microbubbles of the Same Composition, Ultrasound Med. Biol. 46 (2020) 3059–3068.

[241] J. Kim, L. Goel, X. Jiang, Z. Xu, P.A. Dayton, Cavitation-Enhanced High-Pressure Pulsed Sonothrombolysis with Perfluorocarbon Nanodroplets versus Microbubbles in Contracted and Uncontracted Clots, in: 2020 IEEE Int. Ultrason. Symp., IEEE, 2020: pp. 1–4.

[242] L. Goel, H. Wu, B. Zhang, J. Kim, P. Dayton, Z. Xu, X. Jiang, Nanodroplet Mediated Intravascular Sonothrombolysis of Retracted Clots, in: 2020 IEEE Int. Ultrason. Symp., IEEE, 2020: pp. 1–3.

[243] Y. Gao, C.U. Chan, Q. Gu, X. Lin, W. Zhang, D.C.L. Yeo, A.M. Alsema, M. Arora, M.S.K. Chong, P. Shi, Controlled nanoparticle release from stable magnetic microbubble oscillations, NPG Asia Mater. 8 (2016) e260–e260.

[244] B. Zhang, X. Jiang, H. Wu, Ultrasound Thrombolysis with Magnetic Microbubbles Under a Rotational Magnetic Field, in: 2018 IEEE 13th Nanotechnol. Mater. Devices Conf., IEEE, 2018: pp. 1–4.

[245] B. Zhang, H. Kim, H. Wu, Y. Gao, X. Jiang, Sonothrombolysis with magnetic microbubbles under a rotational magnetic field, Ultrasonics. 98 (2019) 62–71.

[246] H. Shangguan, L.W. Casperson, A. Shearin, K.W. Gregory, S.A. Prahl, Photoacoustic drug delivery: The effect of laser parameters on the spatial distribution of delivered drug, in: Laser-Tissue Interact. VI, International Society for Optics and Photonics, 1995: pp. 394–403.

[247] H. Shangguan, L.W. Casperson, A. Shearin, S.A. Prahl, Investigation of cavitation bubble dynamics using particle image velocimetry: Implications for photoacoustic drug delivery, in: Lasers Surg. Adv. Charact. Ther. Syst. VI, International Society for Optics and Photonics, 1996: pp. 104–116.

[248] J. Di, J. Kim, Q. Hu, X. Jiang, Z. Gu, Spatiotemporal drug delivery using laser-generated-focused ultrasound system, J. Control. Release. 220 (2015) 592–599.

[249] P.C. Ray, S.A. Khan, A.K. Singh, D. Senapati, Z. Fan, Nanomaterials for targeted detection and photothermal killing of bacteria, Chem. Soc. Rev. 41 (2012) 3193–3209.

[250] P. Rai, S. Mallidi, X. Zheng, R. Rahmanzadeh, Y. Mir, S. Elrington, A. Khurshid, T. Hasan, Development and applications of photo-triggered theranostic agents, Adv. Drug Deliv. Rev. 62 (2010) 1094–1124.

[251] N. Fomina, J. Sankaranarayanan, A. Almutairi, Photochemical mechanisms of light-triggered release from nanocarriers, Adv. Drug Deliv. Rev. 64 (2012) 1005–1020.

[252] L. Cheng, W. He, H. Gong, C. Wang, Q. Chen, Z. Cheng, Z. Liu, PEGylated micelle nanoparticles encapsulating a non-fluorescent near-infrared organic dye as a safe and highly-effective photothermal agent for in vivo cancer therapy, Adv. Funct. Mater. 23 (2013) 5893–5902.

[253] K. Sivasubramanian, M. Mathiyazhakan, C. Wiraja, P.K. Upputuri, C. Xu, M. Pramanik, Near-infrared light-responsive liposomal contrast agent for photoacoustic imaging and drug release applications, J. Biomed. Opt. 22 (2016) 41007.

[254] L. Zhang, S. Gao, F. Zhang, K. Yang, Q. Ma, L. Zhu, Activatable hyaluronic acid nanoparticle as a theranostic agent for optical/photoacoustic image-guided photothermal therapy, ACS Nano. 8 (2014) 12250–12258.

[255] Y. Wang, E.M. Strohm, Y. Sun, Z. Wang, Y. Zheng, Z. Wang, M.C. Kolios, Biodegradable polymeric nanoparticles containing gold nanoparticles and Paclitaxel for cancer imaging and drug delivery using photoacoustic methods, Biomed. Opt. Express. 7 (2016) 4125–4138.

[256] S. Shi, Y. Liu, Y. Chen, Z. Zhang, Y. Ding, Z. Wu, J. Yin, L. Nie, Versatile pH-response micelles with high cell-penetrating helical diblock copolymers for photoacoustic imaging guided synergistic chemo-photothermal therapy, Theranostics. 6 (2016) 2170.

[257] X. Liu, G. Yang, L. Zhang, Z. Liu, Z. Cheng, X. Zhu, Photosensitizer cross-linked nano-micelle platform for multimodal imaging guided synergistic photothermal/photodynamic therapy, Nanoscale. 8 (2016) 15323–15339.

[258] M. Guo, H. Mao, Y. Li, A. Zhu, H. He, H. Yang, Y. Wang, X. Tian, C. Ge, Q. Peng, Dual imaging-guided photothermal/photodynamic therapy using micelles, Biomaterials. 35 (2014) 4656–4666.

[259] H. Gong, Z. Dong, Y. Liu, S. Yin, L. Cheng, W. Xi, J. Xiang, K. Liu, Y. Li, Z. Liu, Engineering of multifunctional nano-micelles for combined photothermal and photodynamic therapy under the guidance of multimodal imaging, Adv. Funct. Mater. 24 (2014) 6492–6502.

[260] T. Wang, D. Wang, H. Yu, M. Wang, J. Liu, B. Feng, F. Zhou, Q. Yin, Z. Zhang, Y. Huang, Intracellularly acid-switchable multifunctional micelles for combinational photo/chemotherapy of the drug-resistant tumor, ACS Nano. 10 (2016) 3496–3508.

[261] Y. Cai, P. Liang, Q. Tang, X. Yang, W. Si, W. Huang, Q. Zhang, X. Dong, Diketopyrrolopyrrole–triphenylamine organic nanoparticles as multifunctional reagents for photoacoustic imaging-guided photodynamic/photothermal synergistic tumor therapy, ACS Nano. 11 (2017) 1054–1063.

[262] J. Zhang, C. Yang, R. Zhang, R. Chen, Z. Zhang, W. Zhang, S. Peng, X. Chen, G. Liu, C. Hsu, Biocompatible D–A Semiconducting Polymer Nanoparticle with Light-Harvesting Unit for Highly Effective Photoacoustic Imaging Guided Photothermal Therapy, Adv. Funct. Mater. 27 (2017) 1605094.

[263] Q. Fan, K. Cheng, X. Hu, X. Ma, R. Zhang, M. Yang, X. Lu, L. Xing, W. Huang, S.S. Gambhir, Transferring biomarker into molecular probe: melanin nanoparticle as a naturally active platform for multimodality imaging, J. Am. Chem. Soc. 136 (2014) 15185–15194.

[264] R. Zhang, Q. Fan, M. Yang, K. Cheng, X. Lu, L. Zhang, W. Huang, Z. Cheng, Engineering melanin nanoparticles as an efficient drug–delivery system for imaging-guided chemotherapy, Adv. Mater. 27 (2015) 5063–5069.

[265] J. Chen, M. Yang, Q. Zhang, E.C. Cho, C.M. Cobley, C. Kim, C. Glaus, L. V Wang,

M.J. Welch, Y. Xia, Gold nanocages: a novel class of multifunctional nanomaterials for theranostic applications, Adv. Funct. Mater. 20 (2010) 3684–3694.

[266] P. Manivasagan, S. Bharathiraja, N.Q. Bui, I.G. Lim, J. Oh, Paclitaxel-loaded chitosan oligosaccharide-stabilized gold nanoparticles as novel agents for drug delivery and photoacoustic imaging of cancer cells, Int. J. Pharm. 511 (2016) 367–379.

[267] P. Huang, J. Lin, W. Li, P. Rong, Z. Wang, S. Wang, X. Wang, X. Sun, M. Aronova, G. Niu, Biodegradable gold nanovesicles with an ultrastrong plasmonic coupling effect for photoacoustic imaging and photothermal therapy, Angew. Chemie Int. Ed. 52 (2013) 13958–13964.

[268] K. Wilson, K. Homan, S. Emelianov, Biomedical photoacoustics beyond thermal expansion using triggered nanodroplet vaporization for contrast-enhanced imaging, Nat. Commun. 3 (2012) 618.

[269] J. Zhong, S. Yang, L. Wen, D. Xing, Imaging-guided photoacoustic drug release and synergistic chemo-photoacoustic therapy with paclitaxel-containing nanoparticles, J. Control. Release. 226 (2016) 77–87.

[270] S. Duan, Y. Yang, C. Zhang, N. Zhao, F. Xu, NIR-Responsive Polycationic Gatekeeper-Cloaked Hetero-Nanoparticles for Multimodal Imaging-Guided Triple-Combination Therapy of Cancer, Small. 13 (2017) 1603133.

[271] L. Huang, L. Ao, D. Hu, W. Wang, Z. Sheng, W. Su, Magneto-plasmonic nanocapsules for multimodal-imaging and magnetically guided combination cancer therapy, Chem. Mater. 28 (2016) 5896–5904.

[272] G. Fu, W. Liu, S. Feng, X. Yue, Prussian blue nanoparticles operate as a new generation of photothermal ablation agents for cancer therapy, Chem. Commun. 48 (2012) 11567–11569.

[273] X. Liang, Z. Deng, L. Jing, X. Li, Z. Dai, C. Li, M. Huang, Prussian blue nanoparticles operate as a contrast agent for enhanced photoacoustic imaging, Chem. Commun. 49 (2013) 11029–11031.

[274] L. Jing, X. Liang, Z. Deng, S. Feng, X. Li, M. Huang, C. Li, Z. Dai, Prussian blue coated gold nanoparticles for simultaneous photoacoustic/CT bimodal imaging and photothermal ablation of cancer, Biomaterials. 35 (2014) 5814–5821.

[275] L. Cheng, H. Gong, W. Zhu, J. Liu, X. Wang, G. Liu, Z. Liu, PEGylated Prussian blue nanocubes as a theranostic agent for simultaneous cancer imaging and photothermal therapy, Biomaterials. 35 (2014) 9844–9852.

[276] X. Cai, X. Jia, W. Gao, K. Zhang, M. Ma, S. Wang, Y. Zheng, J. Shi, H. Chen, A Versatile Nanotheranostic Agent for Efficient Dual-Mode Imaging Guided Synergistic Chemo-Thermal Tumor Therapy, Adv. Funct. Mater. 25 (2015) 2520–2529.

[277] W. Chen, K. Zeng, H. Liu, J. Ouyang, L. Wang, Y. Liu, H. Wang, L. Deng, Y. Liu, Cell membrane camouflaged hollow prussian blue nanoparticles for synergistic photothermal-/chemotherapy of cancer, Adv. Funct. Mater. 27 (2017) 1605795.

[278] T. Bao, W. Yin, X. Zheng, X. Zhang, J. Yu, X. Dong, Y. Yong, F. Gao, L. Yan, Z. Gu, One-pot synthesis of PEGylated plasmonic MoO3–x hollow nanospheres for photoacoustic imaging guided chemo-photothermal combinational therapy of cancer, Biomaterials. 76 (2016) 11–24.

[279] X. Song, X. Wang, S. Yu, J. Cao, S. Li, J. Li, G. Liu, H. Yang, X. Chen, Co9Se8 Nanoplates as a New Theranostic Platform for Photoacoustic/Magnetic Resonance Dual-Modal-Imaging-Guided Chemo-Photothermal Combination Therapy, Adv. Mater. 27 (2015) 3285–3291.

[280] Z. Sheng, L. Song, J. Zheng, D. Hu, M. He, M. Zheng, G. Gao, P. Gong, P. Zhang, Y. Ma, Protein-assisted fabrication of nano-reduced graphene oxide for combined in vivo photoacoustic imaging and photothermal therapy, Biomaterials. 34 (2013) 5236–5243.

[281] J. Kim, W.-Y. Chang, B.D. Lindsey, P.A. Dayton, X. Dai, J.M. Stavas, X. Jiang, Laser-generated-focused ultrasound transducers for microbubble-mediated, dual-excitation sonothrombolysis, in: 2016 IEEE Int. Ultrason. Symp., IEEE, 2016: pp. 1–4.

[282] H. Wu, H. Kim, Y. Tang, J. Yao, X. Jiang, Fiber-optic laser-ultrasound transducer using carbon nanoparticles for intravascular sonothrombolysis, in: 2019 IEEE 19th Int. Conf. Nanotechnol., IEEE, 2019: pp. 261–264.

[283] H. Wu, Y. Tang, H. Kim, J. Yao, X. Jiang, Fiber based laser ultrasound transducer for intravascular thrombolysis with detective photoacoustic imaging, in: 2020 IEEE Int. Ultrason. Symp., IEEE, 2020: pp. 1–4.

Graphical Abstract